MDPI

Review

A Comprehensive Review of Water-Based Nanolubricants

Afshana Morshed, Hui Wu * and Zhengyi Jiang ***

School of Mechanical, Materials, Mechatronic and Biomedical Engineering, University of Wollongong, Wollongong, NSW 2522, Australia; am294@uowmail.edu.au
* Correspondence: hwu@uow.edu.au (H.W.); jiang@uow.edu.au (Z.J.)

Abstract: Applying nanomaterials and nanotechnology in lubrication has become increasingly popular and important to further reduce the friction and wear in engineering applications. To achieve green manufacturing and its sustainable development, water-based nanolubricants are emerging as promising alternatives to the traditional oil-containing lubricants that inevitably pose environmental issues when burnt and discharged. This review presents an overview of recent advances in water-based nanolubricants, starting from the preparation of the lubricants using different types of nanoadditives, followed by the techniques to evaluate and enhance their dispersion stability, and the commonly used tribo-testing methods. The lubrication mechanisms and models are discussed with special attention given to the roles of the nanoadditives. Finally, the applications of water-based nanolubricants in metal rolling are summarised, and the outlook for future research directions is proposed.

Keywords: water-based nanolubricant; nanoadditive; dispersion stability; tribology; metal forming

1. Introduction

Friction and wear occur between moving materials in contact, the study of which is of fundamental importance in many applied sciences [1]. Lubricants, such as neat oils [2–4] and oil-in-water emulsions [5,6], have been extensively used to reduce the friction and wear, and satisfactory results have been obtained. To further enhance the friction-reduction and anti-wear properties of the oil-containing lubricants, great efforts have been directed towards incorporating different types of nanoadditives into the base lubricants [7–9]. These nanoadditives include metals, metal oxides, metal sulphides, non-metallic oxides, carbon materials, composites, and others such as nitrides [10,11]. The use of these oil-containing lubricants, however, unavoidably leads to adverse effects on the environment, especially when burnt and discharged, and regular maintenance of oil nozzles is always a laborious task. It is thus desirable to use eco-friendly lubricants as alternatives to the oil-containing ones without compromising on the lubrication performance in terms of the decreases in both friction and wear.

Over the past decade, water-based nanolubricants have been emerging as promising eco-friendly lubricants by dispersing nanoadditives into water [12–23], which integrates superb cooling capacity of water with excellent lubricity contributed by the nanoadditives. The use of water-based nanolubricants not only provides protection against friction and wear between the tool and the workpiece, but also improves overall quality of the product, demonstrating a great potential in engineering applications, such as metal forming [24–29]. Despite an increasing number of experimental studies on various nanomaterials as nanoadditives in water, several aspects including dispersion stability, tribological behaviour, and lubrication mechanism have not yet been fully understood. Most importantly, a review of the advances in water-based nanolubricants is still in its infancy [30,31], which brings an urgent need for comprehensive summary of the fundamental knowledge in the field of water-based nanolubrication.

In this review, the recent advances in water-based nanolubricants will be systematically summarised. To begin with, preparation of water-based nanolubricants will be introduced, including the preparation methods and the nanoadditives used in water. Based on the classified lubricants, we will then discuss the dispersion stability of the nanoadditives and the enhancement techniques. Subsequently, the tribo-testing methods used for tribological characterisation of the water-based lubricants will be compared, with a focus on the roles of nanoadditives, to propose the lubrication mechanism. We finally present the applications of the water-based nanolubricants in metal rolling, followed by proposing the outlook for future research directions.

## 2. Preparation of Water-Based Nanolubricants

2.1. Preparation Methods

Preparation of industrial lubricants usually requires the consideration of using various additives, such as antioxidants, corrosion inhibitors, defoamers, emulsifiers, extreme pressure (EP) agents, pour point depressants, and viscosity index improvers for different purposes in practical applications [32]. In particular, water-based nanolubricants are basically prepared by dispersing nano-scale solid particles into base water with the aid of a dispersant or surfactant, followed by mechanical agitation and ultrasonic treatment. In general, two primary techniques including one-step and two-step methods are adopted by most researchers to prepare nanolubricants. These two methods are subdivided in Figure 1.
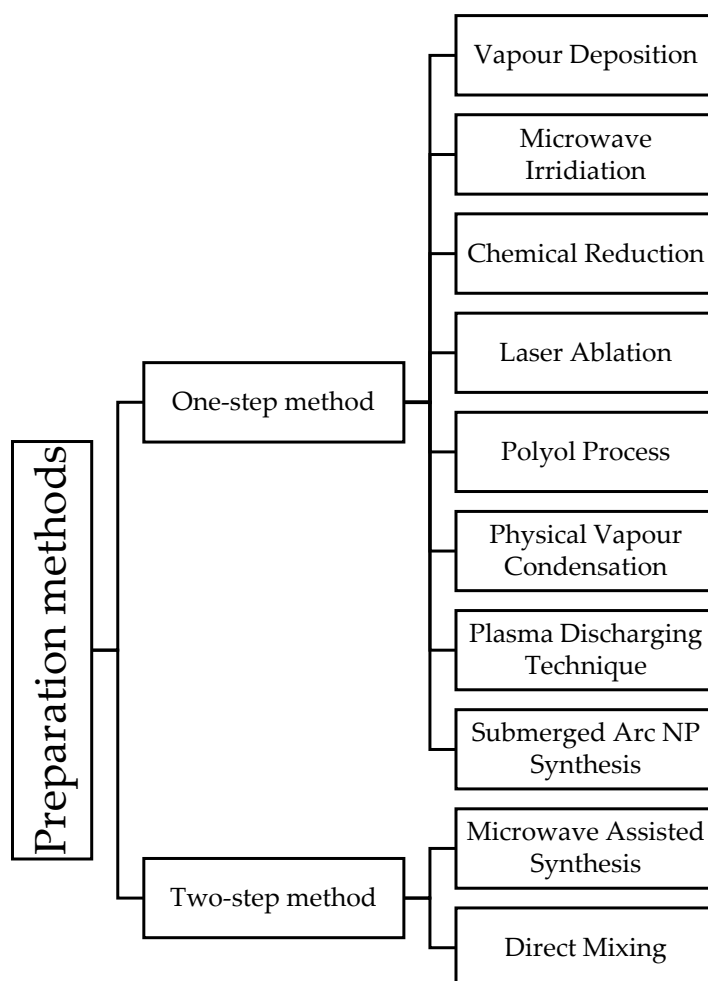
Figure 1. Subdivision of preparation methods of nanolubricants.

One-step method is a procedure that simultaneously combines the production of nanoparticles (NPs) with dispersion of NPs in base lubricant. One of the most commonly

used methods is named vapour deposition, which was developed by Choi and Eastman [33]. The schematic of this method is shown in Figure 2a. First, a flowing thin film made of base liquid is formed on the vessel wall under centrifugal force of the rotating disk. Then the raw material is placed in the resistively heated crucible with heating for evaporation. The produced vapour is condensed into nano-sized particles when contacting the cold base liquid film, and nanolubricant is thus obtained. Another one-step direct evaporation method named vacuum evaporation onto a running oil substrate (VEROS) was developed by Akoh et al. [34], which aimed to produce ultrafine NPs with an average size of around 0.25 nm. Additionally, other techniques in the one-step method include microwave irradiation [35], chemical reduction [36], laser ablation [37], polyol process [38], physical vapour condensation method [39], plasma discharging technique [40], and submerged arc NP synthesis system [41]. However, the disadvantage in the one-step method is that there may be residual reactants such as impurities left in the nanolubricants due to the incomplete reaction which is difficult to avoid.

(**a**)

(**b**)
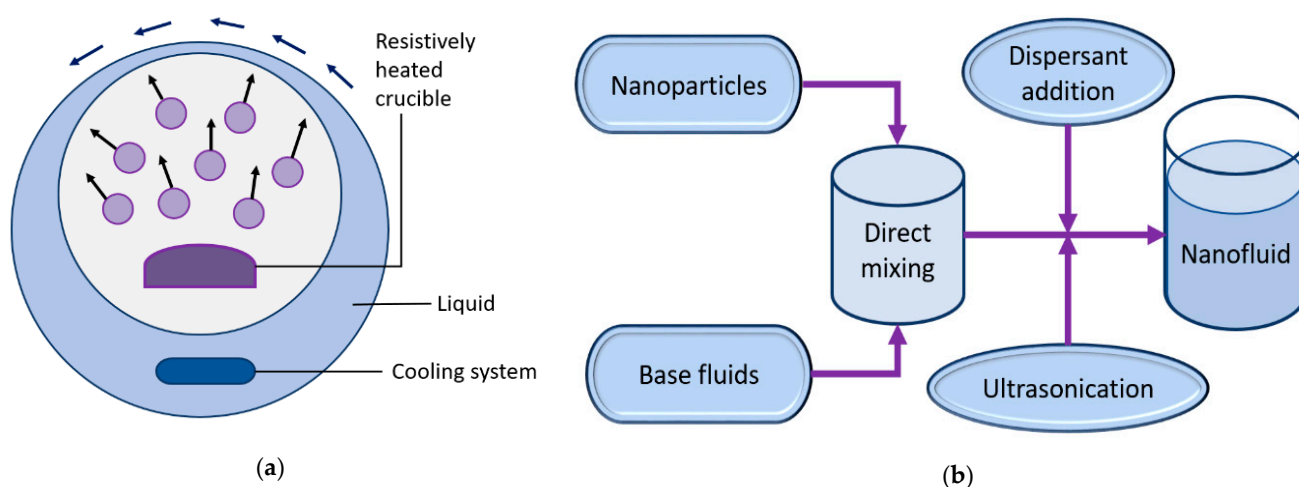
Figure 2. Schematics of preparation methods of nanolubricants: (**a**) one-step method (vapour deposition) [33], and (**b**) two-step method (direct mixing technique) [42].

In contrast, the two-step method is more widely used in the preparation and synthesis of nanolubricants with consideration of raw materials provided by manufacturing companies due to large scalability and cost effectiveness. The schematic of this method involves two procedures (see Figure 2b). The first step is to directly mix NPs with base fluid, followed by subsequent addition of dispersant or surfactant with ultrasonication. If necessary, extra treatments such as magnetic force agitation, mechanical stirring, high-shear mixing, and homogenising at certain temperatures should be combined with the second step to enhance the dispersion stability of the final nanolubricant. Two typical representatives in the two-step methods comprise microwave assisted synthesis and direct mixing technique [42].

2.2. Nanoadditives in Water

Nanomaterials have emerged as one of the most interesting materials in the areas of chemistry, physics, and materials science, and they have been widely applied in many engineering fields. Several varieties of nanoadditives can be dispersed in water, including pure metals, metal and non-metal oxides, metal sulphides, carbon-based materials, composites, and some others such as metal salts, nitrides, and carbides.

Figure 3 reveals a summary of different types of nanoadditives used in water-based lubricants in the past decade. Among all the nanoadditives the most used one is carbon-based materials, accounting for 35%, followed by metal and non-metal oxides (18%) and composites (16%), whereas the least used ones are pure metals (3%) and carbides (2%). More details about various nanoadditives used in water-based lubricants are discussed below.
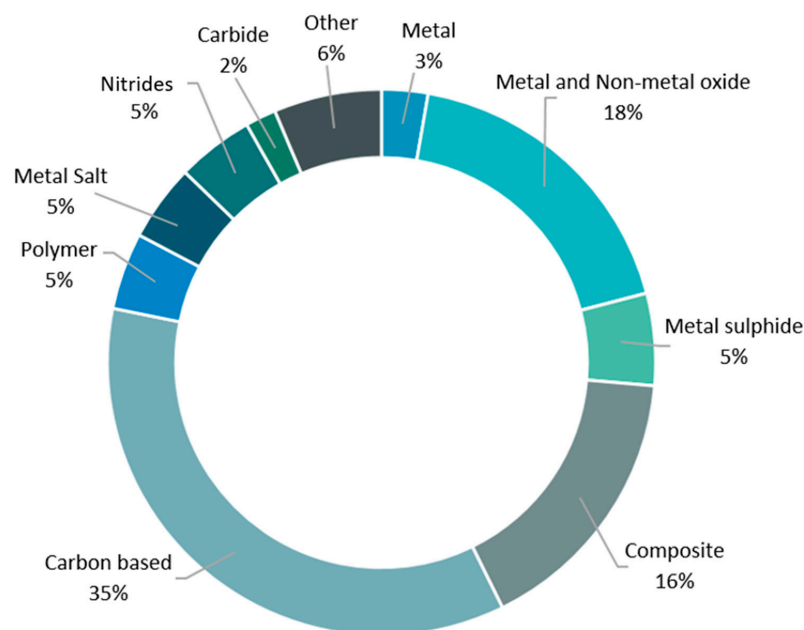
Figure 3. Statistics of nanomaterials used as nanoadditives in water in the past decade.

2.2.1. Pure Metals

Metallic NPs such as Au, Ag, and Cu have been considered to be important additives in base water due to their unique optical, electrical, and photo thermal properties in the fields of physics, chemistry, and biology [43]. These NPs, however, are only weakly compatible with base lubricant because of their high surface activity. This issue can be resolved by surface modification techniques [44]. Among all the candidates, Cu NPs have been suitably used in aqueous lubricants due to their low cost and superb tribological characteristics by acting as nano-bearings and forming metallic and/or tribo-sintered film with low shear stress on rubbed surfaces [45]. For example, Zhao et al. [46] fabricated Cu NPs through in situ surface modification, and then uniformly dispersed varying concentrations of Cu NPs (0.1–2.0 wt.%) into distilled water using prepared water-soluble bis (2-hydroxyethyl) dithiocarbamic acid (HDA) as a capping ligand. A reddish-brown uniform water-based nanolubricant with superior dispersion stability was thus synthesised. Zhang et al. [47] also prepared water-based nanolubricant containing nano-Cu surface-capped with methoxyl-polyethylene-glycol xanthate potassium. The surface-capped Cu NPs had an average diameter of 2 nm and showed no sign of apparent agglomeration in water.

2.2.2. Metal and Non-Metal Oxides

Metallic oxide NPs including Al_2O_3, TiO_2, and ZnO have been widely used as possible lubricating additives in base water. Radice et al. [48] investigated the lubrication behaviour of globular-shaped Al_2O_3 NPs (AKP50) with approximately 0.197 µm in diameter. The lubricant was prepared by diluting AKP50 with an acetate buffer solution (0.1 M $NaCH_3CO_2$ + 0.1 M CH_3CO_2H) in deionised water (DW) under 15 min ultrasound stirring prior to each tribo-test to avoid sedimentation. He et al. [16] used spherical Al_2O_3 NPs of 30, 150, and 500 nm in water to prepare water-based nanolubricants containing 0.2–8 wt.% Al_2O_3 and 10 wt.% glycerol through 400 W ultrasonic agitation for 10 min, and no evident agglomeration was observed until 3 days. It is also of vital importance to report several examples for TiO_2 NPs as water-based nanoadditives. For example, Wu et al. [13–15,25,27] prepared the lubricant by mixing 0.2–8.0 wt.% TiO_2 NPs (20 nm in diameter) into DW by mechanical stirring, stepwise adding 0.002–0.08 wt.% polyethyleneimine (PEI) and 10% glycerol under 30 min high-speed centrifuge at 2000 rpm followed by 10 min ultrasonication. The as-prepared lubricants had no significant sedimentation even after one week. In their recent studies, they prepared industrial-scale water-based nanolubricants using

coarse TiO_2 NPs of 300 nm, with the aid of 0.1–0.2 wt.% of sodium dodecyl benzene sulfonate (SDBS) and 1 wt.% Snailcool by mechanical stirring only. The as-prepared lubricants could be stably dispersed for 24 h [24]. Sun et al. [49–52] also prepared 0.1–5.0 wt.% TiO_2 water-based nanolubricants by adding 20–90 nm TiO_2 particles and different additives, including sodium hexametaphosphate (SHMP) and SDBS which exhibited good stability for 7 days. Additionally, there has been some work conducted on the preparation of water-based nanolubricants using other metal oxide nanoadditives such as CeO_2 [53], CuO [54], γ-Fe_2O_3 [55], MoO_3 [56], and WO_3 [57], and all these nanoadditives can also be well dispersed in water under mechanical agitation and ultrasonic processing.

Non-metallic oxides have also been used extensively as nanoadditives in base water. Silica (SiO_2), one of the typical representatives, is a widely used ceramic material both as a precursor to the fabrication of other ceramic products and as a material on its own. Silica has good abrasion resistance, electrical insulation, and high thermal stability [43]. Ding et al. [58] followed four steps of preparation, including synthesis, modification, purification, and dispersion, to obtain ceramic water-based lubricant with 100 nm SiO_2, which showed no apparent sedimentation for 1 h. Bao et al. [59] also prepared SiO_2 water-based lubricants using 0.1–1 wt.% surface-modified spherical SiO_2 nanoparticles (30 nm in diameter) in 15% ammonia solution under 5 min stirring at room temperature, followed by 30 min stirring at 60 °C with addition of polyethylene glycol-200. The solution was finally mixed using 20 kHz ultrasonic disperser for 5 min, and finally a stably dispersed SiO_2 water-based lubricant was obtained.

To date, many experimental studies have reported the use of metal and non-metal oxides as nanoadditives, as listed in Table 1.

2.2.3. Metal Sulphides

In recent years, lubricant additives based on metal sulphides have received considerable interest in the lubricant industry. It is generally accepted that metal sulphides such as Ag_2S, CuS, and MoS_2 present outstanding lubrication performance when used both as solid lubricants and as additives in liquid lubricants. These materials offer a low-shear resistance to an external shear stress due to their layered structure with strong-interlayer and weak-interlayer bonds [60]. It was reported that Kuznetsova et al. [61] synthesised MPS-capped Ag_2S NPs (2–10 nm) by a simple one-step process as per the following reaction: $2AgNO_3 + Na_2S = Ag_2S\downarrow + 2NaNO_3$, eventually adding MPS (3-mercaptopropyl trimethoxysilane) and ethanol in water by sonication in an ultrasonic bath for 10 min to avoid sedimentation in the solution, and the solution remained stable for up to several months at room temperature. Zhao et al. [62] used HAD-CuS nanoparticles as nanoadditives in water. The nanolubricant was prepared by pouring PEG-400 and HAD in a solution of CTAB, $Cu(NO_3)_2 \cdot 3H_2O$ and distilled water under 10 min stirring, followed by 170 °C heating under 1 h vigorous stirring. The final black homogeneous solution was centrifuged, cleaned, and dried to obtain HAD-CuS NPs that could be uniformly dispersed in water for at least 2 days within the concentration of 0.1–2.0 wt.%.

In the last few years, special attention has been focused on using MoS_2 NPs in water due to their excellent chemical and thermal stability. For example, Meng et al. [63] added multilayer-MoS_2 of 100 nm in water under 10 min magnetic stirring to prepare 0.3–0.5% MoS_2 nanolubricants, and the as-prepared nanolubricants presented good stability for 16 h. To further enhance the dispersion stability of nano-MoS_2 in water, Wang et al. [64] conducted the exfoliation and modification processes on bulk MoS_2 (15 μm in thickness) to prepare functional MoS_2 nanosheets (3.5 nm in thickness) which can be stably dispersed in water for 10 days after ultrasonication for 1 h. In contrast, the unfunctional MoS_2 nanosheets would aggregate in water within a very short time.

2.2.4. Carbon-Based Materials

When compared with metal sulphides, carbon-based nanomaterials have higher chemical stability and superior mechanical properties, which provides outstanding tribological

performance as well as environmentally friendly characteristics for a renewable future. In light of this, carbon-based nanomaterials, such as pure carbon nanomaterials and carbon derivatives, have become potential lubricating additives dispersed in base water.

According to different characteristics, pure carbon nanomaterials include carbon nanotubes (CNTs), carbon dots (CDs), graphene, and nanodiamonds (NDs). Peña-Parás et al. [65] dissolved functionalised CNTs of 30–50 nm in DW and applied a magnetic stirring in an ice bath for 60 h. The as-prepared water-based nanolubricants containing 0.1–2.0 wt.% CNTs remained stable for 4 months even without the aid of dispersing agents. Hu et al. [66] prepared CDs by dissolving thermally carbonized ammonium citrate in DW, followed by high-speed centrifugation, dialysis purification, and freeze-drying. The as-prepared CDs (3–4 nm in diameter) had hydrophilic oxygen-containing groups, thereby exhibiting superb dispersion stability in water for over 6 months. Liang et al. [67] used in situ exfoliated graphene as water-based nanoadditive which remained stable in water for over a month. The authors prepared the graphene enhanced lubricants by dissolving 1.5, 3, and 6 g pristine graphite powder and non-ionic surfactant (Triton X-100) into 1 mg/mL DI-water under 8 h bath sonication, 12 h magnetic stirring, 24 h sedimentation, and 1 h centrifugation. Jiao et al. [68] synthesised a bioinspired copolymer consisting of dopamine and 2-methacryloyloxyethyl phosphorylcholine for surface modification of NDs. Although the modified NDs exhibited remarkable lubricity when added to water-based lubricants, the dispersion stability of NDs in water was not investigated.

Among a variety of carbon-based nanoadditives, graphene and its derivatives stand out owing to their unprecedented structural, chemical, and physical properties. However, it is difficult to prepare stable water-based nanolubricants with graphene due to the formation of irreversible agglomerate caused by its strong π–π stacking and van der Waals interaction [69]. In contrast, graphene oxide (GO) has excellent hydrophilicity because it contains a large number of oxygen-containing functional groups, which enables it to become an ideal nanoadditive in water. Song and Li [70] prepared graphene oxide nanosheets with a diameter of 20–30 nm and a length of 10–30 μm from purified natural graphite by modified Hummers and Offeman's method [71]. The as-prepared GO nanosheets (0.5 mg/mL) were dispersed in water by bath ultrasonication, which resulted in no sedimentation for 5 weeks. After obtaining GO from Hummers' method, min et al. [72] prepared fluorinated GO (FGO) through 12 h hydrothermal treatment at 160 °C with the presence of 0.5 mL nitric acid and 9.5 mL hydrofluoric acid. The produced FGO was dispersed in water with 0.1–1% concentration by ultrasonication, and the as-prepared lubricants exhibited excellent stability for 12 days. Fan et al. [73] prepared 0.5 mg/mL FGO aqueous solution by dispersing 5 mg FGO in 10 mL distilled water under 30 min ultrasonication (300 W), which led to good stability for a week.

Other graphene derivatives, such as reduced GO (RGO) and pH-dependent GO, have been emerging to further enhance the dispersion stability of GO in water, according to the fact that the strong oxygen functionality and flatness together with possible defects of GO may prompt its agglomeration in water. Liu et al. [74] dispersed GO (100 mg) in DW (80 mL) under ultrasonication for 60 min, followed by addition of PEI (5 g) that preliminarily suffered a magnetic stirring with water (100 mL) for 30 min. The mixture was then stirred for 12 h at 80 °C until GO was transformed to RGO, during which the transformation was recognised by the colour change of mixture (from yellowish brown to black). The as-synthesised PEI-RGO was finally dispersed into DW to obtain water-based nanolubricants with concentrations of 0.03–0.1 wt.%, which showed no deposition for over 60 days. Hu et al. [75] proposed a facile process to modify RGO using β-Lactoglobulin (BLG). They dissolved GO (50 mg) with DW (50 mL) via mechanical stirring for 30 min to attain GO aqueous solution which was then mixed with BLG (12.5 mg) and hydrazine hydrate (2 mL). The as-synthesised BLG-RGO was diluted in water to obtain water-based nanolubricants with concentrations of 0.05–1.0 mg/mL, which showed outstanding stability without apparent precipitation for 8 months—the longest stability period as reported in GO-based aqueous lubricants.

In the case of pH-dependent GO as water-based nanoadditives, two studies were reported by He et al. [17] and Meng et al. [76], which proposed two different preparation processes. A mechanical de-agglomeration method was used by He et al. [17] to prepare GO suspension with 0.06 wt.% GO and 0.1 M NaOH in DW under high intensity ultrasonic agitation (400 W) for 10 min, resulting in good dispersion stability for a week. The pH value was adjusted by NaOH and varied from 3.1 to 9.7, which had insignificant influence on agglomeration of GO sheets. In contrast, Meng et al. [76] mixed triethanolamine (TEA) with 0.1 wt.% GO in DIW to adjust the pH value from acidic (pH 2.8) to alkaline (pH 9). They found that the lubricant with pH 9 was the most homogeneous with no precipitation for 50 days.

It has been documented that some researchers have investigated the carbon-based nanocomposites in the formulation of water-based lubricants, including GO/graphene [77], GO/nanodiamond [78,79], GO/carbon [80], and GO/g-C_3N_4 [18]. The detailed information regarding their preparation parameters as well as stability duration is listed in Table 1.

2.2.5. Composites

Nanocomposite which comprises two or more different nano-sized particles is becoming a significant part of nanotechnology and one of the fastest growing research areas in materials science and engineering [81]. The use of nanocomposite is to simultaneously combine physical and chemical properties of the constituent nanomaterials in an attempt to produce a homogeneous phase for better performance than single-component NPs [82]. The composite water-based nanolubricant, therefore, can be prepared by dispersing two or more nanoadditives in the base water.

Over the past few years, much research has been conducted on graphene-based composites including GO/SiO_2 [19,83], GO/TiO_2 [84], and GO/Al_2O_3 [21]. For example, Huang et al. [19] synthesised GO/SiO_2 water-based lubricants by mechanical stirring the aqueous suspension at 25 °C for 30 min, followed by ultrasonic processing (450 W) for 60 min (on/off interval of 5 s) in a chilled water bath. Similar preparation method was used to synthesis the water-based lubricants containing GO/Al_2O_3. Both results indicated that the formation of hybrid nanostructure enabled smaller particle size distribution in water, compared to that of constituent nanoadditives. Some other nanocomposites such as Cu/SiO_2, ZnO/Al_2O_3, Fe_3O_4/MoS_2, TiO_2/Ag, and Ag/C have also been used as nanoadditives in water. For example, Li et al. [85] used a two-step method to prepare 0.05–0.3 wt.% TiO_2/Ag in cooling water by 2 h magnetic stirring, followed by 12 h ultrasonication with 40 kHz frequency and 110 W power, which showed no sedimentation within a month. In contrast, Fe_3O_4/MoS_2 nanocomposite with 0.3–1.2 wt.% concentration was prepared by Zheng et al. [86] by dissolving 5.4 g $FeCl_3 \cdot 6H_2O$, 1.27g $FeCl_2$, 0.48 g MoS_2 nanosheets in 50 mL DW, followed by drop-wise addition of 6 mL $NH_3 \cdot H_2O$ in the solution under ultrasonic state. The precipitates were then centrifuged, washed, and dried for 24 h at 50 °C. The as-prepared nanocomposite Fe_3O_4/MoS_2 showed better dispersibility in water than only Fe_3O_4 NPs or MoS_2 nanosheets. Additional studies on the preparation of different nanocomposites are listed in Table 1.

2.2.6. Nitrides

Among all the nitrides, hexagonal boron nitride (h-BN), as a promising and an ideal alternative to other nanoadditives dispersed in water, has attracted extensive attention due to its exceptional performance, such as high-temperature stability, high thermal conductivity, high electrical resistivity, low coefficient of friction, strong inertness in a wide variety of chemical environments, and environmental friendliness [87]. Cho et al. [88] revealed superb stability of h-BN nanosheets in water without any precipitation within 1 month. The authors synthesised 30 nm thick and 300 nm wide h-BN nanosheets with 0.01, 0.05 and 1 wt.% concentration under 20 h bath sonication excluding any additional surfactants. Moreover, Bai et al. [89] recommended the use of thin hydroxylated BN nanosheets (HO-

BNNS) with 0.0125–0.20 wt.% concentration dispersed in water-glycol (55 wt.% DW and 45 wt.% glycol) under 30 min ultrasonication, which showed good dispersion for 5 days.

2.2.7. Carbides

Recently some research works have been conducted on carbides such as Nb_2C and Ti_3C_2. Cheng and Zhao [90] prepared Nb_2C nanofluid using three different degrees of oxidised Nb_2C nanosheets with the mass ratio of 0.25–1.0 mg/mL of pure water. The Nb_2C nanosheets were obtained by mixing 1 mg/mL accordion shaped Nb_2C powder into 100 mL aqueous solution, followed by 10 mL/50 wt.% TBAOH as intercalation agent, and 20 mg ascorbic acid as anti-oxidant under 12 h magnetic stirring in an ice bath. The pH level of the mixture was balanced by adding hydrochloric acid and 10 min centrifugation at 3000 rpm. The final Nb_2C solution was acquired by freeze-drying method and divided into three parts: Nb_2C of 20 nm (black coloured), after 6 h magnetic stirring at 60 °C water bath; moderately oxidised Nb_2C (MO-Nb_2C) of 12 nm (yellow-coloured), after 7 days magnetic stirring at room temperature; and completely oxidised Nb_2C (CO-Nb_2C) of 6 nm (transparent). The authors also mixed benzalkonium chloride (surfactant) to enhance stability and, among the three groups, MO-Nb_2C showed the best stability even after 1 month. Nguyen and Chung [91] prepared five solutions with 1 wt.%, 2 wt.%, 3 wt.%, 5 wt.%, and 7 wt.% Ti_3C_2 concentrations by adding 0.01, 0.02, 0.03, 0.05, and 0.07 g of Ti_3C_2 to 1 mL of DW respectively. Each solution was mixed under 1 h magnetic stirring at room temperature to ensure uniform dispersion of the NPs in water.

2.2.8. Others

The literature demonstrates that very little research has been conducted on some rare NPs, such as black phosphorus and hydroxides. Tang et al. [92] synthesised 3.9 nm black phosphorus quantum dots (BPQDs) by adding N-methyl-2-pyrrolidone (NMP) under ultrasonic treatment for 8 h. The as-prepared BPQDs with 0.1 wt.% concentration were dispersed into 2.0 wt.% Triethanolamine (TEA) aqueous solution by another 10 min ultrasonic treatment. The BPQDs dispersion showed good stability with no precipitates even after 2 weeks. Metal hydroxides have been demonstrated to perform well as lubricant additives, and layered double hydroxides (LDHs) stand out as particularly impressive examples of this. Wang et al. [93] presented the preparation of 19.42 nm wide and 8.59 nm thick oleylamine-modified Ni-Al LDH (NiAl-LDH/OAm) nanoplatelets as water-based lubricant additives with a concentration of 0.1–1.0 wt.%. The lubricants were synthesised by a microemulsion method under both stirring and ultrasonication in DW followed by 10 h drying at 80 °C. A transparent and stable solution was obtained without additional dispersion or surfactants. The authors also prepared aqueous polyalkylene glycol (PAG) solution by dispersing two different LDHs with 0.5 wt.% concentration under only ul-trasonication, including ultrathin LDH nanosheets (ULDH-NS, 60 nm wide and 1 nm thick), and LDH NPs (19.73 nm wide and 8.68 nm thick) [94]. The ULDH-NS (0.5 wt.%) were uniformly dispersed in water, showing no agglomeration. While 0.5 wt.% LDH-NPs were dispersed in water, a transparent solution was obtained with no precipitates due to the addition of a surfactant 1-butanol and oleylamine under the reverse microemulsion reaction process.

In addition to this, some exceptional NPs such as chitosan [95] and stearic acid [96] were also explored recently. Li et al. [95] used 0.5 wt.% nanoscale liquid metal droplets wrapped by the chitosan (NLMWC) as water-based nanoadditives and compared with 0.5 wt.% gallium based liquid metal $Ga_{76}In_{24}$. The NLMWC was dispersed in water under 15 min ultrasonication in water bath, and the as-prepared aqueous solution remained stable for 1 month without any precipitation and agglomeration. In contrast, the precipitates were observed for $Ga_{76}In_{24}$ in water within 2 h.

The details of different types of nanoadditives used in water-based lubricants are listed in Table 1.

Table 1. List of different types of nanoadditives in water for preparation of various water-based nanolubricants.

Types	Nanoadditives	Size	Shape	Concentration	Stirring	Stability Duration	References
Metals	Cu	3 nm	Spherical	0.1–2.0 wt.%	Magnetic stirring for 10, 20 min	-	Zhao et al. [46]
		2 nm	-	0.5–5 wt.%		-	Zhang et al. [47]
	Ag	10–100 nm	-	1 g/L	-	5 to 19 days	Odzak et al. [97]
	Au	26.7 nm	-	0.018 vol%	Irradiation for 1–18 h	1 month	Kim et al. [98]
Metal and non-metal oxides	Al_2O_3	0.197 μm	Spherical	-	Ultrasonication for 10 min	Few minutes	Radice et al. [48]
		30, 150, and 500 nm	Spherical	0.2–8 wt.%	Ultrasonication for 10 min	3 days	He et al. [16]
	CeO_2	10–40 nm	-	0.05 wt.%	Ultrasonication for 2 min	4 days	Zhao et al. [53]
	CuO	60 nm wide and 230 nm long	Nanorod or spindle	0.1–2.0 wt.%	Magnetic stirring for 60 min	8 h	Zhao et al. [54]
	γ-Fe_2O_3	5 nm	-	0.1–1 wt.%	-	1 h	Pardue et al. [55]
	Fe_3O_4	-	Chain like	1 wt.%	Ultrasonication for 1 h	40 days	Lv et al. [99]
	MoO_3	80–100 nm	2D	0.1, 0.2, 0.3, 0.4, 0.5 wt.%	-	-	Sun et al. [56]
	SiO_2	100 nm	-	0.5 wt.%	-	1 h	Ding et al. [58]
		30 nm	Spherical	0.1–1 wt.%	Magnetic stirring for 10 min	-	Bao et al. [59,100]
		20 nm	Spherical	0.5 wt.%	-	30 days	Lv et al. [101]
	TiO_2	30 nm	-	0.1–2.0 wt.%	Stirring for 0.5 h	-	Gao et al. [102]
		20 nm	Spherical	0.1, 0.2, 0.4, 0.8, 1.6 wt.%	Mechanical stirring and ultrasonic	-	Gu et al. [103]
		0.2–0.4 μm	-	0.25, 0.5, 1.0 wt.$_{NaPa/TiO2}$ %	Stirring and ultrasonication	-	Ohenoja et al. [104]
		40 nm	Non-spherical	1.5 vol.%	Ultrasonication for 2 h	-	Najiha et al. [105]
		15 nm	Spherical	0.1, 0.5, 1.0, 1.5, 2.0 vol.%	Ultrasonic vibration	Several days	Kayhani et al. [106]

Table 1. *Cont.*

Types	Nanoadditives	Size	Shape	Concentration	Stirring	Stability Duration	References
Metal and non-metal oxides	TiO$_2$	20 nm	Spherical	0.2–8.0 wt.%	Mechanical and ultrasonication for 10 min	7 days	Wu et al. [13–15,27,29]
		20 nm	Spherical	0.5–4.0 wt.%	Ultrasonic stirring	-	Huo et al. [26]
		300 nm	Spherical	2.0–4.0 wt.%	Mechanical stirring	48 h	Wu et al. [24]
		50 nm	Spherical	0, 0.25, 0.5, 0.75, 1.0 wt.%	Ultrasonication for 30 min	-	Kong et al. [49]
		~20 nm	-	0.03, 0.05, 0.07 wt.%	Magnetic stirring	-	Ukamanal et al. [107]
		90 nm	-	0.5–1.5 wt.%	Magnetic stirring	7 days	Meng et al. [52]
		20 to 50 nm	-	0.1, 0.4, 0.7, 1.0, 2.0, 3.0, 4.0, 5.0 wt.%	-	-	Sun et al. [50]
		40 nm	-	0.1, 0.5, 1, 2, 4 wt.%	Ultrasonication	30 min	Wang et al. [108]
		20–25 nm	-	-	Magnetic heat for 1 h	7 days	Zhu et al. [51]
	SiO$_2$, TiO$_2$, ZnO	100 nm	Spherical	ASNPs 3 wt.%, AZNPs 1 wt.%, ATNPs 1 wt.%	Magnetic stirring for 6 h	-	Cui et al. [109]
	ZnO, CuO	ZnO (4.5 & 27 nm); CuO (7.5, 45 nm)	-	1 g/L	Ultrasonication for 30 min	19 days	Odzak et al. [97]
	WO$_3$	50 nm	Spherical	0–1 wt.%	Magnetic stirring for 2 h	5 days	Xiong et al. [57]
Metal sulphides	Ag$_2$S	2–10 nm	-	-	Sonication for 10 min	1 h	Kuznetsova [61]
	CuS	4 nm	Uniform spherical	0.1 to 2.0 wt.%	Magnetic stirring for 10 min, 1 h	2 days	Zhao et al. [62]
	MoS$_2$	-	-	0.1 g	-	10 days	Wu et al. [110]
		100–300 nm	layered	-	Stirring for 10, 20 min	-	Zhang et al. [111]
		height 3.5 nm	Chain like layered	0.05 and 0.1 wt.%	Ultrasonication for 1, 2, 3 h	10 days	Wang et al. [64]
		100 nm	-	0.3–0.5 wt.%	Magnetic stirring for 10 min	16 h	Meng et al. [63]

Table 1. *Cont.*

Types	Nanoadditives	Size	Shape	Concentration	Stirring	Stability Duration	References
Composites	graphene-SiO$_2$	Graphene (5 nm thick, interlayer distance 0.34 nm); SiO$_2$ (30 nm)	SiO$_2$ spherical, graphene multi-layered sheet	Graphene:SiO$_2$ (0.4:0.1, 0.3:0.2, 0.2:0.3, and 0.1:0.4)	Stirring for 1hr, ultrasonic bathing for 2 h	-	Xie et al. [112]
	GO-SiO$_2$	GO (1−2 nm thick); SiO$_2$ (30−40 nm)	GO sheet wrinkled folded	0.03–0.5 wt.%	Magnetic stirring for 24 h	60 days	Guo et al. [83]
	GO-SiO$_2$	GO (4–6 nm); SiO$_2$ (25–30 nm)	GO lamellar wrinkled, SiO$_2$ spherical	0.04, 0.08, 0.12, 0.16 and 0.20 wt.%.	Mechanical stirring for 30 min, ultrasonication	-	Huang et al. [19]
	CNT-SiO$_2$	CNT (inner diameter 8 nm, outer diameter 15 nm); SiO$_2$ (30 nm)	SiO$_2$ spherical, CNT tubular	0.5 wt.%	Magnetic stirring for 1 h, ultrasonic bathing for 2 h	-	Xie et al. [113]
	GO-TiO$_2$	TiO$_2$ (25 nm)	TiO$_2$ spherical	0.5 wt.% (0.3 wt.% GO-0.2 wt.% TiO$_2$)	Stirring for 20 min, sonicating for 40 min	30 days	Du et al. [84]
	GO-Al$_2$O$_3$	GO (4~6 nm thick, 10~50 μm lateral sizes), Al$_2$O$_3$ (15, 30 & 135 nm)	Layered	0.25, 0.5, 1.0 and 2.0 wt.%	Magnetic stirring for 30 min, ultrasonic probe for 30 min	1 h	Huang et al. [20]
	GO-Al$_2$O$_3$	GO (10–50 μm in diameter; 1–2 nm thick); Al$_2$O$_3$ (30 nm)	GO layered; Al$_2$O$_3$ near-spherical	0.04, 0.08, 0.12, 0.16, and 0.20 wt.%	Mechanical stirring for 10 min, ultrasonic agitation process	-	Huang et al. [21]
	GO-TiO$_2$/ZrO$_2$	TiO$_2$/ZrO$_2$ (25 nm); GO (3–5 nm thick, 1.5–5.5 μm lateral)	2D GO; zero dimension TiO$_2$/ZrO$_2$	0.5 wt.%	Magnetic stirring and ultrasonication for—30 min, 1 h	-	Huang et al. [12]
	GO-TiO$_2$-Ag	-	-	0.05 wt.%	Sonication for 4 h	-	Zayan et al. [114]
	PTEE-SiO$_2$	413.6 nm (SiO$_2$ layer 20–30 nm)	PTFE rod-like or spherical	0.2, 1 and 3 wt.% (PTFE:SiO$_2$_0.57:0.43)	Ultrasonication for 20 min	12 h	Wang et al. [115]
	Cu-SiO$_2$	20 nm average (Silica layer thick 2 nm)	network-like silica, Cu spherical	0, 0.5, 1.0, 1.5, 2.0 wt.%	Magnetic stirring	-	Zhang et al. [116]
		-	Sphere	0.4 wt.%	Magnetic stirring for 15 min	30 days	Liu et al. [117]

Table 1. *Cont.*

Types	Nanoadditives	Size	Shape	Concentration	Stirring	Stability Duration	References
Composites	MoS$_2$-Al$_2$O$_3$	MoS$_2$-Al$_2$O$_3$ (144.8 nm), MoS$_2$ (178.6 nm), Al$_2$O$_3$ (35.4 nm)	Laminar	2.0 wt.%	Electro-magnetic stirring	168 h	He et al. [118]
	Al$_2$O$_3$, MoS$_2$, hBN, and WS$_2$	Al$_2$O$_3$ (<100 nm), hBN (70−80 nm), MoS$_2$ (80−100 nm), WS$_2$ (80−100 nm)	Al$_2$O$_3$ (spherical); hBN, MoS$_2$, and WS$_2$ (layered structure)	1% each	Ultrasonic bath for 1 h	24 h	Kumar et al. [119]
	Fe$_3$O$_4$-MoS$_2$	MoS$_2$ (100–400 nm), Fe$_3$O$_4$ (10 nm), Fe$_3$O$_4$ on MoS$_2$ (30–60 nm)	Laminated structure	0.3, 0.6, 0.9, 1.2 wt.%	Ultrasonication	-	Zheng et al. [86]
	MWCNT-Fe$_2$O$_3$	Fe$_2$O$_3$ (20–30 nm); MWCNT (10–30 μm length, 10–20 nm outer diameter, 3–5 nm inner diameter)	Multi-walled carbon nanotube	0.1–1.5 vol.% (Fe$_2$O$_3$ 80%, MWCNT 20%)	Sonication for 120 min	1 month	Giwa et al. [120]
	Ag-C	350–400 nm (C shell 100–120 nm thick) Ag 130–180 nm	Core spherical, NPs elliptical (core like short rod)	Ag 28 wt.% in Ag-C	Magnetic stirring for 30 min, ultrasonication for 60 min	5 days	Song et al. [121]
	TiO$_2$-Ag	TiO$_2$ (40 nm)	Ellipsoidal	0.05, 0.1, 0.1, 0.25, 0.3 wt.%	Magnetic stirring for 2 h	1 month	Li et al. [85]
	ZnO-Al$_2$O$_3$	ZnO (70 nm), Al$_2$O$_3$ (45 nm)	ZnO elongated, Al$_2$O$_3$ spherical	0.1–23 wt.%	Ultrasonic bath for 30 min	-	Gara et al. [122]
	WO$_3$-Mn$_3$B$_7$O$_{13}$Cl	22.4 nm	Spherical	0.0, 0.1, 0.3, 0.5, 0.7 and 0.9 wt.%	Ultrasonic vibration for 1 h	48 h	Liang et al. [123]
Carbon-based materials	Carbon	outer diameter ~177 nm	Toroidal	2.0, 1.5, 1.2, 1.0, 0.5, and 0.1 wt.%	Magnetic stirring for 60 h	4 months	Peña-Parás et al. [65]
		130, 170, 200 and 250 nm	Spherical	0.05, 0.1, 0.15, 0.2, 0.3 wt.%	Ultrasonication	5–10 h	Wang et al. [124]

Table 1. *Cont.*

Types	Nanoadditives	Size	Shape	Concentration	Stirring	Stability Duration	References
Carbon-based materials	Carbon nanotube	10–20 nm diameter; 1–2 μm axial dimension	Short and tube	0.1 wt.%	Sonication for 2 h	30 min	Peng et al. [125]
		90 nm diameter	Long rod like	0.1, 0.3, 0.5, 0.7, and 1.0 wt.%	Stirring for 0.5, 1, 3 h	-	Sun et al. [126]
		20–30 nm in outer diameter; 10–30 μm in length	Pentagonal and heptagonal	0.05, 0.10, 0.15, 0.20, and 0.25 wt.%	Proper stirring	12 days	min et al. [127]
		SWCNTs (2 nm diameter), MWCNTs (25 ± 10 nm diameter)	Sphere	50–100 μL	-	Few hours	Kristiansen et al. [128]
		8–50 nm in diameter, 0.5–30 μm in length	-	-	Magnetic stirring and ultrasonication for 2 h	168 h	Ye et al. [129]
	Carbon dots	CDs-IL 4.4 nm	Spherical	3, 12.2, 34.9, 19.4 wt.%	Magnetic stirring for 6 h	60 min	Tang et al. [130]
		Sulphur doped CQDs 4.8 nm	Spherical	0.25, 1.25, 2.5, 5, and 10 wt.%	Ultrasonication for 30 min	7 days	Xiao et al. [131]
		CDs-GO 3–4 nm	-	0.06, 0.08, 0.1, 0.2, 0.3 mg/mL	-	6 months	Hu et al. [66]
	Graphene	1 nm	-	23.8, 69.9, and 110 mg/mL	Magnetic stirring for 12 h	1 month	Liang et al. [67]
		100 nm	2D nanosheet	0.2 mg/mL	Stirring for 4 h	-	Fan et al. [132]
		Size several micrometres, interlayer spacing 0.63 nm	Crystal	0.5, 1.0, 1.5, 2.0, and 2.5 mg/mL	Ultrasonication for 30 min	-	Ma et al. [133]
		0.67–0.87 nm	Multiple layered	0, 0.5, 1, 2, and 4 mg/mL	Stirring for 4 h, ultrasonication 8 h	-	Ye et al. [134]

Table 1. *Cont.*

Types	Nanoadditives	Size	Shape	Concentration	Stirring	Stability Duration	References
Carbon-based materials	Graphene	2 nm	-	0.5, 1.5, 2.5, 4, 5, and 8 mg/mL	-	-	Qiang et al. [135]
		-	Flat flake	0.1, 1 wt.%	-	30 days	Piatkowska et al. [136]
	Diamond	3–10 nm	spherical	0.1, 0.5, 1, 2, 4, and 6 wt.%	Probe sonication, stirring	-	Mirzaamiri et al. [137]
		5–10 nm	-	0.01−0.07 wt.%	Simple stirring	-	Jiao et al. [68]
	Graphene oxide	1.20 & 1.45 nm	Sheet	0, 0.3, 0.5, and 1 mg/mL	Ultrasonication for 30 min	1 week	Fan et al. [73]
		10–50 μm thick, 0.335 nm high	Single monolayer	0.01 wt.%	Ultrasonication for 5 min	-	Kinoshita et al. [138]
		4 nm	-	0–2 wt.%	Ultrasonication	-	Elomaa et al. [139]
		200–1000 nm	Transparent nanosheet	0.1, 0.3, 0.5, 0.7, 1 wt.%	Ultrasonication	12 days	min et al. [72]
		0.5–5 μm diameter; 0.8–1.2 nm thick	-	0.01, 0.05, 0.1, and 0.5 wt.%	Sonication for 2 h	-	Singh et al. [140]
		500 nm–5 μm diameter; 0.8–1.2 nm thick	Ultra-thin	0.025, 0.05, 0.075, and 0.1 vol.%	Ultrasound, stirring	3 months	Bai et al. [141]
		20–30 nm outer diameters; 10–30 μm length	2D sheet	0.5 mg/mL	Stirring for 30 min	5 weeks	Song et al. [70]
		0.335 nm thick	Ultrathin and transparent	0.8, 1.2, and 1.6 mg/mL	Stirring for 24 h, ultrasonication	2 weeks	Gan et al. [142]
		10–50 μm lateral size; 1–2 nm thick	Spherical	0.06 wt.%, 0.5 wt.%	Stirring for 30 min, ultrasonic bath for 10 min	7 days	He et al. [17]
		2–5 nm thick 10–20 μm lateral size	-	0.1 wt.%	Stirring for 30 min ultrasonic bath for 20 min	50 days	Meng et al. [76]

Table 1. *Cont.*

Types	Nanoadditives	Size	Shape	Concentration	Stirring	Stability Duration	References
Carbon-based materials [18]	Graphene oxide	1 nm thick	initially sheet shape, then parabolic shape	0.2 mg/mL	Sonication	-	Kim et al. [143]
		1.3 nm	Thin film	0.05 to 1.0 mg/mL	Mechanical stirring for 30 min	8 months	Hu et al. [75]
		0.8 μm lateral size 1.96 nm thick	Bathtub	0, 0.03, 0.05, 0.07, and 0.1 wt.%	Magnetic stirring for 12 h, ultrasonication for 1 h	90 days	Liu et al. [74]
	GO & carbon	C (30–60 nm) and GO (30–60 nm)	C onion-like spherical; GO 2D nanosheet	C 0.06 wt.%; GO 0.02–0.06 wt.%	-	-	Su et al. [80]
		oxidised wood-derived nano carbons 640–1300 nm and GO 50–200 nm	aggregated chain-like	0.001 and 1 wt.%	Ultrasonication for 30 min	1 month	Kinoshita et al. [144]
	GO & chitosan	GO 0.05–0.2 μm	GO optical 3D; copolymer brush-like	2 mg/mL	Stirring for 6, 12 h ultrasonication	30 days	Wei et al. [145]
	GO & 3-APS	3-APS (525.39 nm)	-	2 mg/mL	Stirring for a certain period	-	Li et al. [146]
	GO & graphene	GO 4.2 nm, graphene 5 nm	Multi-layered	0.2, 0.5, 0.7 and 1.0 wt.%	Stirring for 1 h, ultrasonic bath 2 h	-	Xie et al. [77]
	GO & diamond	GO 2.5 nm and nanodiamond 2–10 nm	GO laminar	0, 0.2, 0.4, 0.6, 0.8, 1.0 wt.%	Magnetic stirring for 9 h	-	Wu et al. [78]
		GO 30 nm, 2–3 nm thick; modified diamond 30 nm	GO lamellar and MD 3D structure	GO colloid (0.7 wt.%) and MD colloid (0.5 wt.%)	Ultrasonic ethanol bath for 5 min	2 months	Liu et al. [79]
	GO & graphitic CN	graphitic carbon nitride and GO 10–50 μm lateral size, 1–2 nm thick	unique one-layer	0.06 wt.% each	Stirring for 30 min, ultrasonic bath for 10 min	-	He et al. [18]
	PEGlated graphene	20 nm	laminar	0.005, 0.01, 0.03, 0.05, and 0.1 wt.%	Mechanical stirring for 3, 4 h	7 days	Hu et al. [147]

Table 1. *Cont.*

Types	Nanoadditives	Size	Shape	Concentration	Stirring	Stability Duration	References
Polymers	Cellulose	Length 200 ± 25 nm, Size 1–50 μm	Chain like, crystalline	1, 1.5, 2, 2.5, 3, and 4 wt.%	-	-	Shariatzadeh et al. [148,149]
	Fullerene–styrene and –acrylamide	3–40 nm	Ideal spherical	0.5 wt.%	-	-	Lei et al. [150]
		average 46 nm	Ideal spherical	0, 0.2, 0.4, 0.6 & 0.8 wt.%			Jiang et al. [151]
	Hydrogel	-	Fibrous-3D network	3, 4 & 5 wt.%	Stirring for 3–4 h, mechanical sheared	-	Wang et al. [152]
	Naphthalene	-	-	0.02, 0.04, 0.06, 0.08, 0.1, 0.15, 0.2 mol/L	Stirring for 24 h	-	Yang et al. [153]
Metal salts	LaF$_3$	LaDTP-10 (19.6 nm) and LaDTP-20 (8.5 nm)	LaDTP-10 polycrystalline; LaDTP-20 sphere	1 wt.%	Continuous magnetic stirring for 1 h	-	Zhang et al. [154]
	Proton type-ionic liquids	-	Chain like	0, 0.25, 0.5, 0.75 & 1 wt.%	Stirring for 2 h		Zheng et al. [155]
		-	Bilayered	1 wt.%	Stirring for 12 h	-	Dong et al. [156]
		-	brushy-like soft layer	0.1 & 1 wt.%	Magnetic stirring for 2 h, ultrasonication for 10 min	60 min	Khanmohammadi et al. [157]
		-	-	1 wt.%	Magnetic stirring for 10 min	-	Kreivaitis et al. [158]
Nitrides	Hydroxylated boron nitride (HO-BNNS)	0.6–0.8 nm	Thin flat	HO-BNNS/water-glycol (0.0125, 0.025, 0.05, 0.10, 0.20 wt.%)	Ultrasonic process for 30 min	5 days	Bai et al. [89]
	Hexagonal boron nitride	76.14 nm	-	0.2 to 1.0 wt.%	Ultrasonication	7 days	He et al. [159]
		-	-	0.1–5.0 vol.%	-	-	Abdollah [160]
		300 nm wide and 30 nm thick	-	1, 0.05 or 0.01 wt.%	Sonicator bath for 20 h	30 days	Cho et al. [88]
	Silicon nitride	Silica 20, 50, 100, 200 nm	-	-	-	-	Lin et al. [161]

Table 1. *Cont.*

| Types	Nanoadditives	Size	Shape	Concentration	Stirring	Stability Duration	References
Carbides	Nb$_2$C	20 nm (Nb$_2$C), 12 nm (MO-Nb$_2$C), 6 nm (CO-Nb$_2$C)	Accordion like, Crystalline	1.0, 0.75, 0.5, and 0.25 mg/mL	Magnetic stirring for 6, 12 h, 7 days; ultrasonic stirring	CO-Nb$_2$C 15 days; MO-Nb$_2$C 30 days	Cheng et al. [90]
	Ti$_3$C$_2$	Lateral size 0.2–3 μm Layer thick 20 nm	Layered, Planar	1, 2, 3, 5 and 7 wt.%	Magnetic stirring for 1 h	-	Nguyen et al. [91]
Others	Black phosphorus	3.9 nm	Crystalline	0.001–0.02 wt.%	Ultrasonication for 8 h	2 weeks	Tang et al. [92]
		500 nm	Honey-comb	91.17% (wt.%)	Ultrasonication for 10 h	-	Wang et al. [162]
		100 nm wide; 7 nm thick	Multilayered	35, 70, and 200 mg/L	Stirring for 10 min, ultrasonication	-	Wang et al. [163]
	LDH	19.73 nm wide; 8.68 nm thick	-	0.5 wt.%	Ultrasonication	-	Wang et al. [94]
		19.42 nm wide; 8.59 nm thick	Layered	0.1–1.0 wt.%	Stirring for and ultrasonication	-	Wang et al. [93]
	Chitosan	70–145 nm	Crystalline	0–0.5 wt.%	Ultrasonication for 15 min	30 days	Li et al. [95]
	Stearic acid	-	2D layered	0.25, 0.5, 0.75 & 1.0 mg/mL	Ultrasonication	-	Ye et al. [96]

3. Dispersion Stability of Nanoadditives

3.1. Evaluation Methods

Research on dispersion stability of nanoadditives in water is of vital importance for the development of water-based nanolubricants, and it has become one of the key challenges in restricting their widespread practical application. Stable nanosuspension is usually considered as a prerequisite for the successful preparation of water-based nanolubricants. In general, there are some methods that can be used to effectively evaluate the dispersion stability, including microscopy, zeta potential, UV-vis spectral analysis, dynamic light scattering, and sedimentation.

3.1.1. Microscopy

Microscopic methods using optical microscope (OM), transmission electron microscope (TEM), and scanning electron microscope (SEM) are very useful to distinguish the size and shape of NPs, and the dispersion stability of NPs in water can be evaluated as per the distribution and agglomeration of NPs under microscopic observation. Among all the microscopic methods, the use of OM is the easiest and quickest technique to examine the agglomeration behaviour and trend of the nanolubricants even at micrometre scale. However, the limited resolution of OM is the main disadvantage of viewing the size and shape of NPs at nanometre scale.

Currently, electron microscopy is the most commonly used method to evaluate the NPs stability in a base lubricant due to its high resolution. TEM and SEM are two of the most popular methods for observing the morphology and size distribution of NPs. TEM samples are prepared by placing a nanolubricant drop on a carbon-coated copper grid until complete evaporation of the base lubricant. SEM samples are prepared by dropping a small amount of nanolubricant onto a tape that is attached to the top of a sample holder before heating and drying under vacuum [164,165]. During the sample preparation processes for both TEM and SEM, NPs may somewhat agglomerate, leading to inaccurate evaluation of NPs stability in base lubricant. In spite of this, it is still acceptable to evaluate the dispersion stability of NPs between different concentrations or formulations by comparing the NP size difference. Figure 4 shows TEM images of TiO_2 NPs with 2.0 wt.% and 4.0 wt.% concentrations in water. It can be found that the NPs were uniform and well dispersed in water, and no visible agglomeration was observed even at 4.0 wt.% concentration. With the increase of concentration, however, there is a trend of few NPs agglomeration.

(a)	(b)
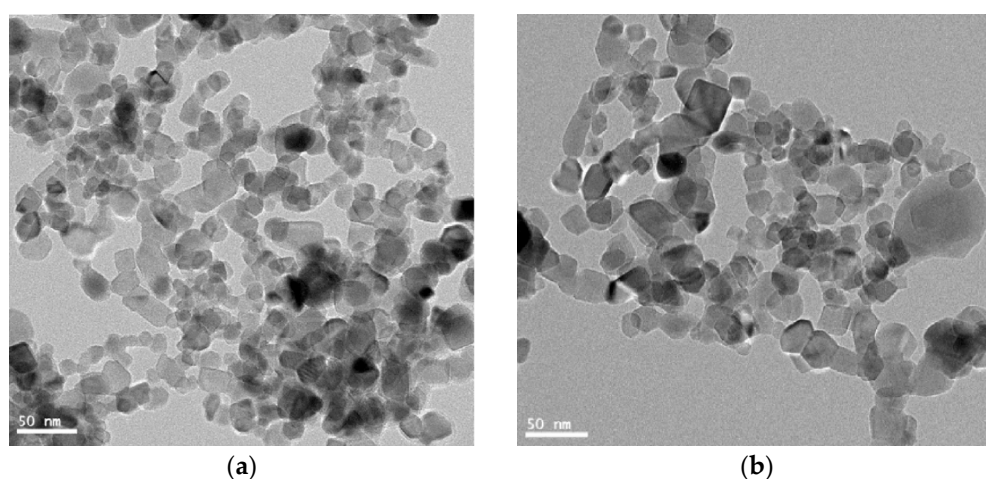
Figure 4. TEM image of TiO_2 NPs in water-based lubricants with concentrations (**a**) 2.0 wt.%; (**b**) 4.0 wt.% [15].

Given the shortcomings of using TEM and SEM, scientists recommend the use of freeze etching replication TEM (FERTEM) or cryogenic electron microscopy (cryo-TEM) [166–168] to observe the nanolubricants because each of them is appropriate to characterise wet

samples, and the size and morphology of NPs can be kept the same as those in the original nanolubricants.

3.1.2. Zeta Potential Test

Zeta potential (ZP) test shows the potential difference between the static fluid layers adhered to the dispersed particles and the dispersion medium [166,169]. The nanofluid stability is evaluated by observing the fluid's electrophoretic behaviour, as a layer of charged particles is formed when the free charge in the base fluid is attracted by the surface opposite charges of dispersed particles [166]. ZP values range from a positive value at low pH to a negative value at high pH in any nanofluid. A nanofluid with relatively high ZP absolute value (>30 mV) is electrically stable due to a strong repulsive force between NPs. Instead, a nanofluid with relatively low ZP absolute value (<15 mV) tends to have NPs agglomerate because an attractive force dominates. In particular, a ZP absolute value above 60 mV indicates excellent dispersion stability of a nanofluid.

ZP test has been used in many studies to determine the size distribution and stability of water-based lubricants [63,90,93,95,111,170]. Figure 5 demonstrates a bar graph of the ZP (mV) vs. nanolubricant with 0.12 wt.% GO, 0.12 wt.% Al_2O_3, and 0.12 wt.% GO-Al_2O_3 (1:1) suspension [21]. It can be seen that the GO-Al_2O_3 lubricant exhibits comparatively higher ZP absolute value (40 mV) than Al_2O_3 (30 mV) and GO lubricants (35 mV), signifying a greater level of stability.
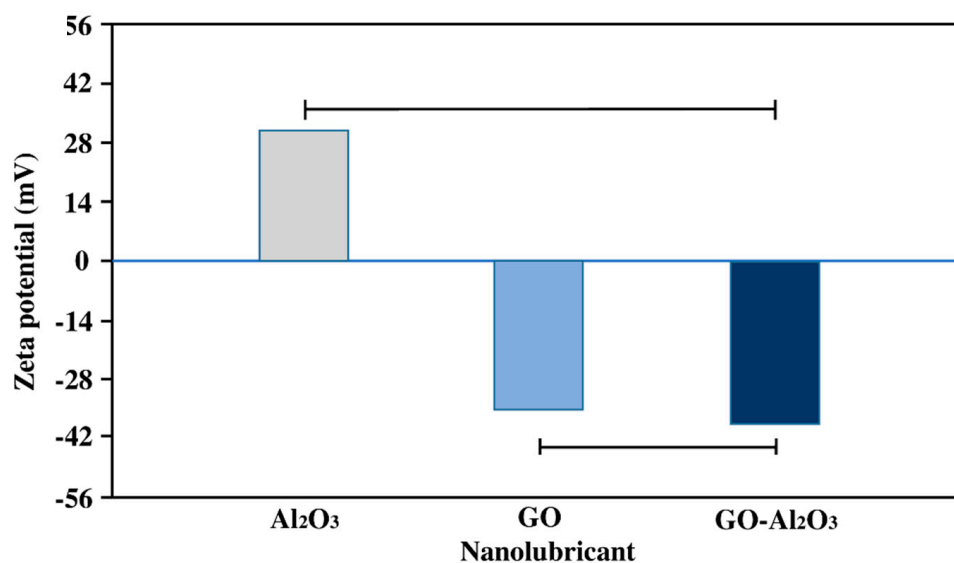

Figure 5. Zeta potential rate of GO, Al_2O_3, and GO-Al_2O_3 [21].

3.1.3. UV-Vis Spectral Analysis

One of the reliable methods to measure the dispersion stability and durability of nanofluids is spectral absorbency analysis against NPs concentration in nanofluids utilising an ultraviolet-visible (UV-vis) spectrophotometer which follows the Beer-Lambert law [171,172]. The stability of suspension is determined by calculating the volume of sediment relative to the time of sediment. The intensity of light different from the scattering and absorption of light passing through the fluid is used in the UV-vis spectrophotometer. It evaluates the absorbance of a fluid within a wavelength of 200–900 nm to analyse various dispersions in the fluid [173]. One of the unique aspects of this method is that it is capable of obtaining quantitative data of NP concentration in nanofluid and is applicable for all boundary fluids [174].

Research has been undertaken using UV-vis spectrometer to analyse the liquid absorbance, physical properties, and chemical state of NPs in water-based lubricants such as graphene [17,74,135], boron nitride [89], and copper [46,116]. For example, the absorbance of 0.05 wt.% hydroxylated boron nitride nanosheets (HO-BNNS) in water was measured

within 5 days, as shown in Figure 6. A good dispersion of HO-BNNS in water can be observed from the slight drop of absorbance, probably because of the hydrogen bond existence between the hydroxyl groups in HO-BNNS and water-glycol. The NPs absorbency ratio is directly proportional to the nanofluid concentration. However, the use of UV-vis is limited by the dispersion of high concentration nanofluids, mainly for carbon nanotube CNT solutions [175] or when the colour of the base lubricant is too dark to distinguish the deposits of NPs.
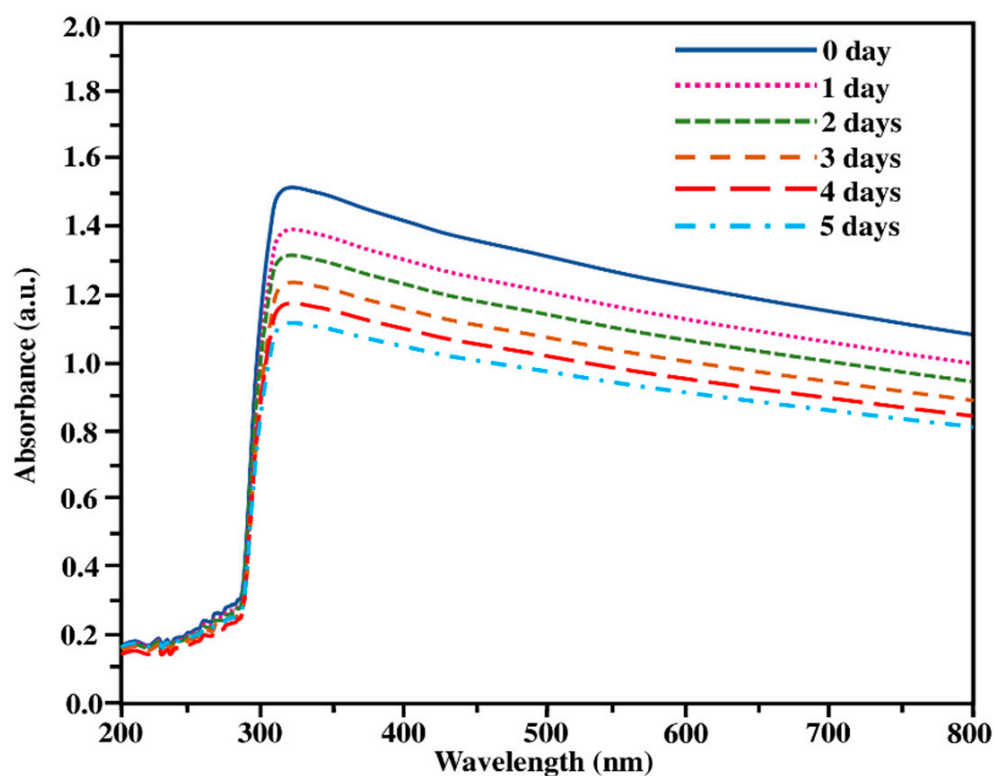

Figure 6. UV–vis absorption spectra of 0.05 wt.% HO-BNNS in water within five days [89].

Generally, a linear relationship exists between the NP concentration and the absorption intensity [166,176,177]. For instance, Liang et al. [123] assessed NP stability using an absorbance method for 48 h and noted that the dispersion stability was obtained for $Mn_3B_7O_{13}Cl$-WO_3:Eu^{3+} from a linear graph (absorbance vs. time), as shown in Figure 7a. The results also showed that WO_3: Eu^{3+} and $Mn_3B_7O_{13}Cl$ exhibited a decrease in relative absorbance over time, indicating that NPs settled more rapidly in acidity solution than that in alkalinity solution. Compared to $Mn_3B_7O_{13}Cl$, $Mn_3B_7O_{13}Cl$-WO_3:Eu^{3+} showed lower relative absorbance, thus presenting better stability. Similarly, Figure 7b revealed that the relative absorbance of the BN, BNNS, and HO-BNNS decreased with the increase in settling time [89]. The settling rate was different for these three additives. To be specific, the settling rate of BN was higher because of its larger mass. BNNS showed a better stability compared to BN due to fewer hydroxyl groups on its surface. While HO-BNNS exhibited the best dispersion stability due to the presence of more hydroxyl groups on its surface. It is worth noting that at higher nanofluid concentration this method might not work accurately because the absorption range is outside the system's highest limit [178].
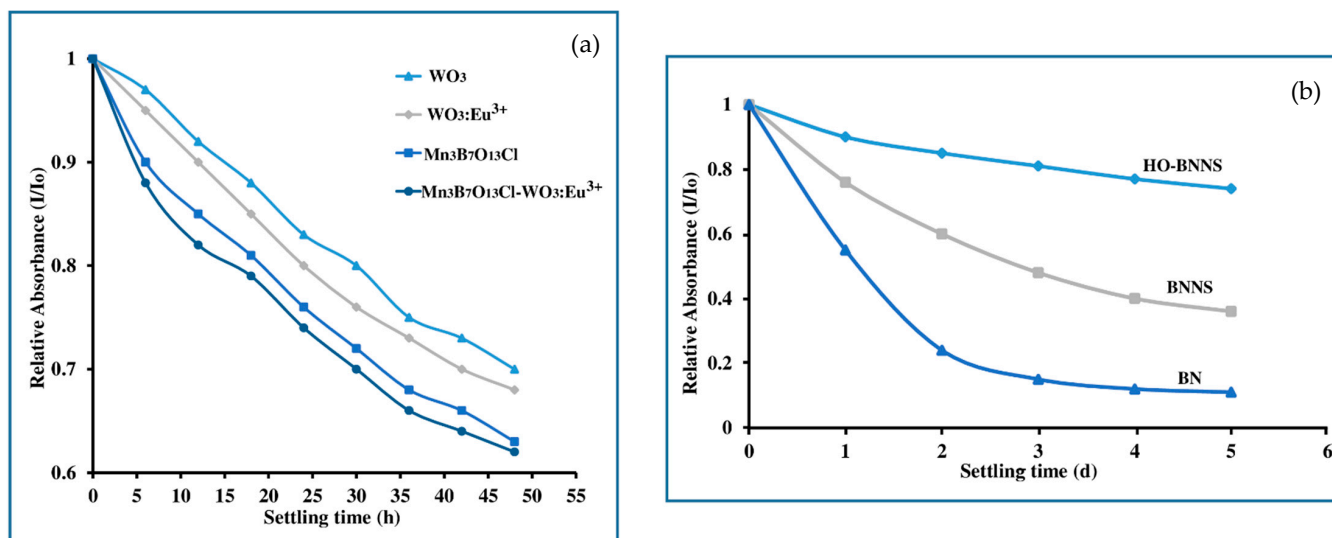
Figure 7. Relative absorbance under different time of (**a**) WO_3, $WO_3:Eu^{3+}$, $Mn_3B_7O_{13}Cl$, and $Mn_3B_7O_{13}Cl\text{-}WO_3:Eu^{3+}$ NPs [123] and (**b**) BN, BNNS, and HO-BNNS [89].

3.1.4. Dynamic Light Scattering

The dispersion stability of lubricants over time can also be evaluated by measuring the NPs size distribution using the dynamic light scattering (DLS) method through analysing the autocorrelation index function [177,179,180]. This method evaluates the particle diffusion moving in Brownian motion and uses the Stokes-Einstein ratio to convert them into particle size ranging between 0.3 nm to 10 μm [181]. Numerous researchers use the DLS method in order to determine the diameter of NPs, although this method is also promising for estimating the size distribution of water-based nanoadditives such as graphene [132,141], ceria [53], and copper [65,117,118,182]. The more stable dispersion of NPs in base lubricant, the greater the impact is on the scattered light intensity, and vice versa. DLS was used to monitor colloidal stability of $Cu@SiO_2$ NPs in DW over time, as illustrated in Figure 8. After 30 days of storage at ambient conditions, very limited size variation was observed, and the hydrodynamic diameter (HD) stayed constant at 230 nm, demonstrating no agglomeration of $Cu@SiO_2$ NPs in DW.
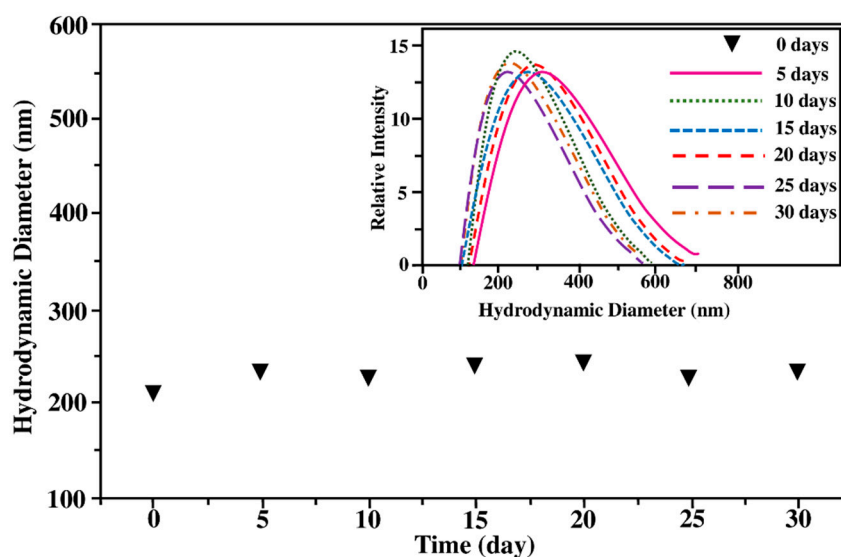
Figure 8. Dynamic light scattering (DLS) observation of $Cu@SiO_2$ NPs in water [117].

Basically, before measurement, thick nanolubricants must be diluted, which may change the microstructure nature of the NPs [168,171]. Therefore, a suitable method is needed to determine the particle size of nanolubricant without changing the particle's microstructure.
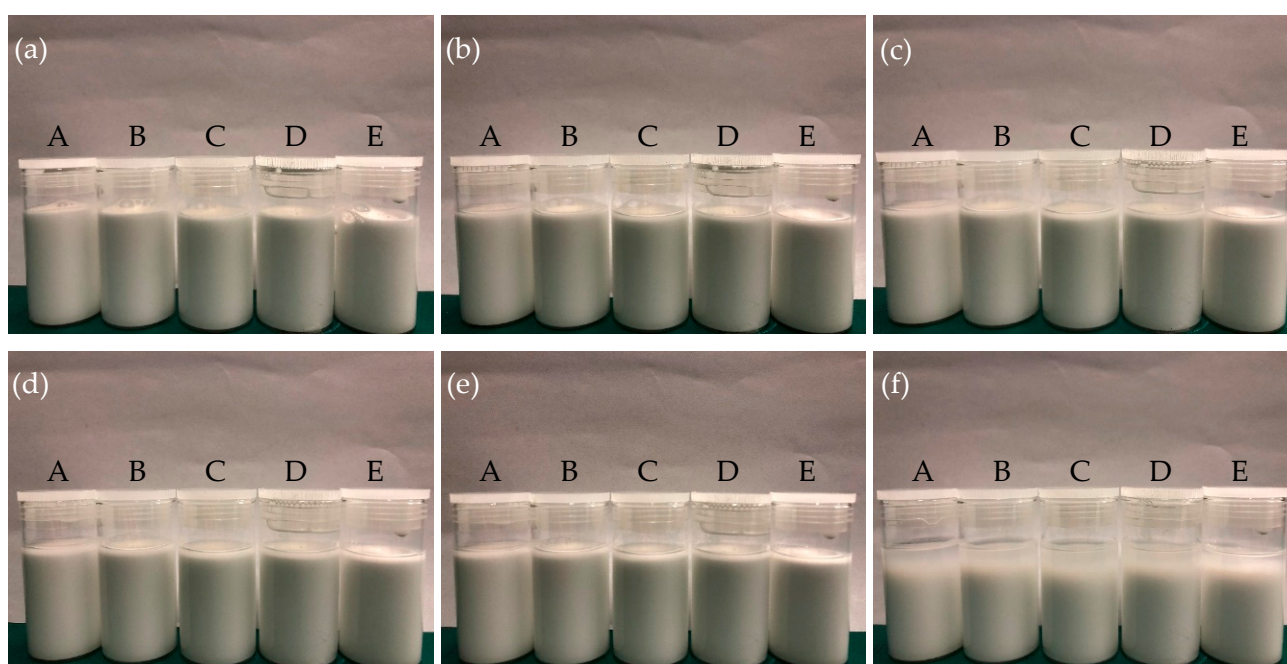
3.1.5. Sedimentation

The basic and low-cost method to analyse the dispersion stability of nanolubricants is the sedimentation method. It is a process in which NPs settle or precipitate as sludge at the lubricant base. Additionally, it is related to the balance of friction force and buoyancy [183]. In nanofluid, the NPs sediment volume or weight is an indicator of nanofluid stability under an external force field.

According to Stokes' law [171], the rate of NP sedimentation rate is calculated:

$$v_o = 54.5d^2 \frac{(\delta - \rho)}{\mu} \text{ (for spherical shape)} \tag{1}$$

where d is the diameter (cm) of NP. δ is the density (g/cm^3) of NP. ρ is the density (g/cm^3) of base lubricant and μ is the viscosity (Pa·s) of base lubricant.

Photography of nanofluid sedimentation using a camera over a time period is the simplest method to monitor the nanofluid stability and sedimentation coefficient [166,184]. Comparing the photos is widely used in nanofluid research, and many examples were mentioned for water-based nanoadditives such as TiO$_2$ [15,24,29,51]. The stability analysis using sedimentation is usually conducted immediately after the dispersion of NPs in the base lubricant, and the disturbance or movement should be avoided to ensure its reliability. Wu et al. [24] carried out the sedimentation experiment to compare the precipitation of TiO$_2$ NPs in different as-prepared water-based nanolubricants, as shown in Figure 9. They found that all the lubricants remained stable without apparent particle sedimentation at the bottom within 120 min as long as the dispersants such as sodium dodecyl benzene sulfonate and Snailcool were added into water. After standing the lubricants for 24 h, the TiO$_2$ NPs began to settle down slightly, and a shallow supernatant appeared.

Figure 9. Sedimentation of TiO$_2$ NPs dispersed in different water-based nanolubricants at settling time of (**a**) 0; (**b**) 30 min; (**c**) 60 min; (**d**) 90 min; (**e**) 120 min and (**f**) 48 h [24].

Moreover, the sedimentation rate of NPs in a certain time is measured by the change in the mass/volume concentration in the base fluid using a highly sensitive analytical balance. According to the following formula, the NPs suspension fraction *F* at a specific time is calculated:

$$F = \frac{(W_o - W)}{W_o} \tag{2}$$

where W_o is the total mass of all NPs in the base fluid; W is the mass of the sediment NPs at a certain time [185].

The nanofluid is considered to be stable if the concentration of NPs in the base fluid stays constant over time, and vice versa [186]. This is a simple method that just requires an accurate and sensitive balance to quantify the volume of the deposited NPs. The only limitation of this method is that it cannot detect small NP aggregates that are not considered to settle at a reasonable amount [166,187].

3.1.6. Other Methods

There are some other methods applicable for evaluating dispersion stability of nanofluids, including three-omega, centrifugation, and density measurement, each of which has its own characteristics. For example, a densitometer can be used in the density measurement method to monitor NP concentration varying with time due to NPs aggregation and precipitation [188]. The three-omega method determines colloidal stability with large volume fractions of NPs through thermal conductivity [187,189]. In centrifugation method, analysis is carried out using the centrifugal force acting on the nanofluids at various speeds and time [164,177,180]. It is acknowledged that centrifugation is a faster way to determine nanofluids stability compared to sedimentation photography [164].

3.2. Factors Affecting Dispersion Stability

3.2.1. pH Control

Altering the pH of nanofluids affects the surface of NPs and enhances the stability of dispersed NPs [190]. Nanofluids are characterised by their electrokinetic properties, which influence their stability. Therefore, an increase or decrease in nanofluid pH is accompanied by an increase or decrease in zeta potential. As previously noted, NPs repel one another when their zeta potentials increase above +30 mV or decrease below −30 mV. With the objective to change the pH of a nanofluid, suitable acidic or alkaline solutions should be added [191].

In order to enhance the nanofluids' stability, it is necessary to modify its pH level. The pH of nanofluids must be equal to a specific critical value in order for them to have zero net charges. As the electrostatic force is diminished, the NPs begin to break apart. At this point, the system is at the point of zero charge (PZC) or an isoelectric point (IEP). Aggregation and sedimentation of NPs peaks at this stage [166]. At an IEP, both surface charge and zeta potential are zero. By enhancing repulsive forces among particles and zeta potential, a pH value far from the IEP demonstrates better durability. When a pH is far away from IEP and the zeta potential is high, it leads to a stable suspension with almost no particle coagulation [191]. The effect of pH on the stability of water-based lubricants has been investigated by many researchers using NPs such as graphene oxide (GO). For instance, Meng et al. [76] discovered that alkaline GO water-based lubricant (pH 9.0) presented the most effective lubricity, and an increase in lubricant pH value can modify the GO structure, improving the dispersibility of GO in water.

3.2.2. Ultrasonication

Generally, chemical or physical methods are used to generate NPs as dry powders that are then distributed into water for synthesising aqueous lubricants [192]. Every chemical treatment-based procedure changes the surface chemistry of the NPs distributed in boundary fluids, protecting them from agglomeration and sedimentation, and improving their long-term stability [166]. In contrast, physical methods such as magnetic stirring,

shear homogenizer, and probe and bath ultrasonication are also widely used for producing stable nanofluids with a two-step method [188]. In comparison to bath ultrasonication, probe ultrasonication is expected to produce a nanofluid with better dispersion stability. Furthermore, it has been demonstrated that ultrasonication is more effective than mechanical stirring in reducing the agglomeration of NPs in water. In ultrasonication, an ultrasonic wave is spread through a periodic motion, leading to unstable cavitation bubbles bursting. Implosion occurs when unstable cavitation bubbles break up aggregates [193,194]. The produced ultrasonic waves can break up the attractive force between NPs to increase the stability of the nanofluid [195]. It should be noted that an excessive ultrasonication time may result in rapid sedimentation of NPs.

3.2.3. Surface Modification

In the surface modification method, the surface-modified NPs are straightforwardly added into water to attain stable water-based nanolubricants without the aid of surfactants. Surface modifiers are necessary to modify NPs' surface activity. Table 2 demonstrates a list of surface modifiers used for different types of NPs. For example, Tang and Cheng [196] modified ZnO NPs to enhance the stability in an aqueous solution using polymethacrylic acid (PMAA). Nano-ZnO has hydroxyl groups that interact with carboxyl groups of PMAA and develop zinc methacrylate complexes on nano-ZnO surfaces, which enables ZnO NPs to be stably dispersed in water. Zhao et al. [46] implemented an in situ modification of water soluble Cu NPs, which involves both the preparation and surface modification simultaneously. The two polar groups of Bis (2-hydroxyethyl) dithiocarbamic acid (HDA) that act as capping agents enhance the dispersibility of Cu NPs in water. Through in situ surface modification, they also synthesised water soluble CuO with different morphologies (nanorods, nanobelts, and spindle shapes) using polyethylene glycol (PEG, a guiding agent) and polyvinyl pyrrolidone (PVP, a stabilising agent), showing improved stability [54].

It is possible to obtain long-term nanofluid stability by functionalising the NP surface. Therefore, in order to prepare self-stabilised nanofluid, functionalised NPs are added to the base fluid. In this context, appropriate functional organic groups are selected that will most likely adhere to the NP surface, thereby assisting self-stabilisation. Functional groupings can be presented in two ways. The first technique requires bifunctional organic compounds to introduce all of the functional ligands in one step. The NP surface is attached with one functionality, and the other group is used to functionalise the NP. In the second method, bifunctional compounds are combined through reaction, in which a group acts as a bonding point, and can later be transformed to an ultimate functionality [197]. Kayhani et al. [106] functionalised spherical TiO_2 NPs (15 nm) by mixing with hexamethyldisilazane ($C_6H_{19}NSi_2$) at 2:1 mass fraction ratio to produce stable TiO_2/water nanofluid. The mixture was sonicated for 1 h at 30 °C to obtain soaked NPs which were dried and dispersed in distilled water for 3–5 h by ultrasonic vibration. No agglomeration was observed in the nanofluids for several days. The stable behaviour of TiO_2 NPs resulted from the hydrophilic ammonium group. In addition to this, Yang and Liu [198] succeeded in maintaining the stability of 10 wt.% SiO_2 water-based nanolubricant by functionalising with silanes of (3-glycidoxylpropyl) trimethoxysilane, and found no sedimentation existed for a year.

3.2.4. Surfactant Addition

In general, NPs will not agglomerate as long as the nanofluid surface tension is low. It is reported that surfactants can be used to reduce the surface tension of nanofluids [199]. The presence of surfactants decreases the interfacial tension between two liquids or between a liquid and a solid, supporting the spread of liquids [200]. In aqueous solutions, surfactants addition can significantly improve NP stability. It is not only necessary to investigate the influence of surfactants on base nanofluids, but also important to discover new surfactant candidates with the potential to enhance the stability while minimising the damage to native nanofluid properties [188].

Popular surfactants used in literature to maximise the dispersion stability have been listed in Table 2. It is essential to select the right surfactant, which is either cationic, anionic or non-ionic. For instance, the performance of sodium dodecyl sulfate (SDS) and polyvinylpyrrolidone (PVP) was compared by Xia and Jiang [201] to present the dispersion stability of Al_2O_3 NPs in DW. Based on this study, PVP demonstrated better dispersibility than SDS by improving stability at 0.5, 1.0, and 2.0 wt.% surfactant concentration. The nonionic PVP performed comparatively better because of its extended alkyl chain. Kakati et al. [202] prepared 0.1–0.8 wt.% Al_2O_3 and ZnO water-based nanolubricants with the aid of 0.03 wt.% SDS. The results showed that the nanofluid with SDS had 4–5 days stability while without SDS the NPs agglomerated within 1 h after preparation.

Table 2. A list of surface modifiers and surfactants used in various water-based nanolubricants.

NPs Type	Surface Modifier	Surfactant
Pure metals	Bis (2-hydroxyethyl) dithiocarbamic acid (HAD) [46], Methoxylpolyethyleneglycol xanthate potassium ($MPEGOCS_2K$) [47]	Polyvinylpyrrolidone (PVP) [46,97]
Metal and non-metal oxides	polyethylene glycol-200 [59], oleic acid (OA) [102], polyethyleneimine (PEI) [13,15,26–28], sodium hexametaphosphate (SHMP) [50], KH-570 [103]	(3-mercaptopropyl)trimethoxysilane (MPS) [85], sorbitan monostearate [53], polyvinylpyrrolidone (PVP) [54,97], polyethylene glycol (PEG) [54], cetrimonium bromide (CTAB), and sodium dodecylbenzene sulfonate (SDBS) [24,25,51,52,99], sodium silicate [51,52], snailcool [24], hexadecyl trimethyl ammonium bromide (CTAB) [101]
Metal sulphides	Bis (2-hydroxyethyl) dithiocarbamic acid (HDA) [62], sodium oleate soap, triethanolamine oleate, fatty alcohol polyethylene glycol ether (MOA), polyethylene glycol octyl phenyl ether (OP-4) [110],	(3-mercaptopropyl) trimethoxysilane (MPS) [61], cetrimonium bromide (CTAB), and sodium dodecylbenzene sulfonate (SDBS) [111], oleic acid, triethanolamine [111],
Carbon-based materials	Dopamine methacrylamide (DMA) 2-methacryloyloxyethyl phosphorylcholine (MPC) [68],	humic acid (HA) [128], sodium dodecyl sulfate (SDS) [119,120], Triton X-100 ($C_{34}H_{62}O_{11}$) [67]
Composites	hexadecyldithiophosphate (DDP) [117], 3-mercaptopropyl trimethoxysilane (MPTS) [116], polydopamine (PDA) [118],	sodium dodecyl sulfate (SDS) [124,125], polyvinylpyrrolidone (PVP) [119], Igepal CO-520 [117], cetrimonium bromide (CTAB), and sodium dodecylbenzene sulfonate (SDBS) [119,184]
Others	dialkyl polyoxyethylene glycol thiophosphate ester (DTP-10, DTP-20) [154], oleylamine [93]	benzalkonium chloride [90], sodium polyacrylate (PAAS) [159], SHMP (sodium hexametaphosphate), 1,4-butylene glycol [203], coconut diethanol amide (CDEA) [204]

3.3. Theories of Dispersion Stability

In addition to the above discussion, the dispersion stability of nanofluids can be explained by a number of theories including DLVO (Derjaguin and Landau 1941, Verwey and Overbeek 1948), depletion and steric stability theory. The DLVO theory describes the dispersion stability by electrostatic repulsive forces and van der Waals forces, which is only applicable for spherical NPs. When the van der Waals force is less than electrostatic repulsion, molecule agglomeration and collision are reduced significantly, resulting in more stable suspension [176,205]. The NPs tend to reassemble while the van der Waals force plays a main role. A DLVO potential is calculated as follows:

$$G_T(h) = G_e(h) + G_A(h) \tag{3}$$

where $G_e(h)$ denotes the repulsive potential and $G_A(h)$ denotes the attractive potential. $G_T(h)$ is the total potential at varying values of h. Both are influenced by the distance between NPs [206], as shown in Figure 10.
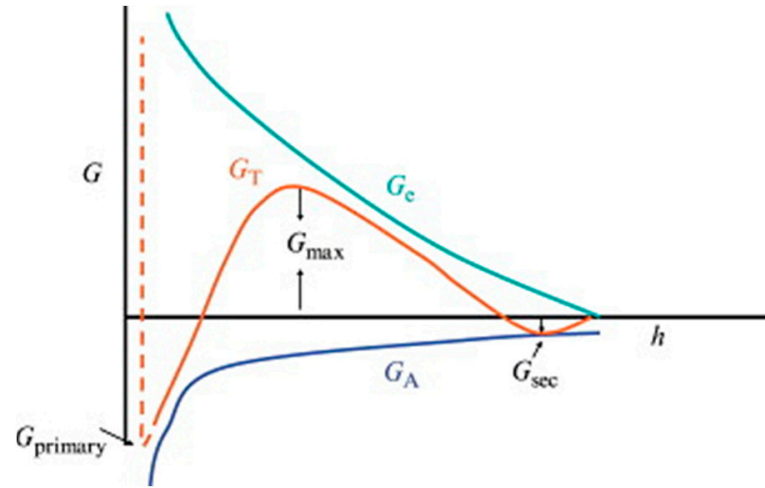

Figure 10. DLVO potential variation with a certain range of NPs distance [206].

Additionally, the electrostatic repulsive potential and van der Waals attraction potential can be determined using the following equations [207]:

$$\text{Repulsive potential } G_e(h) = 2\pi\varepsilon a\psi_o^2 \ln[1 + exp(-\kappa h)] \tag{4}$$

$$\text{van der Waals attractive potential } G_A(h) = -\frac{A}{6}\left[\left(\frac{2a^2}{h^2 + 4ah}\right) + \left(\frac{2a^2}{h^2 + 4ah + 4a^2}\right) + \ln\left(\frac{h^2 + 4ah}{h^2 + 4ah + 4a^2}\right)\right] \tag{5}$$

where *a* is particle radius; ψ_o is particle's surface potential; ε is medium's permittivity; κ is inverse Debye length that is influenced by the thickness of electrical double layer; *h* is the distance between NPs; and *A* is Hamaker constant. The electrostatic repulsion is influenced by three factors: size, distance, and surface potential of NPs, while the van der Waals force is influenced by the distance and radius of NPs. NPs aggregate when their distance is below a certain value due to the molecular attraction [207].

However, for NPs with platelet, rod, ellipse, or other shapes, both the depletion and steric stability theories have to be taken into account. The steric stability theory is explained by van der Waals force and elastic steric force in nanofluids with different NPs, ionic/non-ionic surfactants or absorbed polymers. The steric force is influenced by the chemical composition of the suspension and thickness, and the density of absorbed polymer layers [208–211]. The depletion theory contributes to nanofluids with free polymer additives, and depletion force is present between the NPs and non-absorbed polymers which results in depletion layer formation [212]. For depletion force, the concentration of free polymers is the influencer. When the polymer concentration is low, the NPs aggregate due to the attractive potential energy, whereas repulsive potential energy is strong with more free polymers developing more stable nanofluids.

Apart from the van der Waals, depletion, and steric stability forces, the Brownian force [213,214], buoyancy force [215], hydration force [216], and interphase resistance [217] may also contribute to the dispersion stability of nanofluids under specific conditions.

4. Tribo-Testing Methods

The American Society of Lubrication Engineers (ASLE) has compiled 234 apparatus for tribo-testing which are classified by their geometries. Tribometers that have been designed with advanced instrumentation are equipped with instruments that enable the measurement of coefficients of friction, friction forces, wear rates, noise, vibrations, and

temperature of a system [218]. Several tribo-testing methods, including four-ball, pin-on-disk, ball-on-disk, ball-on-plate, ball-on-three-plates, and block-on-ring have been primarily used to evaluate the tribological performance of as-prepared water-based lubricants.

4.1. Four-Ball

A four-ball tribometer is one of the most common type of tribometers for analysing lubricant performance. Figure 11 shows a diagram of the four-ball tribometer. This structure consists of three balls fixed in a lubricant bath. The rotating ball is placed above the three fixed balls [218,219]. During the tribo-testing, a normal force is exerted pneumatically to the rotating ball at a constant speed, and the force is increased until the balls are welded together under the frictional heat. This tribometer can not only be used for measurement of COF and wear scar diameter (WSD), but also be applicable for assessment of load-carrying capacity and extreme pressure (EP) property. ASTM standard (D2783) is followed while conducting the tests. The EP characteristics can be evaluated by measurement of P_B (last non-seizure load, the last load at which the measured scar diameter is not more than 5% greater than the compensation value at that load) and P_D (weld point, the lowest applied load at which sliding surfaces seize and then weld). In principle, higher P_B and P_D values indicate better EP properties. It should be noted that the feasibility of evaluating EP properties is the unique feature of the four-ball test, which is independent of other types of tribo-testing configurations.
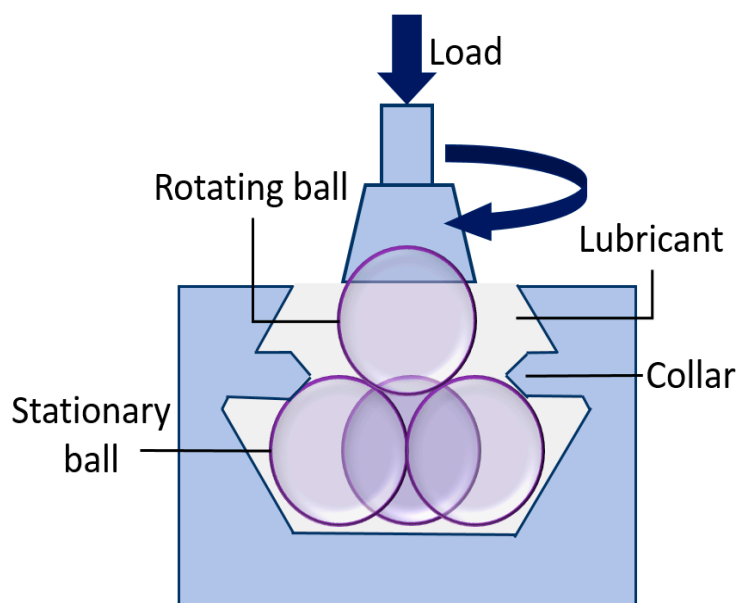

Figure 11. Four-ball tribometer.

The studies found in the literature using four-ball tribometer to evaluate lubricant properties are listed in Table 3. For instance, Zhang et al. used this tribometer to investigate the tribological properties of surface capped Cu [47] and Cu/SiO$_2$ [116] nanocomposite as additives in DW, and found that the water-based nanolubricants exhibited excellent load carrying capacity and reduced wear and friction. Furthermore, multiple studies have been conducted with TiO$_2$ NPs using four-ball tribometer to evaluate the tribological performance [49,52,102,103]. For example, Sun et al. [50] investigated the tribological behaviour of nano-TiO$_2$ water-based lubricant using the four-ball tribometer under 196 N load at a speed of 60 rpm for 30 min, which resulted in a significant reduction of wear by 30.6%, COF by 64%, with an optimal concentration of 0.7 wt.%. Additionally, with the increase of nano-TiO$_2$ concentration, the P_B increased. To be specific, for 0.1 wt.% nano-TiO$_2$ the P_B raised by 6.5%, ultimately reached 784 N at 5.0 wt.%. Meng et al. [52] also conducted tribo-testing with nano-TiO$_2$ using four-ball tribometer for 30 min at 1200–1760 r/min

under 392 N. The test result indicated that adding nano-TiO_2 in lubricant assisted with the increase in P_B by 62.5%, along with the reduction in COF and wear by 33.8% and 47.4%, respectively. Many factors such as load, speed, optimal concentration, and temperature can be modified for testing tribological characteristics with various simulated circumstances.

4.2. Pin-on-Disk

The pin-on-disk tribometer shown in Figure 12a is used according to standard testing procedures. The arrangement consists of a fixed pin and a rotating disk. A circular sliding path is established on the rotating disk, while the load cells and sensors measure the frictional and tangential force generated by the fixed pin. The loading force is applied on the pin which is placed on the disk surface with a distance away from the disk centre. The disk is driven by a servo motor with a certain rotation speed (rpm). The applied pins are generally cylindrical in form, with flat, truncated, or spherical conical ends. The wear of pin can be measured by monitoring its dimensional changes, such as the length of pin, the WSD of the contact face, or by measuring weight loss. If the weight loss is too little to be weighed, it can be calculated or evaluated using wear area obtained from surface profile under a 3D microscope.
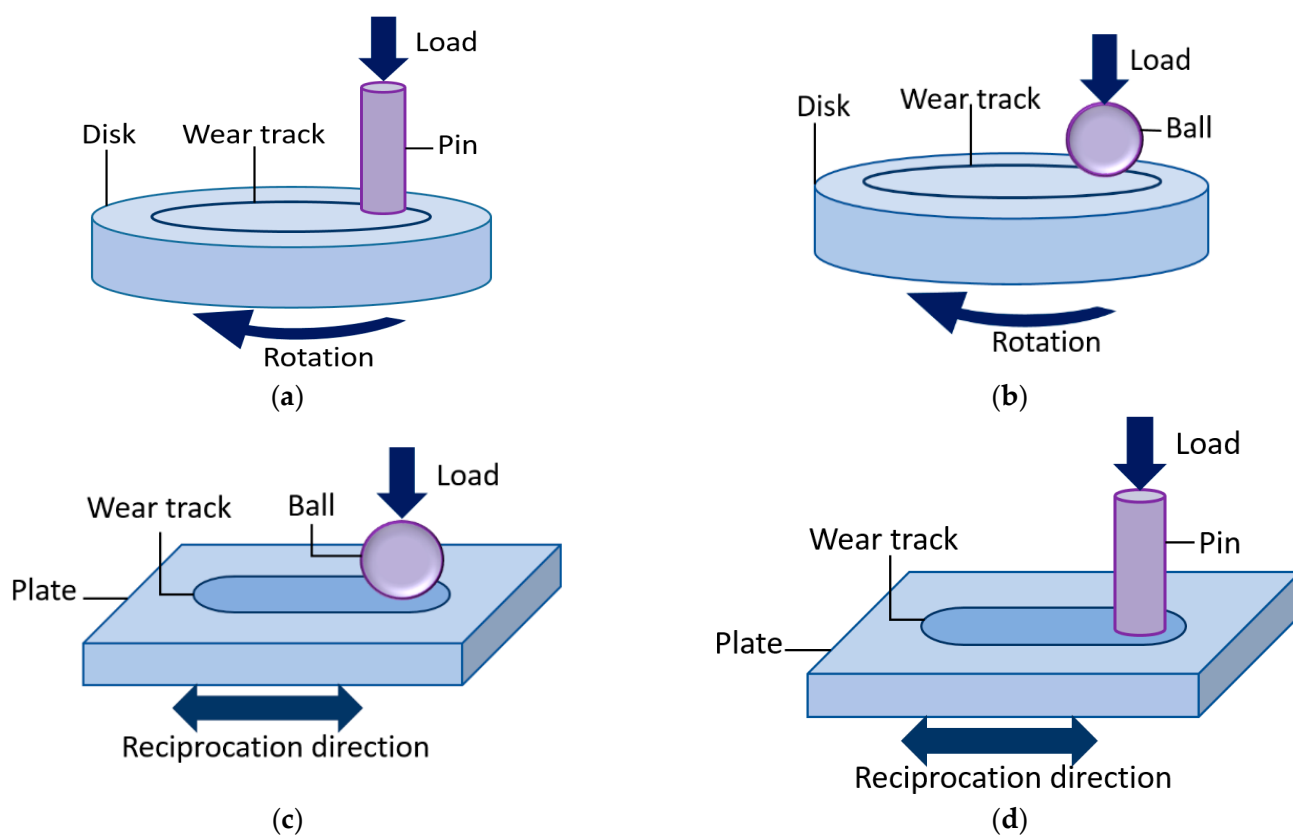
Figure 12. (**a**) Pin-on-disk, (**b**) ball-on-disk, (**c**) ball-on-plate, and (**d**) pin-on-plate.

In the field of tribology, this type of tribometers has been widely used in simulating practical working conditions. The pin-on-disk tribo-testing can be used for research on bearing systems, brake systems, train wheel systems, and manufacturing industries. This mechanism can be carried out under both the dry and lubricating conditions [218,219]. The pin-on-disk tribometer was used by He et al. [159] to evaluate the tribological properties of hexagonal boron nitride (h-BN) in base water at 300 rpm for 30 min under 400–600 N loads, which revealed an excellent reduction in WSD by 14.6% and COF by 29.1% with an optimal concentration of 0.7 wt.% h-BN. Zhao et al. [53] also used pin-on-disk tribometer to conduct 30 min tribological test at 50 mm/s using 0.05–0.2 wt.% cerium dioxide (CeO_2)

water-based nanolubricant. The results indicated 20% reduction in COF and 49% reduction in wear track depth. In a similar way, Elomaa et al. [139] conducted tribo-testing with graphene oxide (GO) water-based nanolubricant and found that the optimal parameters for significant friction and wear reduction can be achieved using 1 wt.% GO under 10 N.

4.3. Ball-on-Disk

The term pin-on-disk is substituted by ball-on-disk in the presence of the spherical cap end, which is also used extensively in tribo-testing configurations due to massive application of ball bearings in engineering. In this case, the parameters of the ball including diameter, Poisson's ratio, and elastic modulus are supposed to influence the Hertzian contact stress when contacting the disk. The initial experimental conditions, therefore, are quite different, which affects the final results of the tribological test. Normally, the working principles of the pin-on-disk and ball-on-disk arrangement are quite similar. The only difference is that the contact type is set by pin or ball. The ball-on-disk tribometer includes a ball and a circular flat disk, and a contact is established between these two surfaces of contact. The ball usually remains stationary when the flat disk rotates around its central axis, as shown in Figure 12b. A pre-set normal load is applied on the fixed ball, and a circular sliding path is generated on the disk after testing. Load cells and sensors can be used to measure the friction or tangential force generated between the fixed ball and the rotating disk. Usually, the tests are conducted in accordance with the standard test procedure (ASTM G99) [219].

There is a great demand for ball-on-disk tribometers to investigate the performance of water-based nanolubricants. For example, ball-on-disk tribometer was used by Radice and Mischler [48] to inspect the effect of Al_2O_3 NPs in aqueous solutions on the tribocorrosion behaviour of steel/alumina sliding surface under 4–10 N and 10–40 mm/s, which resulted in COF and wear rate reduction by 40–50%. Ball-on-disk tribometer has also drawn the attention of many researchers to analyse the tribological properties of nanoadditives including nanocomposite, graphene based, and ionic liquids. For example, tribological properties of carbon dots (CDs) [66] and poly ethylene glycol-graphene (PEG-G) [147] nanoadditives were evaluated under 10 N and a sliding velocity of 5 Hz. Superior friction-reduction and anti-wear properties were obtained with 0.05 wt.% PEG-G in water, indicating 39.04% wear rate reduction and 81.23% COF reduction. The use of CDs in water-based lubricants revealed outstanding tribological behaviour compared to pure water, with 39.66% COF reduction and 38% wear rate reduction. Table 3 contains a list of studies related to the use of ball-on-disk tribometers.

4.4. Ball-on-Plate

A ball-on-plate configuration is designed for sliding reciprocating motions (Figure 12c). Under certain conditions, the ball slides linearly along the plate. When compared to a ball-on-disk configuration, where the ball moves unidirectionally over a circular track, a ball-on-plate apparatus performs an alternating linear movement of the ball back and forth over the stationary plate at a constant speed [219]. The normal load is applied on the ball, and COF can be recorded against time during the sliding process. The wear track produced by reciprocating motion is much shorter than that produced by rotating motion for the same dimension of specimen under the same linear speed and testing duration. Therefore, ball-on-disk test is used more often than ball-on-plate test due to its higher efficiency for wear loss generation and more spots yielded for wear track observation.

There have been quite a few researchers who have used a ball-on-plate tribometer to characterise the tribological properties of graphene-based NPs. A reciprocating ball-on-plate tribometer was used by Xie et al. to evaluate the tribological properties of graphene/GO [77] and SiO_2/graphene [112] as nanoadditives in water-based lubricant for magnesium alloy sheets under 3 N normal load at a speed of 0.08 m/s for 30 min. Compared to pure water, 0.5 wt.% GO enabled 77.5% COF reduction and 90% wear rate reduction, while 0.5 wt.% graphene showed only 21.9% COF reduction and 13.5%

wear rate reduction. Furthermore, the best tribological properties were obtained using SiO_2/graphene (0.1:0.4) combination in water compared to only 0.5 wt.% graphene in water, presenting decreases in COF and wear volume by 48.5% and 79%, respectively. Moreover, black phosphorus quantum dots served as a high-efficient nanoadditive in water-based lubricant with an ultra-low concentration of 0.005 wt.%, not only exhibiting remarkable wear reduction by 56.4%, COF reduction by 32.3%, but also indicating an increment in load-carrying capacity from 120N to 300 N [92]. In recent years, ball-on-plate tribometer has been used consistently for various nanoadditivies including GO, nanodiamond, copper, ionic liquids, and naphthalene (listed in Table 3).

4.5. Ball-on-Three-Plates

The ball-on-three-plates tribometer is another device that researchers can use to examine the tribological properties of lubricants. Such a configuration is also called ball-on-pyramid. This device is composed of a spherical shaped ball and three plates that move independently in all directions. In order to efficiently distribute a normal load on the upper ball's three points of contact, the bottom plates need to be placed at 45° along the loaded axis. Results can be inaccurate when normal loads are unevenly distributed on three plates. It is possible to adapt the system to the desired material combinations since the balls and the plates are interchangeable [218,219]. Figure 13a shows a ball-on-three-plates tribometer that is commonly used for testing lubricants. He et al. [16] conducted studies to investigate the tribological behaviour of water-based Al_2O_3 nanosuspensions using a ball-on-three-plates tribometer under 10–40 N load at 20–100 mm/s sliding speed. Results indicated that, compared to water/glycerol solution, 1–2 wt.% Al_2O_3 (30 nm) nanolubricant presented the highest reductions in COF and wear mark by 27% and 22%, respectively. The authors also used this tribometer at a sliding speed of 50 mm/s under a normal load of 20 N to assess the tribological characteristics of GO sheets in water. By using 0.06 wt.% GO nanolubricant, vibration and noise in tribo-testing were minimised simultaneously, and the COF and WSD were reduced by 44.4% and 17.1%, respectively [17]. He et al. [18] also examined the tribological properties of pure GO and $g\text{-}C_3N_4$ nanosheets in water applying 10–35 N normal load with varying sliding speeds between 25–125 mm/s at 25 °C. With optimal concentration of 0.06 wt.% GO, $g\text{-}C_3N_4$ and $g\text{-}C_3N_4$/GO (1:1), reductions in COF by 37%, 26%, and 37% and WSD by 19.1%, 16.0%, and 19.6%, respectively, were observed. Thus, $g\text{-}C_3N_4$/GO presented better tribological performance than only GO and $g\text{-}C_3N_4$ in water under varying loads and speeds.
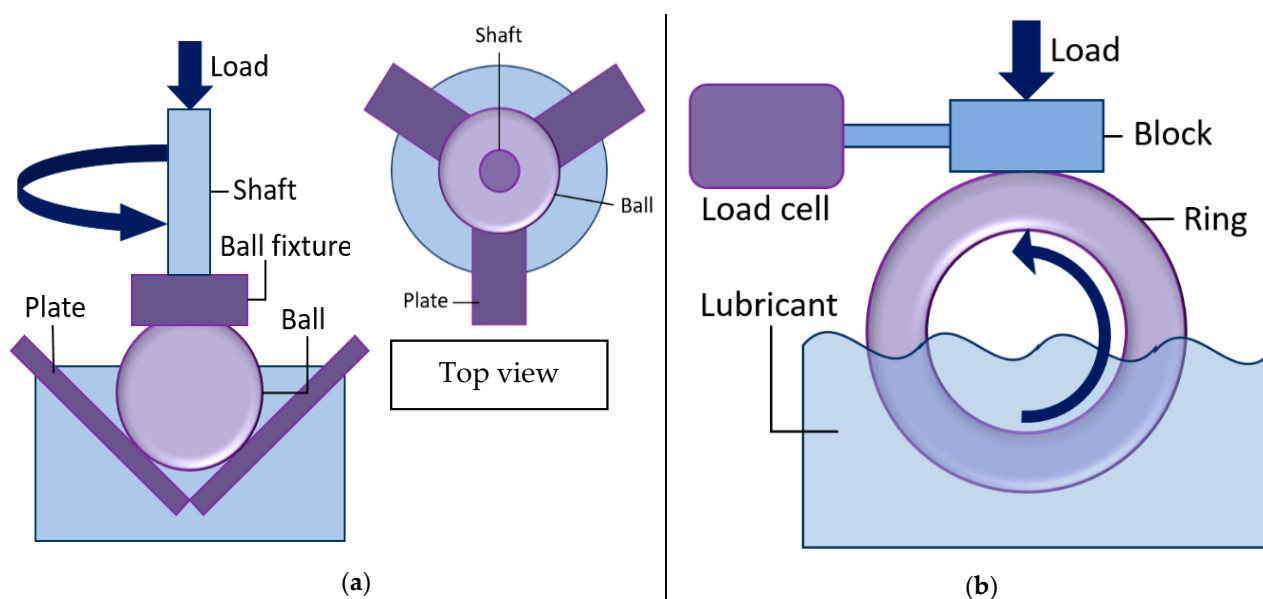

Figure 13. (**a**) Ball-on-three-plates configuration and (**b**) block-on-ring configuration.

4.6. Block-on-Ring

In the block-on-ring setup, as shown in Figure 13b, the block is placed against the rotating ring under a predetermined load. The COF between the block and the ring is recorded when the ring rotates at a certain rate. Block-on-ring tribometers have been extensively used to study nanolubricants, coatings, and polymers. This type of tribometer configuration can evaluate the wear and COF between sliding surfaces in contact such as lubricating films, rings, and bearings.

Huang et al. [21] used a block-on-ring tribometer to study the role of GO, Al_2O_3, and GO-Al_2O_3 as nanoadditives in water-based lubricants under varying loads from 10 to 30 N and varying sliding speeds from 100 to 400 mm/s at 20–25 °C. Compared to individual 0.06 wt.% GO and 0.06 wt.% Al_2O_3 solutions, 0.12 wt.% GO-Al_2O_3 (1:1) lubricant showed significant decreases in COF by 47% and 64%, respectively, and surface roughness was improved by 60% and 63%, respectively. The authors conducted tribo-testing with 0.16 wt.% GO/SiO_2 water-based slurry under 20 N and 109 rpm, leading to a surface roughness (R_a) reduction by 35% and an increase in material removal rate (MRR) by 28% [19]. Huang et al. [12] conducted another study using a block-on-ring tribometer for testing water-based nanosuspension containing ZrO_2/TiO_2 NPs and GO with a normal load of 100 N and a sliding speed of 400 mm/s. The results demonstrated that the use of GO- ZrO_2/TiO_2 hybrid nanosuspension resulted in 65% surface roughness improvement and 25% reduction in COF. The studies using block-on-ring tribometers are summarised in Table 3.

4.7. Others

There are several tribometers with a wide range of testing capabilities used for different applications. For example, piston ring-on-cylinder line is used to analyse wear and friction phenomena in ring-piston pairs in combustion engines, compressors, and pumps, as shown in Figure 14a. Two-disk tribometers are used to measure relative displacement among two cylindrical surfaces to determine the wear on gears, rollers, bearings, and wheel systems [218,220], as shown in Figure 14b. Furthermore, a ring-on-ring tribometer is used to study the wear and friction of cylindrical tribological pairs, such as camshafts, clutches, and bearings, as shown in Figure 14c. Contact areas between rings typically vary based on their topology, which can be either tangential or concentric [218].

In recent months, a novel ultrahigh speed ball-on-disk tribometer with a sliding speed up to 50 m/s has been developed [221], which may be used to characterise the lubricants in a large speed range. This ultrahigh sliding speed can be achieved through a combined solution of on-line precision cutting and in situ dynamic.

In the tribological studies related to water-based lubricants, some researchers used other tribometers including ring-on-plate [222], ball-on-block, pin-on-cylinder [148,149], and 2-ball-plate tribometers [126] according to the testing parameters. In recent years, Ye et al. used ball-on-block tribometer to evaluate the tribological properties of multi-walled carbon nanotubes [129], stearic acid [96], and urea-modified fluorinated graphene [134] as water-based nanoadditives by analysing their anti-wear and friction-reduction properties.

Table 3 demonstrates a list of tribological studies summarised in the field of water-based nanolubrication using different tribometers.
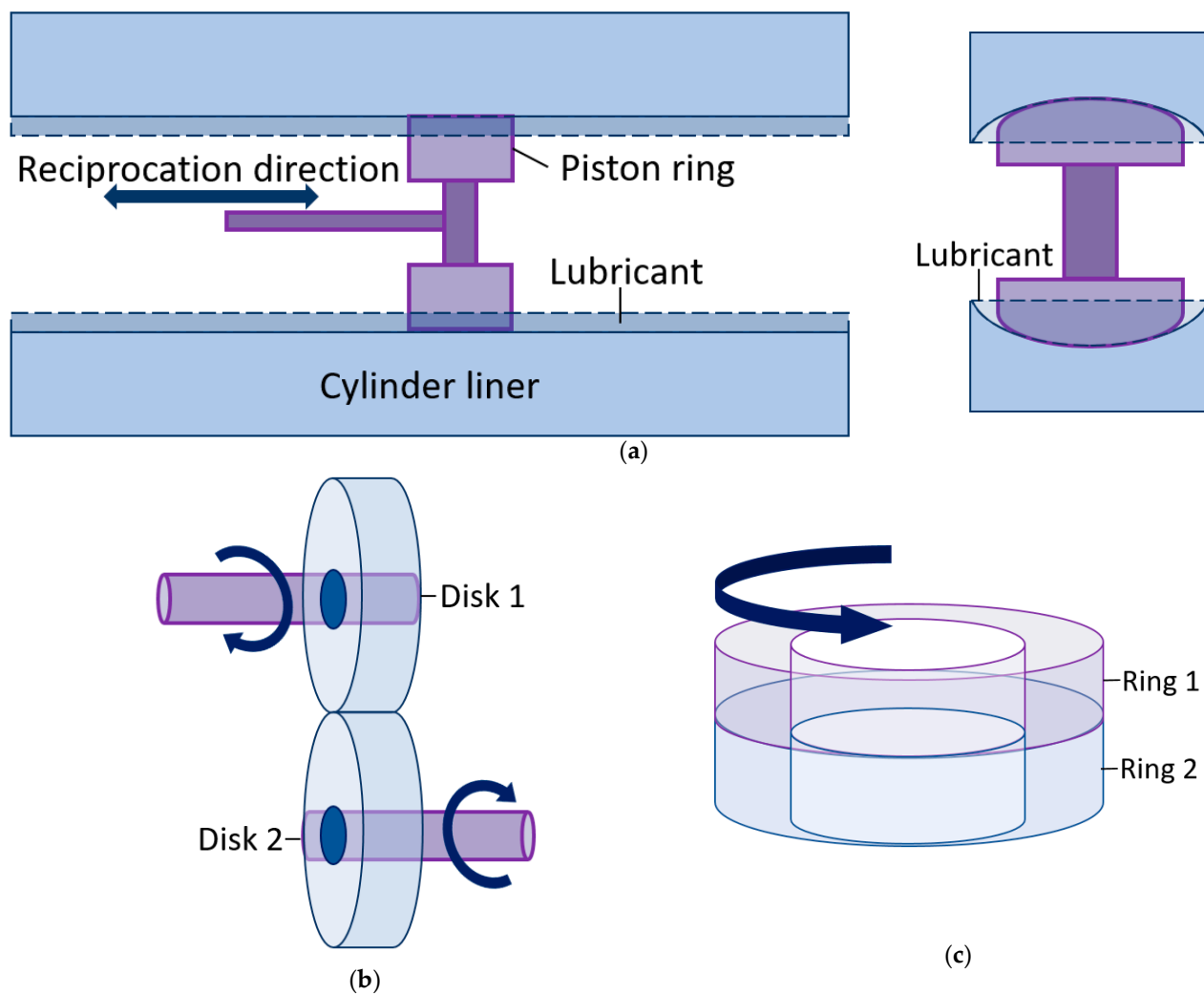
Figure 14. (**a**) piston ring-on-cylinder line, (**b**) two-disk, and (**c**) ring-on-ring configurations.

Table 3. A summary of different tribometers used for testing water-based nanolubricants.

Tribometer	Nanoparticle	Test Parameters			Testing Results			Reference
		Force	Speed	Temp. & Duration	Wear Reduction	Friction Reduction	Optimum Concentration	
Four-balls	hBN	100 N	120–440 rpm	Room temp., 30 min	95.73%	60%	0.05 wt.%	Bai et al. [89]
	Capped Cu	-	1450 rpm	25 °C, 30 min	-	-	-	Zhang et al. [47]
	Cu-SiO$_2$	50 N	1450 rpm	25 °C, 30 min	37%	-	1 wt.%	Zhang et al. [116]
	hBN	392 N	1200 rpm	25 °C, 30 min	14.6%	29.1%	0.7 wt.%	He et al. [159]
	Novel C	0–7200 N	500 rpm	25 °C, 18 s	96%	76%	1.2–2.0 wt.%	Peña-Parás [65]
	MWCNT	-	1450 rpm	Room temp., 30 min	-	-	-	Peng et al. [125]
	CDs-IL	30–80 N	600 rpm	Room temp., 30 min	64%	57.5%	0.015 wt.%	Tang et al. [130]
	Fe$_3$O$_4$-MoS$_2$	294 N	0.479 m/s	30 min	29.7%	34.6%	-	Zheng et al. [86]
	LaF$_3$	100–900 N	1450 rpm	20 °C, 30 min	-	-	0.75–1 wt.%	Zhang et al. [154]
	fullerene–styrene	200 N	1450 rpm	20 °C, 30 min	-	-	-	Lei et al. [150]
	fullerene–acrylamide	200 N	1450 rpm	20 °C, 30 min	-	-	-	Jiang et al. [151]
	GO-TiO$_2$	392 N	1200 rpm	20 °C, 30 min	-	-	0.5 wt.%	Du et al. [84]
	MoO$_3$	392 N	1200–1760 rpm	1800 s	-	-	0.4 wt.%	Sun et al. [56]
	MoS$_2$ and MoO$_3$	392 N	1200–1760 rpm	1800 s	-	-	0.3–0.5 wt.%	Meng et al. [63]
	Multilayer-MoS$_2$	588 N	1200 rpm	30 days	-	-	-	Zhang et al. [111]
	SiO$_2$	-	1760 rpm	Room temp., 10 s	-	-	0.3 wt.%	Bao et al. [59]
	Dual-Coated TiO$_2$	147 N	1440 rpm	-	34.8%	0.17%	1.6 wt.%	Gu et al. [103]
	OA–TiO$_2$	-	1450 rpm	25 °C, 30 min	-	-	0.5 wt.%	Gao et al. [102]
	Nano-TiO$_2$	196 N	60 rpm	30 min	30.6%	64.9%	0.7 wt.%	Sun et al. [50]
	Nano-TiO$_2$	200 N	1200–1450 rpm	Room temp., 30 min	-	-	0.5 wt.%	Kong et al. [49]

Table 3. *Cont.*

Tribometer	Nanoparticle	Test Parameters			Testing Results			Reference
		Force	Speed	Temp. & Duration	Wear Reduction	Friction Reduction	Optimum Concentration	
Four-balls	Nano-TiO$_2$	392 N	1200–1760 rpm	30 min	47.4%	33.8%	-	Meng et al. [52]
	Eu doped	392 N	-	60 min.	0.62–0.37 mm	0.083–0.065	0.5 wt.%	Liang et al. [123]
	Eu	-	-	45–55 °C, 2 h	0.62–0.35 mm	0.083–0.055	0.6 wt.%	Xiong et al. [57]
Pin-on-disk	hBN	400–600 N	300 rpm	25 °C, 30 min	14.6%	29.1%	0.7 wt.%	He et al. [159]
	Ceria	-	50 mm/s	Room temp., 30 min	49%	20%	0.05–0.2%	Zhao et al. [53]
	Cr$_2$O$_3$	20–150 N	50 mm/s	-	-	-	-	Cheng et al. [223]
	GO	10 N	0.02 m/s	21–23 °C, 30 min	-	57%	1 wt.%	Elomaa et al. [139]
	Two phase fluids	20 N	100 rpm	22 °C	-	~0.05	-	Pawlak et al. [224]
Ball-on-disk	Ag-C	1–9 N	100–500 rpm	Room temp., 30 min	40.4%	80.6%	1.0 wt.%	Song et al. [121]
	Polyalkylene Glycol	3 N	24 mm/s	Room temp.	-	Around 20%	0.5 wt.%	Wang et al. [94]
	Al$_2$O$_3$ (also disk on ball)	4–10 N	10–40 mm/s	-	40–50%	40–50%	-	Radice and Mischler [48]
	C dots	10 N	-	Room temp., 1 h	38%	39.66%		Hu et al. [66]
	CQD	2 N	150 cycles/min	Room temp., 12 min	-	30%	-	HuaPing et al. [131]
	Urea modified C	3–7 N	200–400 rpm	30 min	96.70%	80.86%	0.15 wt.%	min et al. [127]
	Hexagonal BN	5.64 N	10.2 mm/s	Room temp, 30 days	-	-	-	Cho et al. [88]
	DDP-Cu	1–4 N	-	25 °C, 30 min	60.5%	45.5%	0.2–0.4 wt.%	Liu et al. [117]
	Diamond	-	80 mm/s	30 °C	88%	70%	2 wt.%	Mirzaamiri [137]
	γ-Fe$_2$O$_3$	4 N	0.20 m/s	Room temp.	-	-	0.6 wt.%	Pardue et al. [55]
	GO/Chitosan	100 N	-	-	47%	84%	-	Wei et al. [145]

Table 3. *Cont.*

Tribometer	Nanoparticle	Test Parameters			Testing Results			Reference
		Force	Speed	Temp. & Duration	Wear Reduction	Friction Reduction	Optimum Concentration	
Ball-on-disk	Graphene quantum dots	100 N	-	Room temp., 60 min	58.5%	42.5%	-	Qiang et al. [135]
	GO-MoS$_2$	0.5–3 N	60 rpm	25 °C	-	50%	-	Liu et al. [225]
	FGO	5 N	300 r/min	30 min	88.1%	41.4%	0.7 wt.%	min et al. [72]
	GO	5–20 N	0.005–0.1 m/s	Room temp	68%	78.5%	0.1 wt.%	Singh et al. [140]
	GO-OLC	2–10 N	200 rpm	Room temp	-	-	0.06 wt.%	Su et al. [80]
	Nanofilm GO	2 N	12 mm/s	25 °C, 60 min	79.7%	43.6%	-	Li et al. [146]
	SiO$_2$-GO	10 N	-	25–35 °C	78.3%	-	0.05 wt.%	Guo et al. [83]
	PEGlated graphene	10 N	-	30 min	81.23%	39.04%	0.05 wt.%	Hu et al. [147]
	Hydroxide	2N	0.024 m/s	25 °C. 45 min	43.2%	83.1%	0.5 wt.%	Wang et al. [93]
	Al$_2$O$_3$-WS$_2$-MoS$_2$	10 N	320 rpm	Amb. Temp.	23.4%	53.89%	-	Kumar et al. [119]
	Black phosphorus	10–70 N	-	-	97.1%	25%	-	Wang et al. [162]
	BP	8–15 N	150 r/min	30 min	61.1%	32.4%	-	Wang et al. [163]
	Si$_3$N$_4$	15, 30, 60 N	0.25 m/s, 0.5 m/s	27 °C, 3600 s	-	-	-	Lin et al. [161]
	Ti$_3$C$_2$	3–10 N	120 rpm, 0.126 m/s	24–26 °C, 1 h	48%	20%	5 wt.%	Nguyen and Chung [91]
	TiO$_2$	5 N	50 mm/s	25 °C, 30 min	-	16.3%	0.4–8.0 wt.%	Wu et al. [14]
	TiO$_2$	20–80 N	50 mm/s	10 min	70.5%	84.3%	4 wt.%	Wu et al. [25]
	NaCl saline	10–100	50 mm/s	1 h	-	-	3.5 wt.%	Wu et al. [226]
	ZnO and Al$_2$O$_3$	10 N	100 mm/s	-	-	56.9%	-	Gara and Zou [122]
	Ceramics	30 N	0.5 m/s	Room temp., 3600 s	54.0%	78.8%	-	Cui et al. [109]
	Chitosan	5–30 N	12–36 mm/s	25 °C, 30 min	69%	40%	0.3 wt.%	Li et al. [95]

Table 3. *Cont.*

| Tribometer	Nanoparticle	Test Parameters			Testing Results			Reference
		Force	Speed	Temp. & Duration	Wear Reduction	Friction Reduction	Optimum Concentration	
Ball-on-disk	Individual additives	3 N	20 mm/s	Room temp. 1 h	-	12%, 30%	0.05%, 0.1%	Tomala et al. [203]
Ball-on-plate	Hard C microsphere	100–300 mN	10 mm/s	30 min	-	-	0.1 wt.%	Wang et al. [124]
	Cu	1–4 N	0.02 m/s	22 °C, 30 min	85–99.9%	80.6%	0.6 wt.%	Zhao et al. [46]
	CuO	-	20 mm/s	22 °C, 30 min	72.6–89.1%	43.2–52.2%	0.8 wt.%	Zhao et al. [54]
	Nano diamond	1 N	360 rpm	25 °C, 30 min	-	40%	-	Jiao et al. [68]
	Graphene and GO	1–8 N	0.08 m/s	30 min	13.5%	21.9%	0.5 wt.%	Xie et al. [77]
	Fluorinated GO	20 N	4 mm/s	Room temp., 2000 s	47%	-	-	Fan et al. [73]
	MGO	5–25 N	-	Room temp., 3000 s	74%	-	-	Gan et al. [142]
	GO-ND	0–1 N	0.4 mm/s	25 °C, 1800 s	-	-	0.1 wt.% GO, 0.5 wt.% ND	Wu et al. [78]
	GO-MD	-	-	250 s	-	0.6–0.01	0.7 wt.% GO, 0.5 wt.% MD	Liu et al. [79]
	Graphene water-based	10 N	0.01 m/s	-	-	-	0.1 wt.% graphene flakes. 1% wt.% graphite	Piątkowska et al. [136]
	Graphene-SiO$_2$	3 N	0.08 m/s	Room temp., 30 min	79%	48.5%	0.5 wt.%	Xie et al. [112]
	Monolayer GO	1.88 N	0.5 mm/s	-	Marginal after 60,000 cycles	~0.05 after 60,000 cycles	0.01 wt.%	Kinoshita et al. [138]
	Oxide graphene	10 N	120 rpm	10 min	-	-	<0.1 wt.%	Song and Li [70]
	Metal doped CDs	40–500 N	-	20–120 min	Up to 43.1%	Up to 73.5%	1.0 wt.%	Tang et al. [227]
	Reduced GO	50–200 N	4mm/s	-	70 µm after 100,000 cycles	Around 0.1 after 100,000 cycles	0.01 wt.%	Kim and Kim [143]

Table 3. *Cont.*

Tribometer	Nanoparticle	Test Parameters			Testing Results			Reference
		Force	Speed	Temp. & Duration	Wear Reduction	Friction Reduction	Optimum Concentration	
Ball-on-plate	PEI-RGO	-	9000 r/min	-	45%	54.6%	0.05 wt.%	Liu et al. [74]
	Protic ionic (PILs)	2–4 N	-	30 °C, 30 min	85%	80%	1 wt.%	Kreivaitis et al. [158]
	MoS_2	20 N	-	25 °C	-	-	0.1 wt.%	Wang et al. [64]
	Naphthalene	100 N	1475 rpm	30 min	-	-	-	Yang et al. [153]
	BPQDs	40–300 N	10 mm/s	30 °C, 20–120 min	56.4%	32.3%	0.005 wt.%	Tang et al. [92]
	CNT/SiO_2	5 N	120 rpm	10 min	-	66.4%	0.5 wt.%	Xie et al. [113]
	rGO	20 mN	4 mm/s	-	-	12 times	5 µL/min	Kim et al. [228]
Ball-on-three-plates	Alumina	10–40 N	20 to 100 mm/s	10 min	22%	27%	2 wt.%	He et al. [16]
	$g\text{-}C_3N_4/GO$	10–35 N	25 to 125 mm/s	25 °C	19.6%	37%	0.06 wt.%	He et al. [18]
	pH-GO	20 N	50 mm/s	-	17.1%	44.4%	0.06 wt.%	He et al. [17]
	MR fluid	0.5 N	1.18 m/s	2–10 min	-	-	1 vol%	Rosa et al. [229]
Block-on-ring	Novel C	245 N	300 rpm	1200 s	96%	76%	2 wt.%	Peña-Parás [65]
	$GO\text{-}Al_2O_3$	10 to 30 N	100 to 400 mm/s	20–25 °C, last 7 min	-	47–64%	0.06 wt.%	Huang et al. [21]
	ZrO_2/TiO_2	100 N	400 mm/s	-	65%	25%	-	Huang et al. [12]
	$GO\text{-}SiO_2$	20 N	109 rpm	Ambient Temp.	-	-	0.16 wt.%	Huang et al. [19]
Ring-on-plate	Alkyl glucopyranosides (AGPs)	50 N	0.1 m/s	Room temp, 1 h	-	>95%	-	Chen et al. [222]
Ball-on-block	MWCNT	50 N	-	30 min	66%	-	-	Ye et al. [129]
	urea-modified FG							Ye et al. [134]
	Stearic acid	-	-	30–500 °C	57–90%	68–83%	-	Ye et al. [96]
Piston ring-on-cylinder	Cellulose	50 N	130–300 rpm	Room temp.	>50%	~75%	2 wt.%	Shariatzadeh and Grecov [148,149]
2 ball-plate	Px-CNTs	5 N	120 rpm	10 min	-	66.4%	0.5 wt.%	Sun et al. [126]

5. Lubrication Mechanism

Due to small sizes and high surface areas, NPs have unique properties that are different from bulk materials. Hence, research groups have focused on the addition of NPs to lubricant dispersions for enhancing the thermophysical and tribological properties [230,231]. Scientists have been committed to understanding the roles of nanoadditives in base lubricants and the lubrication mechanism of synthesised nanolubricants in terms of friction-reduction and anti-wear properties. Numerous mechanisms, including rolling effect, protection film, mending effect, polishing effect, and synergistic effect [232], have been proposed to explain the enhancement of the lubricity.

5.1. Rolling/Ball Bearing Effect

According to the theory of rolling/ball-bearing effect, nanolubricants have outstanding lubricity due to two factors. First, NPs are spherical and they can act as ball bearings under friction. Second, the NPs flatten and create a sliding system between the two friction surfaces, eventually reducing friction and wear [233]. Figure 15a illustrates the rolling/ball bearing mechanism. NPs with a sphere, quasi-spherical, or hemispherical shape play this role. Generally, spherical NPs reduce the COF by converting sliding friction to rolling friction as a result of their morphological properties [233–235]. Some scholars have revealed that these NPs themselves might roll or embed into surfaces [236–238]. Moreover, many scholars have mentioned the ball bearing effect in lubrication mechanism analysis of the water-based nanoadditives including metal and non-metal oxide [54,59,100], composite [86,119], and many more [68,78,92,124,137,159]. In the past few years, it has been noted that due to their spherical shape, metal and non-metal oxides such as SiO_2 [59,100] and TiO_2 [15,25,29] generate a ball bearing effect between sliding surfaces, converting the friction mechanism from sliding to rolling and thus causing friction reduction. NPs will maintain their shape and stiffness under mild conditions [239–241].
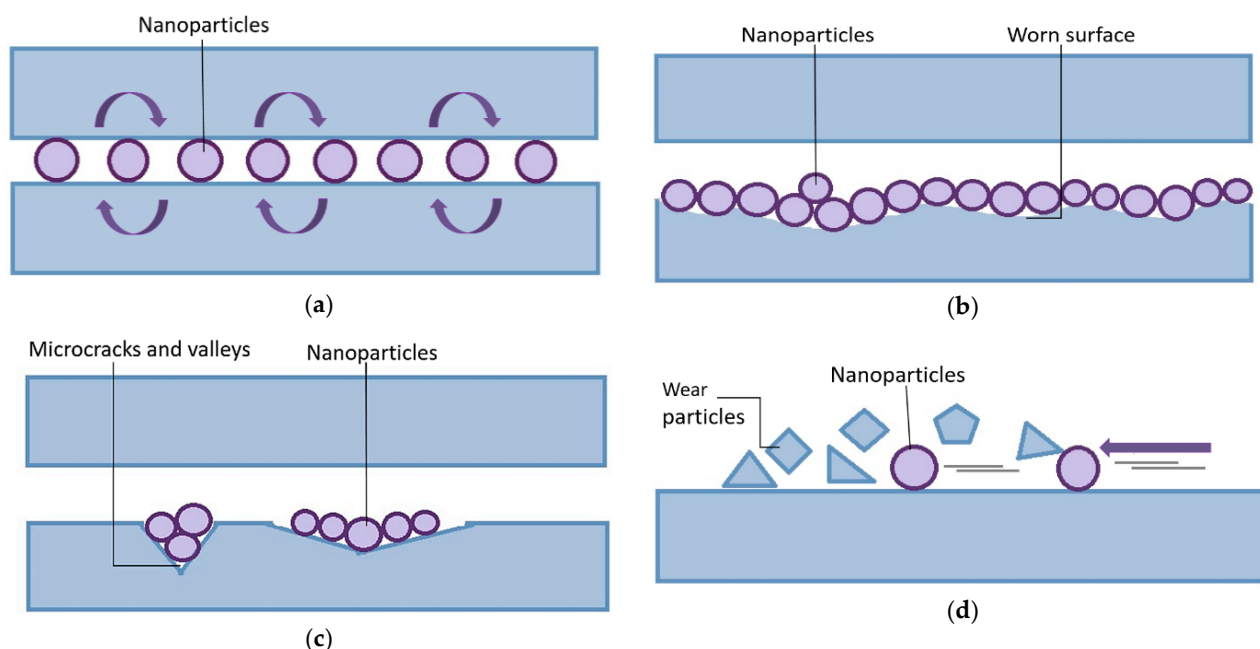
Figure 15. (**a**) Rolling/ball bearing mechanism; (**b**) protective film/tribo-film formation; (**c**) mending effect; and (**d**) polishing/smoothing effect.

On the other hand, stable spherical NPs can enhance bearing capacity and performance under maximum pressure [242,243]. The ball bearing effect of spherical NPs is influenced by the film thickness, and NPs with a diameter close to the film thickness will retain their shape. A transfer film is generated when the film's thickness is less than the NPs'

diameter [59]. During the hot rolling test, Wu et al. [25,29] found that the rolling effect of spherical shaped nano-TiO_2 assisted in reducing wear and friction to a large extent, thereby decreasing the roll roughness and rolling force.

5.2. Protective Film/Tribo-Film

The idea behind this method is the formation of a thin protective film consisting of NPs on the area of frictional contact [236]. The protective film refers to coating the friction surfaces by separating them from direct contact, and it is derived from three aspects. First, the NPs are able to be deposited or adsorbed on the rubbing surfaces to form a boundary film. Second, the NPs are melted as a protective film under friction heat to cover the friction surfaces. Third, the formation of the protective film is produced by tribo-sintering of the NPs, and the compacted and smooth tribo-film is conducive to the decreases in friction and wear. Figure 15b shows the schematics of protective film/tribo-film formation.

It is believed by scientists that the nanofluids have better lubricity than the base lubricant because the NPs can form a protective film over friction surfaces and thereby prevent the friction surfaces from sliding [244–246]. Multiple studies have mentioned the significance of protective film formation using NPs such as graphene based [73,75,77,134,145,147], ionic liquids [155–157], and phosphorus [162]. Some other NPs such as metal oxides [27–29,56–58], diamond [137], and composites [19,113,115,123] are also able to form a protective film on friction surfaces. Based on previous studies, it is concluded that the protective film not only reduces the friction and wear between friction pairs but also helps in isolating air, thus leading to reduced oxide scale thickness during hot steel rolling [27–29]. It is also found that the enhanced wettability of nanofluids caused by the addition of NPs promotes the formation of protective film.

5.3. Mending Effect

Mending effect is very important in moving mechanical parts that are repeatedly loaded and might fail from the crack, as there is the possibility that cracks can spread outside the contact area to other parts of the metal body. Using this technology, the metal surface can become hardened by sintering and filling NPs into macroscopic cracks [236], as shown in Figure 15c. A mending effect has been observed in numerous studies [16,21,27,66,92,117,121]. Many results reveal that NPs act with a mending effect by filling in the surface defects, thereby improving the surface quality [247–249]. Bao et al. [59,100] used SiO_2 NPs to improve the tribological performance of water-based lubricants through the mending effect, which contributed to the decreases in scratches and pits on friction surface with enhancement of anti-wear and friction-reduction properties. To compensate for weight loss, it is particularly important to deposit NPs on the interaction surface [11,59,171,234,249].

Scientists proposed the roles of NPs to self-heal or repair surfaces by depositing them in grooves or scars, which can prevent further wear [250]. Tribo-sintering may occur in the mending process when the frictional heat generated is strong enough to melt the scattered NPs, thus causing permanent deposition of the NPs on the worn surface [219,233]. It is reported that soft metals with a face-centred cubic structure are generally capable of self-repairing [233]. However, the mending effect does not simply include the deposition of the NPs on the friction surface. The melting point of NPs falls significantly as their size decreases. These NPs are thus easy to melt at a high friction surface temperature, thus forming a uniform filler and tightly bonding to the friction surface [233].

5.4. Polishing/Smoothing Effect

The polishing effect can be observed prior to and after using lubricants that contain nanoadditives. The surface roughness is decreased because of NPs deposition on the surface profile [251]. In the polishing/smoothing effect, NPs are used to minimise the roughness of the lubricated surface by abrasion treatment [252], as shown in Figure 15d. NPs deposited on the hollow contour provides smoothness to the metal surface. A number of studies demonstrated that the polishing effect can be contributed by some types of NPs

such as phosphorus [92], metal oxide [27–29,100], and nitride [159]. Under high pressure and speed, NPs flatten the surface peaks to make a smooth tool surface, which in turn greatly improves the surface quality of workpiece.

Nanofluid is an ideal polishing substance that mechanically polishes the friction surface. The tribo-pair contact area increases when harder nanoparticles are used to polish a smoother surface, which reduces friction and meanwhile increases the load-carrying capacity of the nanolubricant. However, the mechanical properties of NPs are poor on a very rough surface. Due to their small size, NPs can only restore rough surfaces at an atomic scale. In other words, a mechanical polishing effect is more evident when the surface of tribo-pair is relatively smooth. In addition to the polishing effect, NPs can be deposited easily in microcracks and valleys as per the mending effect, which also produces smooth surfaces [233].

5.5. Synergistic Effect

Lubricants and modified friction surfaces are often combined with nanoadditives to generate a synergistic effect. Most of the time, NPs perform their lubrication effects through not just one mechanism, but rather a combination of various mechanisms. Furthermore, lubrication conditions can change when various mechanisms are modified. Research on lubrication mechanism analysis has always been focused on the roles of NPs in base lubricants. It is also important to consider the interaction among the NPs, the dispersant, and the base lubricant [233].

Synergistic lubrication effect may improve the tribological performance of nanolubricants by integrating two or more mechanisms, and this effect is usually contributed by composite nanoadditives [21,78,84,115,118,121,225]. A synergistic effect is also reported for some other nanoadditives such as metal carbide [90], nitrides [159,160], and oxides [73,96,108,130,146,147,154], and these nanoadditives themselves play multiple roles in combining two or more lubrication effects together for enhanced lubricity.

5.6. Exfoliation

For the NPs with layered structure, the lubrication mechanisms are different from those of spherical NPs. Tevet et al. [253] pointed out three main lubrication mechanisms in terms of fullerene-like (IF) NPs which have layered hollow polyhedral structure. First, the IF NPs may act as a spacer between the friction pairs, which supplies low frictional force during sliding process, as shown in Figure 16a. Second, the IF NPs can also behave as ball bearings that roll on the friction surface, as shown in Figure 16b. Third, the IF NPs can be exfoliated into nanosheets under certain shear force. The evolved nanosheets are deposited on the asperities of friction surface and thus supply an easy shearing for the subsequent friction process, as shown in Figure 16c. The "exfoliation" is typical lubrication mechanism for layer-structure NPs dispersed in base lubricant.
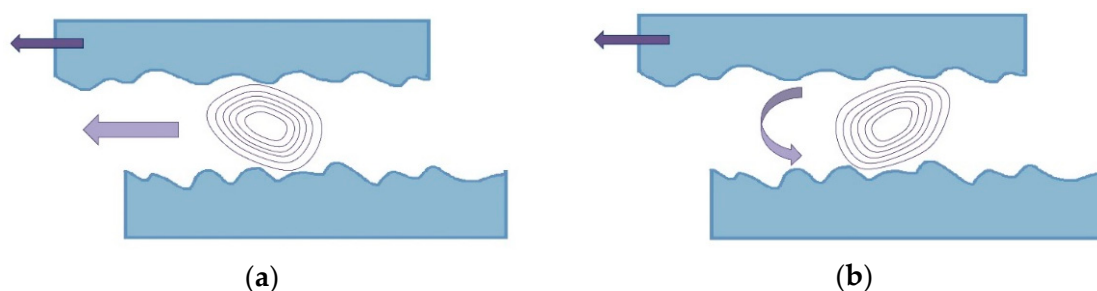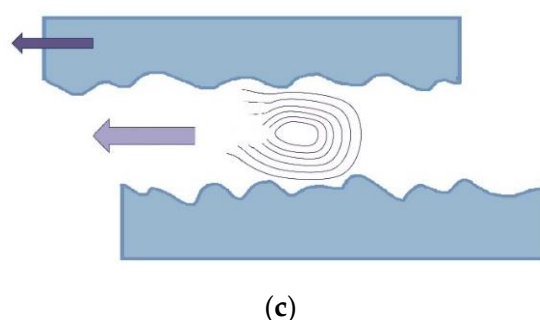

(**a**)　　　　　　　　　　(**b**)

Figure 16. *Cont.*

(c)

Figure 16. Schematic of lubrication mechanism for the lubricants containing nanoadditives with layered structure: (**a**) sliding; (**b**) rolling; and (**c**) exfoliation [253].

IF NPs are inorganic and layered compounds such as fullerenes and carbon nanotubes, with spherical or tubular structures. These concentric layered materials are often solid, though hollow sometimes, and are arranged in an onion shape [254]. This onion morphology is spherical outside and lamellar inside. It is more likely that the onion may have spherical morphology if it is stable, otherwise it may exfoliate and turn into a sheet [255]. One of the benefits of onion structure is the sphere-like shape and the lack of dangling bonds [256]. Su et al. [80] evaluated the lubrication performance of onion-like carbon (OLC) NPs and graphene oxide (GO) sheets, and reported that due to its onion-like structure, OLC may reduce friction and wear in water, producing rolling motion and tribo-film formation during sliding. Due to the protective film formation between adjacent wear surfaces, the 2D structure of GO provided better sliding and shear between adjacent wear surfaces, exhibiting excellent lubricity. Another layer-lattice-structured NPs, hexagonal boron nitride, has also exhibited superb friction-reduction properties, probably through a similar mechanism [246,257].

5.7. Hydration Lubrication

In water-based lubricants, regardless of whether NPs are added or not, water is absolutely the largest component. The water molecule, due to its positive (H atoms) and negative charges (O atom), interacts strongly with charged ions or zwitterions to form stable hydration layers (thin water films) in aqueous media [258]. The hydration layers form hydrated charges between sliding surfaces, which can sustain large pressures due to the reluctance of the hydration water to be squeezed out and meanwhile generate a fluid response to shear [259]. The hydration lubrication mechanism enables a significant friction reduction between surfaces which expose or slide across such hydrated layers under low shear stresses. This striking lubrication mechanism is expected to provide new insight into the boundary lubrication processes in water-based lubricant.

Although these mechanisms are well established, it has always been a matter of debate among researchers. In fact, it has been difficult for any single theory to fully explain the lubrication mechanism in water-based nanolubricants. In this case, further research is needed to establish a more accurate theory of nanolubrication.

6. Application of Water-Based Nanolubricants in Metal Rolling

6.1. Physicochemical Properties of Applied Lubricants

Traditional water-based lubricants are often restricted in practical metal rolling due to their low viscosity, poor wettability on roll surface, and harsh corrosion of base water, despite their eco-friendliness, low-cost, noninflammability, and outstanding cooling performance. The physicochemical properties of applied lubricants including viscosity, wettability, and corrosivity are crucial to the lubrication performance.

Viscosity is a measurement of the tendency of liquid to resist flow, and it is defined as the ratio of the shear stress to the shear rate [82]. The liquid is known to be Newtonian or non-Newtonian when the viscosity is constant or varies, respectively, at different val-

ues of shear rate [260]. The viscosity of lubricant is dependent on many factors, and it influences lubrication performance in most cases. It has been reported that the viscosity of base lubricant increases with the addition of NPs [25,261,262], and it also increases with the increase of their mass fraction [173]. In addition, the viscosity decreases with the increase of temperature [263], and it is a function of pressure throughout the inlet zone in metal rolling [264]. Most importantly, a higher viscosity leads to a lower COF due to a transition of lubrication regime from boundary lubrication into mixed or hydrodynamic lubrication [241], which indicates an increase in the thickness of lubricating film as per the well-known Stribeck curve [4]. This increased film thickness restrains the work rolls and workpiece from direct contact, leading to decreased friction in the contact zone.

Wettability is one of the most important lubricant characteristics, which reveals how well a lubricant can wet a solid surface [265]. Wetting of surfaces in contact is of vital importance to decrease friction and wear, which relates directly to the decreases of rolling force and roll wear in metal rolling [29,266]. This result is ascribed to the phenomena that excellent wettability facilitates the formation of a lubricating film [112], and also helps retain the effective lubricants on work roll surfaces [28]. In general, wettability can be characterised by the measurement of contact angle on a solid surface, and a smaller contact angle indicates a better wettability [267]. It has been reported that the wettability of base lubricant can be significantly improved by adding NPs, and the addition of dispersant or surfactant also enables improved wettability due to their functional groups [25].

Corrosivity of water-based lubricants often plays a negative role in aggravating the surface quality of rolled products, especially for ferrous materials. Water itself and pH values of the lubricants both determine the corrosion effect of as-prepared water-based lubricants on metal surfaces. It has been proved that the corrosion resistance of water can be enhanced by adding water-soluble additives. For example, nanoadditives such as fluorinated graphene [72], surface-modified CuS NPs [62], and GO-TiO$_2$ [84] are able to retard the corrosion of steel by forming a protective film on the steel surface. Corrosion inhibitors such as Triethanolamine (TEA) [92] and sodium dodecyl benzene sulfonate (SDBS) [63], have also been used to minimise the corrosivity of water-based lubricants. On the other hand, water-based lubricant with a pH value of 7 and above leads to insignificant corrosion on the rolled surface [76]. Nevertheless, the optimal pH values in the lubricants should be determined with the consideration of their effects on the dispersion stability of the lubricants. In some cases, the corrosion resistance of water-based lubricants may be negligible, especially in hot rolling of steels and cold rolling of non-ferrous metals such as aluminium and magnesium. However, special attention should be given to the corrosion effect of water-based lubricants on cold rolling of ferrous metals.

6.2. Hot Rolling of Steels

Hot rolling of steels is applied to obtain not only the required dimensions and mechanical properties, but also satisfying surface finish [268]. Friction and wear are unavoidably generated between the work rolls and the workpiece, which results in increased consumption of energy and damage of work rolls [269,270]. Water-based nanolubricants are emerging to substitute the traditional oil-containing lubricants to resolve these issues with environmental concern. The use of water-based nanolubricants in hot steel rolling also exhibits a great potential in reducing the thickness of oxide scale, improving the surface quality of rolled products, and refining the grains in rolled steel. The water-based nanolubricants can also act as better coolants of work rolls than conventional cooling water due to their enhanced thermal conductivity [271], which further prolongs the roll service life by replacing the cooling water using a lubricant supply system. In view of these, energy consumption of the rolling mill can be lowered, and rolling high-strength steels with heavy reduction can thus be readily achieved within the limits of mill load. Meanwhile, the roll changing frequency would be reduced, and the mill configuration would be simplified, thus leading to increased productivity and decreased operation cost. The overall quality and yield together with the properties of rolled products are therefore greatly enhanced.

As the hot rolling process involves harsh working conditions such as high temperature and pressure, special requirements are placed on the physicochemical properties of the nanoadditives and other chemical additives. The applications of different types of water-based nanolubricants in hot rolling are comprehensively reviewed in the subsequent sub-sections in terms of their effects on rolling force, surface morphology, oxidation behaviour of steel, and microstructure obtained after rolling.
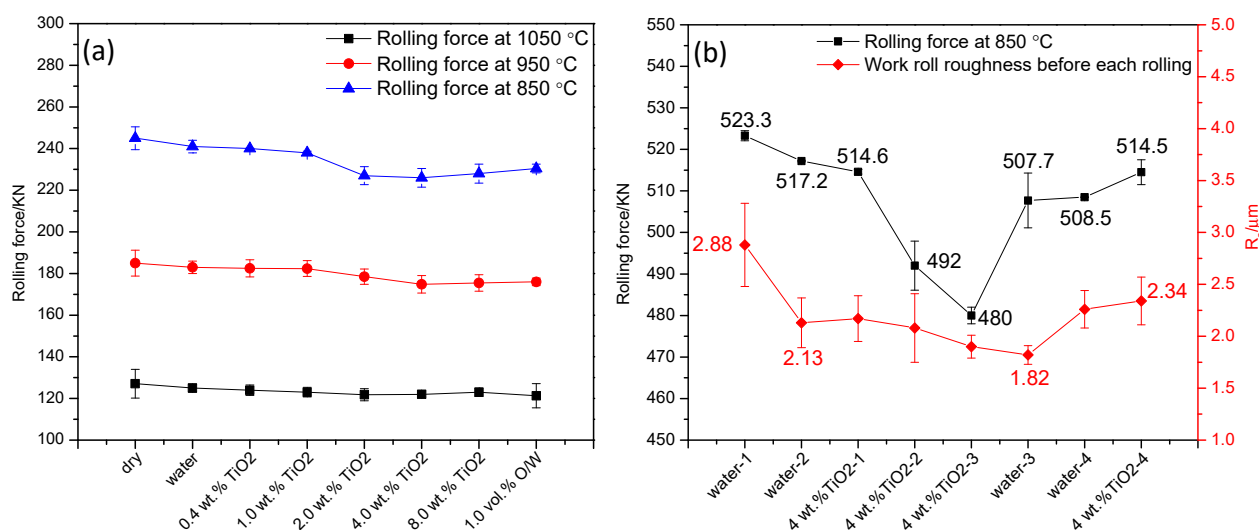
6.2.1. Rolling Force

In general, rolling force data during hot steel rolling are measured through two individual transducers placed at both the drive and the operation sides over the bearing blocks of the top work roll. The presence of lubricants between the work rolls and the workpiece enables a decrease in friction and hence the rolling force is lowered by up to 25% [272]. The value of rolling force is one of the key indicators that evaluates the energy expenditure during hot steel rolling.

TiO_2 water-based nanolubricants used in hot steel rolling were first reported in [273]. The rolling force obtained using the lubricant with 2% anatase TiO_2 decreased in each pass, and the total decrease reached up to 20%, in comparison to that obtained under dry condition. However, there was a lack of experimental evidence to underpin the analysis of lubrication performance, and the role of TiO_2 NPs was not well understood. The effects of TiO_2 concentration and rolling parameters on the rolling force were not discussed either. In light of this, single-pass hot steel rolling tests were conducted to investigate the influences of TiO_2 concentration and rolling temperature on the rolling force [29]. It was found that the use of 4% TiO_2 lubricant led to the lowest rolling force at rolling temperatures of 850 and 950 °C, while the rolling force obtained under 1050 °C did not vary significantly under all the lubrication conditions (see Figure 17a). The mechanisms of the decrease in rolling force were dominated by rolling and mending effects together with the formation of protective film, and they were demonstrated through cross-sectional SEM-EDS analysis. The hot rolled steel samples observed under SEM are, in fact, inevitably involved in grinding and polishing processes, which may affect the distribution of TiO_2 NPs and therefore the understanding of corresponding lubrication mechanisms. To overcome this drawback, a focused ion beam (FIB) foil was cut from the surface of rolled steel, and then observed under TEM to identify the NP distribution through EDS mapping [28]. The synergistic effect of lubricating film, rolling, polishing, and mending was thus confirmed to contribute to the predominant lubrication mechanisms. The effect of work roll roughness on the rolling force was also examined, which has been neglected by the majority of researchers in the field of hot steel rolling [25]. This revealed a significant research finding that the continuous use of TiO_2 water-based nanolubricants was inclined to enable a successive decrease in rolling force up to 8.3% due to the polishing on work roll surface (see Figure 17b). Some other researchers applied composite nanomaterials such as MoS_2-Al_2O_3 as the nanoadditives in water, and the average rolling force within five rolling passes was reduced by 26.9% compared with the base fluid [118]. Another notable finding was that the effect of MoS_2-Al_2O_3 lubricant on the decrease in rolling force was superior to that of the lubricant with individual nanoadditive, owing to the synergistic effect of the composite nanoadditives.

Although significant decrease in rolling force has been achieved in [25,28,29,118,273], the nanoadditives used in these lubricants all had particle sizes less than 100 nm, which brought forth extremely high material cost especially when large quantities of lubricants were applied, let alone the combination of two or more nanoadditives. Beyond this, the nanolubricants have always been prepared using complex chemical agents, followed by subsequent processes including ultrasonic treatment, which led to extra production cost. All these disadvantages have greatly restricted the application and popularisation of water-based nanolubricants in industrial-scale hot steel rolling. Accordingly, relatively coarse TiO_2 NPs (~300 nm in diameter) were adopted to replace the expensive nanosized particles in water-based lubrication formula [24]. Novel dispersant (SDBS with a linear structure) and extreme pressure agent (Snailcool) were added to compensate the degradation of

lubrication performance caused by coarsened TiO_2 NPs. These TiO_2 water-based nanolubricants were prepared using mechanical agitation without applying ultrasonic treatment. Nevertheless, the rolling force could be decreased up to 8.1% in a single-pass hot rolling at 850 °C when using 4% TiO_2 lubricant.

An overview of the typical representatives of the use of water-based nanolubricants in decreasing rolling force is presented in Table 4. The total decrease in rolling force is expected to be more significant upon the use of lubricants in multi-pass hot steel rolling.

Figure 17. (**a**) The rolling force obtained in each single pass under different lubrication conditions at 1050, 950, and 850 °C [29]; (**b**) the rolling force varying with the work roll roughness at 850 °C under water and 4 wt.% TiO_2 lubrication [25]. (Rolling reduction of 30% in each single pass; rolling speed of 0.35 m/s).

Table 4. The decrease in rolling force using different types of water-based nanolubricants under certain rolling parameters.

| Workpiece & Dimensions	Lubricant	Benchmark	Rolling Temp.	Rolling Reduction	Rolling Speed	Decrease in %	Ref.
Mild steel with 30 mm in thickness	2% anatase TiO_2, SHMP	Dry condition & Water	~950–750 °C	~81.8% in five passes	-	Up to 20% in the final pass	[273]
Mild steel 300 × 50 × 8 mm³	0.4–8% TiO_2, 0.004–0.08% PEI, 10% glycerol	Dry condition & Water	~1050–850 °C	~30% in one pass	0.35 m/s	Up to 8%	[29]
Mild steel 300 × 100 × 8 mm³	1–8% TiO_2, 0.01–0.08% PEI, 10% glycerol	Dry condition & Water	~850 °C	~30% in one pass	0.35 m/s	Up to 6.8%	[28]
Mild steel 300 × 91 × 8.5 mm³	2% & 4% TiO_2, 0.2% & 0.4% SDBS, 10% glycerol	Water	~850 °C	~30% in one pass	0.35 m/s	Up to 8.3%	[25]
Mild steel 100 × 70 × 30 mm³	MoS_2-Al_2O_3, glycerol, TEOA, SDBS, and SHMP	Base fluid	~1000–800 °C	~86.7% in five passes	1 m/s	Up to 26.9%	[118]
Mild steel 300 × 100 × 12 mm³	2% & 4% TiO_2, 0.1% & 0.2% SDBS, 10% glycerol, 1% Snailcool	Water	~850 °C	~27% in one pass	0.35 m/s	Up to 8.1%	[24]

6.2.2. Surface Morphology of Rolled Steel

Surface morphology of hot rolled steel strips, i.e., the surface topography of oxide scale, can be characterised in terms of surface roughness measurement and microscopic observation, which is directly related to the assessment of surface quality. In the case of pickle-free as-hot-rolled steel strip, in particular, the surface roughness plays an important role in the downstream processing such as sheet metal forming, coating, and stamping [274,275]. It has been of great interest in recent years to use TiO_2 water-based lubricants to improve the surface morphology of as-hot-rolled steel strips [24,25,28,29,52]. Among these studies, a typical example is the use of 4% TiO_2 lubricant dispersed with PEI and glycerol, which yielded the smoothest strip surface after rolling according to the 3D surface morphologies (see Figure 18) [28]. The surface roughness of the rolled strip under dry condition can thus be improved by up to 19.5% (see Figure 19). Some other researchers used SiO_2 NPs (<0.5%) as nanoadditives in the base lubricant to improve the surface morphology of hot rolled strips [100]. The main mechanisms of the decrease in surface roughness were derived from mending and polishing effects of SiO_2 NPs. These SiO_2 NPs not only filled the surface defects such as pores and cracks, but also removed the peaks protruded from the surface [29]. The other mechanism that contributed to the decrease in surface roughness was the formation of tribofilm, and hence the direct contact between the work roll and the workpiece was relieved [276]. When the concentration of nanoadditive exceeded the optimal one, the agglomeration of NPs might aggravate the friction and wear in the contact zone, thereby increasing the surface roughness. On the contrary, a nanoadditive concentration lower than the optimal one resulted in insufficient lubrication, and therefore an insignificant effect on the decrease in surface roughness.
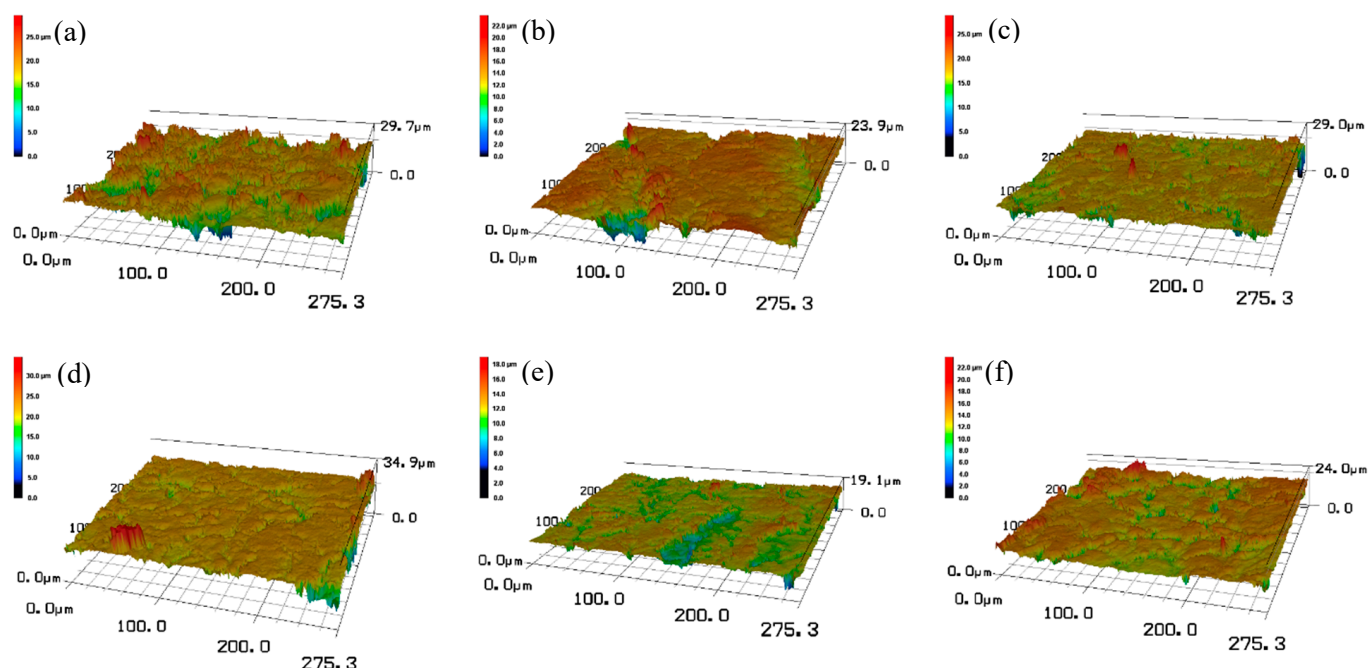
Figure 18. 3D profiles of surface morphologies of rolled steels at 850 °C under different lubrication conditions of (**a**) dry, (**b**) water, (**c**) 1.0 wt.% TiO_2, (**d**) 2.0 wt.% TiO_2, (**e**) 4.0 wt.% TiO_2, and (**f**) 8.0 wt.% TiO_2 [28]. (Rolling reduction of 30% in each single pass; rolling speed of 0.35 m/s).
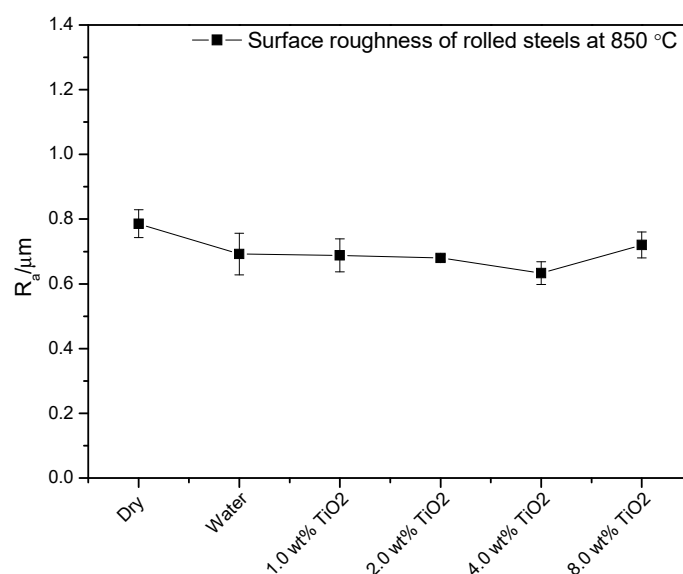
Figure 19. Surface roughness of rolled steels at 850 °C under different lubrication conditions as shown in Figure 18 [28]. (Rolling reduction of 30% in each single pass; rolling speed of 0.35 m/s).

6.2.3. Oxidation Behaviour of Steel

As hot steel rolling is normally conducted at the temperatures ranging from 800 to 1050 °C, significant oxidation occurs instantaneously in air [268]. The oxide scale formed on a hot rolled steel strip plays a prominent role in the subsequent industrial processes, including pickling, cold rolling, heat treatment, and electrolytic tinning [277]. In most cases, as-hot-rolled steel strip needs to suffer pickling, during which the oxide scale is removed by the use of acid treatment to obtain a high-quality surface for upcoming cold rolling. The oxides descaled as such have a dramatic impact on the consumption of acid and the yield of finished products. Decreasing oxide scale thickness is thus a highly desirable target in practical hot rolling production line. In some other cases, it is required to produce pickle-free as-hot-rolled steel strip that has 'tight oxide scale' formed on the strip surface prior to downstream forming [278]. Besides the roughness of the strip surface, the constitution of oxide phases in the scale also has a significant effect on the tribological feature during metal working [279]. Taking the oxide scale formed in mild steel as an example, hematite increases friction and wear as abrasive behaviour due to its high hardness, while magnetite and wustite are more ductile and hence resistant to wear [280]. As a whole, thin and tight oxide scale with considerable amounts of magnetite and wustite is always preferred after hot steel rolling.

Several studies were devoted to decreasing the oxide scale thickness during hot steel rolling by the use of various nanoadditives in water, including Eu-doped $CaWO_4$ NPs [276], SiO_2 NPs [100], MoS_2-Al_2O_3 nanocomposite [118], and TiO_2 NPs [24,28,29,52]. Some possible mechanisms of the decrease in oxide scale thickness have been proposed. First, the increase in strip deformation leads to the decrease in oxide scale thickness [275]. Second, the NPs fill in the voids of oxide scales and then prevent oxygen from penetrating into steel matrix for further oxidation [52]. Third, the NPs deposit on the strip surface to form a protective film that isolates oxygen and thus reduces the diffusion of O^{2-} into oxide layers [118]. These so-called 'mending effect' and 'protective film' can be characterised using SEM or TEM, in which the distribution of NPs can be clearly identified in the oxide layers [28,29]. The effects of using water-based nanolubricants on steel oxidation in these studies, however, were only confined to the entire thickness of oxide scale. It is also very important to systematically examine the formation and evolution mechanisms of different oxide phases during hot steel rolling. Given this point, Wu et al. [27] detailed the effect of water-based nanolubrication on the oxidation behaviour of steel through quantitative

analyses of the oxide phases by the use of Raman microscope and SEM along with image processing software Image J. The schematic illustration of oxide scale formed on steel surface under no deformation (sampled from the tapered edge of steel workpiece), dry or water condition, and TiO_2 nanolubrication is presented in Figure 20. For non-deformed steels (see Figure 20a), a typical three-layered oxide scale was formed with a dominant inner layer of wustite, intermediate layer of magnetite, and top layer of hematite, as well as the magnetite seam at the scale/substrate interface and proeutectoid magnetite precipitated inside the wustite layer. For the steel under dry or water condition (see Figure 20b), considerable amounts of cracks and pores were generated, thereby causing fast conversion of magnetite to hematite near the scale surface and wustite to magnetite close to the scale/substrate interface. When TiO_2 water-based nanolubricants were used (see Figure 20c), TiO_2 NPs not only reduced the friction and the rolling force due to rolling effect, but also enabled the formation of protective film which was a barrier to inhibit oxygen diffusion. These effects decreased the extent of oxide deformation and therefore the porosity and cracks in oxide scale. As a result, the channels for oxygen penetration were reduced, which thus slowed down the conversions of wustite to magnetite and magnetite to hematite.
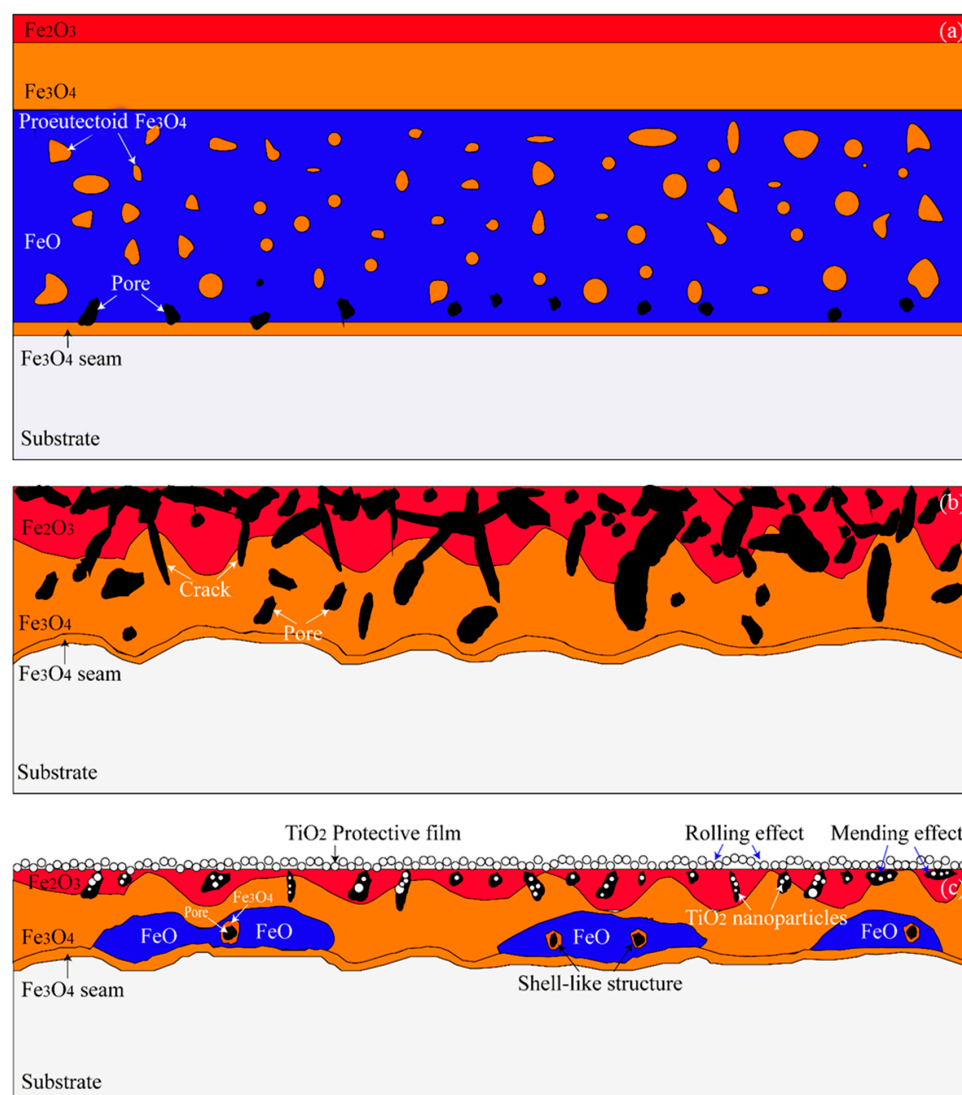
Figure 20. Schematic illustration of oxide scale formed on steel surface under (**a**) no deformation, (**b**) dry or water condition, and (**c**) TiO_2-containing nanolubrication condition during hot steel rolling [27].

For the steel experiencing hot rolling, in general, the conversions between different oxide phases follow the reactions below [27]:

$$6FeO + O_2 = 2Fe_3O_4 \tag{6}$$

$$4Fe_3O_4 + O_2 = 6Fe_2O_3 \tag{7}$$

$$4FeO = Fe_3O_4 + \alpha\text{-}Fe \tag{8}$$

Equations (6) and (7) exist at a temperature above 570 °C, while Equation (8) exists during cooling process at temperatures below 570 °C. The formation of proeutectoid magnetite and magnetite seam is related to the eutectoid reaction in Equation (8) [281,282].

6.2.4. Microstructure of Rolled Steel

It has been widely accepted that the steel's microstructure largely determines its mechanical properties which can be greatly enhanced by grain refinement and phase transformation [283]. For a steel with specified chemical compositions, controls of deformation during rolling and cooling rate after rolling are the dominating strategies to attain desired microstructure and targeted mechanical properties [284]. During hot steel rolling, heavy reduction and accelerated cooling are two of the most effective ways to refine the grains in steels [285]. In recent years, some researchers have been committed to applying water-based nanolubricants during hot steel rolling, instead of conventional ways, to achieve grain refinement. Nanolubricants containing 0.1–0.5 wt.% SiO_2, for instance, were used to refine the grain size in microstructure during hot rolling of ASTM 1045 steel within 5 passes from 1000 to 750 °C [100]. Nano-TiO_2 lubricants were also used to refine the grain size of rolled strips by around 50% after 5-pass hot rolling [52]. In particular, Wu et al. [28] conducted single-pass hot steel rolling at 850 °C using TiO_2 water-based nanolubricant, and found that the grain size of ferrite was refined up to 50.5% through statistical analysis of size distribution in the surface microstructure of rolled steels (see Figure 21). The possible factors that contribute to the decrease in grain size during hot steel rolling include the cooling rate of nanolubricant and the actual rolling deformation. On one hand, adding NPs into water increases the lubricant's thermal conductivity, and therefore the enhancement in cooling rate [185,261,286,287]. At an instant contact of work rolls with the workpiece, the lubricant in between acts as a coolant that offers a higher cooling rate than that of non-lubrication conditions. In this case, the increase in cooling rate leads to the increase in the number of nucleation sites for ferrite grains, and meanwhile a higher cooling rate enables the ferrite grains to pass through the high temperature region faster, thus shortening the time for ferrite growth [288]. Therefore, both the increased nucleation of ferrite and the retarded grain growth prompt the grain refinement due to enhanced cooling rate. On the other hand, the decrease in rolling force enabled by the use of nanolubricants gives rise to the decrease in exit thickness due to reduced spring-back value according to the Gaugemeter equation [289], where the exit thickness is the sum of the height of roll gap and the spring-back value. Given the increase in rolling deformation, the lattice distortion energy increases, and the dislocation density also increases, which respectively provides the driving force and nucleation sites for grain nucleation and therefore the grain refinement [290]. In some other cases, however, the grain size of surface microstructure would not change significantly after hot rolling with water-based nanolubricants [118,276], which might be ascribed to the slight differences in the deformation rate and the cooling rate of the lubricants being used.
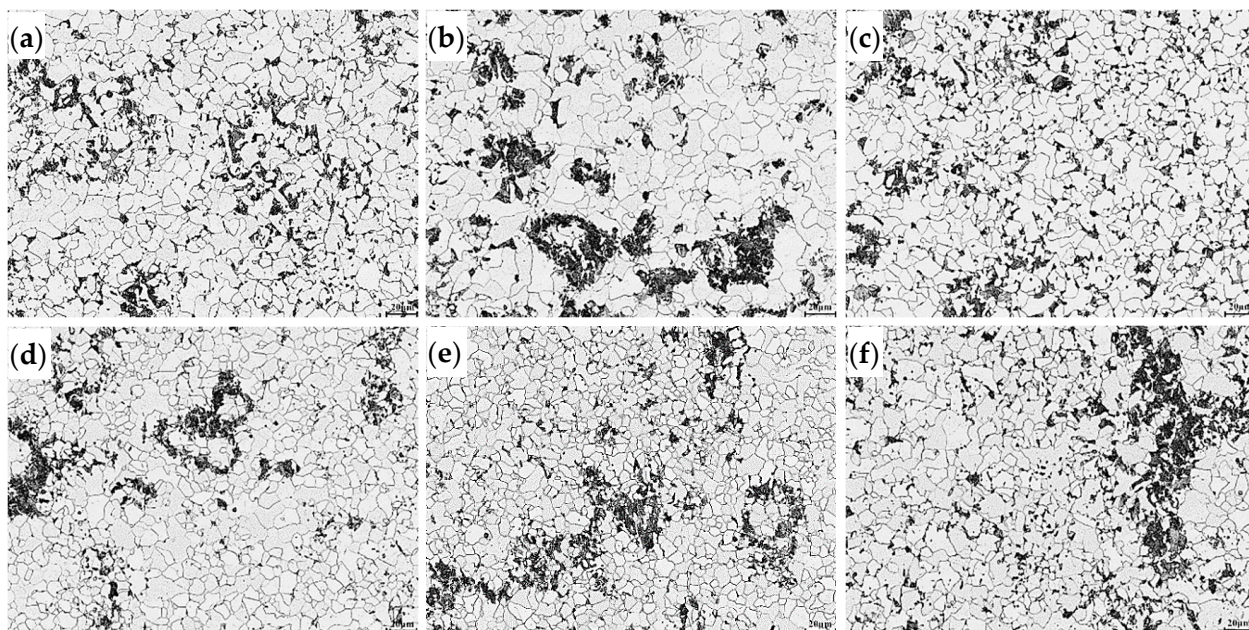
Figure 21. Surface microstructures of rolled steels at 850 °C under different lubrication conditions of (**a**) dry, (**b**) water, (**c**) 1.0 wt.% TiO_2, (**d**) 2.0 wt.% TiO_2, (**e**) 4.0 wt.% TiO_2, and (**f**) 8.0 wt.% TiO_2 [28]. (Rolling reduction of 30% in each single pass; rolling speed of 0.35 m/s).

6.3. Cold Rolling of Steels

In most cases, hot rolled steel strips experience subsequent cold rolling which is conducted at ambient temperature to obtain higher surface quality, special surface textures, or dimensional accuracy [291]. Due to the plastic deformation of workpiece in cold rolling, similar to hot rolling, friction exists between the work roll and the workpiece, and therefore the wear of work rolls is generated. To relieve the friction and wear occurred in the contact zone, rolling lubricants are also extensively applied in cold steel rolling. The requirements for cold rolling lubricants are a bit different from those for hot rolling ones in terms of rolling temperature and corrosive property of the lubricants. Nevertheless, the lubrication mechanisms, in general, are at least similar for both rolling processes.

It has been reported that the use of 0.7 wt.% nano-TiO_2 water-based rolling lubricant would largely decrease the surface scratches and adhesion defects on rolled steel surface [50]. However, the corresponding lubrication mechanisms were not well understood. Furthermore, 2D materials such as MoS_2, MoO_3, and graphene have also presented great potential in cold steel rolling due to their weak interlayer interaction and easy sliding nature between neighbouring atomic layers [292]. For example, water-based MoS_2 nanolubricant was applied in cold rolling of a low-carbon steel, and the results revealed that both the rolling force and the minimum rolling thickness obtained under base lubricant were decreased even using the recycled MoS_2 nanolubricant [63]. As nano-MoS_2 used as a lubricant additive would be readily oxidised and then converted to nano-MoO_3 under cold rolling conditions, they also applied MoO_3 water-based lubricant in a four-high cold rolling mill [56]. The rolling force and power were found to be significantly reduced in each rolling pass, and the minimum rolling thickness was apparently thinned, owing to a lubricating film composed of MoO_3, MoO_2, and $Fe(OH)_3$ formed on strip surface. Graphene, as another promising nanoadditive in water, has also been extensively studied over the past five years [67,132]. As a matter of fact, graphene oxide (GO) instead of graphene has been more commonly used in water due to the presence of hydrophilic groups such as hydroxyl, carboxyl, and epoxy which relieve the agglomeration caused by π-π stacking interaction [142,145]. However, the pristine GO suspension without pH modification is acidic, which is detrimental to the strip quality [17]. In light of this, Meng et al. [76] used tri-

ethanolamine (TEA) to prepare alkaline GO aqueous lubricants that were feasibly applied in cold steel rolling. The results demonstrated that the use of alkaline lubricant with pH 9 resulted in the best lubrication performance by distinctly reducing the rolling force in each pass, and the minimum rolling thickness after 7-pass rolling was 21.36% lower than that without using lubricant. The lubrication mechanisms were proposed as the combination of mending effect and formation of physically adsorbed layers.

Given the excellent tribological characteristics of 0D and 2D materials as individual additives in water, GO-based composites are attracting considerable research interest in the area of water-based nanolubrication, which exhibits improved tribological properties by combining two or more components through a synergistic effect [12,19–21]. In light of this, Du et al. [84] conducted cold steel rolling by means of 0.5 wt.% GO-TiO_2 nanolubricants in comparison with 0.5 wt.% GO and 0.5 wt.% TiO_2 nanolubricants. The results indicated that the hybrid nanolubricant exhibited better tribological performance than the lubricant with individual nanoadditive. Beyond that, the strip rolled with GO-TiO_2 nanolubricant had the minimum rolling thickness and surface roughness, and meanwhile the rolling force was the lowest among all the lubricants being used. The exceptional lubricating properties of GO-TiO_2 nanocomposite were caused by the excellent dispersion stability and the formation of absorption films, carbonaceous protective films and transfer films.

6.4. Cold Rolling of Non-Ferrous Metals

Magnesium (Mg) alloys, owing to their exceptional physicochemical properties such as low density, high strength/weight ratio, good damping performance, superb biocompatibility, excellent machinability, and castability, have been widely used in many engineering applications including transportation, electronics, aerospace, biomedical, and energy sectors [293]. During the forming of Mg alloys, generating severe friction and wear between the tool and the workpiece is inevitable, which may result in inhomogeneous deformations, shortened tool life, and poor surface quality of workpiece [294]. To overcome these disadvantages, the use of suitable lubricants is essential in the forming process. Although some eco-friendly lubricant additives, for instance, N-containing compounds [295], borates [296], and ionic liquids [297] have been developed for forming Mg alloys, they still raise some issues such as poor extreme pressure property, complex synthesis process, and high material cost. To date, there have been few choices of lubricants for the forming process of Mg alloys, while water-based nanolubricants are becoming increasingly popular due to their minimum impact on the environment, low cost, desirable recyclability, and exceptional lubrication performance. For example, graphene and graphene oxide (GO) have been adopted as water-based lubricant additives for steel-Mg alloy contacts through ball-on-plate tribo-testing, and 0.5 wt.% GO lubricant has been proposed for the forming of Mg alloys due to its prominent tribological performance in the reduction of COF and wear rate of Mg alloy plate [77]. It has been always anticipated that hybrid nanolubricants provide possibilities to further improve the tribological performance of the lubricant with individual nanoadditive through a synergistic effect of two or more components. Based on this, SiO_2/graphene composite was dispersed in water to evaluate their tribological performance for Mg alloy rolling [112]. It was found that the combinations of 0.1 wt.% nano-SiO_2 and 0.4 wt.% graphene displayed the best friction-reduction and anti-wear properties among all the SiO_2/graphene mixing ratios. During the cold rolling of Mg alloy under a single-pass reduction of 10%, the rolling force and rolled surface roughness obtained with dry rolling were decreased by up to 12% and 42.4%, respectively, when using the nanolubricant with the optimal SiO_2/graphene combinations. It has also been documented that SiO_2/nanotube hybrid water-based nanolubricant with a mass ratio of 0.3:0.2 can be used for Mg alloy forming according to its excellent tribological properties and load-carrying capacity as well as formation of stable lubricating film on the surface of Mg alloy [113]. These research findings have provided new insights into the potential of applying carbon-based aqueous nanolubricants in Mg alloy forming.

7. Conclusions and Outlook

In this paper, we provide a comprehensive overview of recent advances in water-based nanolubricants with particular emphasis on the preparation of different types of nanolubricants, the methods to evaluate their dispersion stability and tribological properties, the discussion on lubrication mechanisms, and their application in metal rolling. Among all the candidate nanoadditives used in water, carbon-based nanomaterials have attracted the most attention due to their exceptional physicochemical properties and unique chemical structures. Nanocomposites with carbon-based nanomaterials as constituent materials have shown better performance and greater potential than individual component in water-based nanolubricants. Although some water-based nanolubricants have presented remarkable performance in metal rolling, great efforts are still needed to well understand the behaviours of the nanoadditives and reduce their material and preparation costs for accelerating their applications on an industrial scale. Some research directions that deserve further exploration are provided as follows.

- Ensuring long-term dispersion stability of nanoadditives in water is still a big challenge. The interaction among different lubricant components needs to be investigated for the perfection of the theories of dispersion stability.
- For the application in metal rolling, the formulation of water-based nanolubricants needs to be optimised to further enhance their physicochemical properties in terms of dispersion stability, wettability, and extreme pressure property. Special attention should be given to the strategies for reducing material and preparation costs of the applied nanolubricants.
- The application of water-based nanolubricants in hot steel rolling has exhibited positive effects on the decreases in rolling force, rolled surface roughness, and oxide scale thickness, and also enabled refined grains in microstructure. However, the lubrication effects on controls of profile, flatness, and texture have been rarely involved. More studies are also needed to examine the grain refinement mechanism and attain maximally refined grains, which is a promising and economical technique to significantly promote the overall properties of hot rolled steels.
- For the case of application of cold steel rolling, it is of vital importance to have more focus on the study of the corrosive property of applied water-based nanolubricants. In addition to the lubrication effects on rolling force and surface quality, extra attention should be paid to those on rolling texture and shape control.
- Although certain water-based nanolubrication mechanisms in rolling of steels have been proposed through analysis of post-rolling specimen by means of electron microscopy, in situ observation of NPs and demonstration of their motion behaviour have not been specifically conducted. To have a systematic and comprehensive understanding of the lubrication mechanisms, varying rolling parameters such as rolling temperature, rolling reduction, and speed should be employed, and corresponding multi-scale numerical simulation can be carried out.
- As pointed out earlier, work roll service life can be prolonged using water-based nanolubricants, which largely reduces the roll changing frequency and thus enhances the productivity of rolling mill. However, no research has been conducted to quantitatively evaluate the wear of work rolls under water-based nanolubrication conditions.
- The use of green lubricant is becoming mainstream in sustainable manufacturing. It is of vital importance to develop a cost-effective recycling technology for waste water-based nanolubricants.

References

1. Bhushan, B.; Israelachvili, J.N.; Landman, U. Nanotribology-Friction, Wear and Lubrication at the Atomic-Scale. *Nature* **1995**, *374*, 607–616. [CrossRef]
2. Fu, Y.; Batchelor, A.W.; Loh, N.K.; Tan, K.W. Effect of lubrication by mineral and synthetic oils on the sliding wear of plasma nitrided AISI 410 stainless steel. *Wear* **1998**, *219*, 169–176. [CrossRef]
3. Haus, F.; German, J.; Junter, G.-A. Primary biodegradability of mineral base oils in relation to their chemical and physical characteristics. *Chemosphere* **2001**, *45*, 983–990. [CrossRef]
4. Sotres, J.; Arnebrant, T. Experimental Investigations of biological lubrication at the nanoscale: The cases of synovial joints and the oral cavity. *Lubricants* **2013**, *1*, 102–131. [CrossRef]
5. Dubey, S.; Sharma, G.; Shishodia, K.; Sekhon, G. Study on the performance of oil-in-water emulsions during cold rolling of steel strip. *Tribol. Trans.* **2005**, *48*, 499–504. [CrossRef]
6. Hu, X.; Wang, Y.; Jing, H. Application of oil-in-water emulsion in hot rolling process of brass sheet. *Ind. Lubr. Tribol.* **2010**, *62*, 224–231. [CrossRef]
7. Xia, W.; Zhao, J.; Wu, H.; Jiao, S.; Zhao, X.; Zhang, X.; Xu, J.; Jiang, Z. Analysis of oil-in-water based nanolubricants with varying mass fractions of oil and TiO$_2$ nanoparticles. *Wear* **2018**, *396–397*, 162–171. [CrossRef]
8. Xia, W.Z.; Zhao, J.W.; Wu, H.; Jiao, S.H.; Jiang, Z.Y. Effects of oil-in-water based nanolubricant containing TiO2 nanoparticles on the tribological behaviour of oxidised high-speed steel. *Tribol. Int.* **2017**, *110*, 77–85. [CrossRef]
9. Xia, W.Z.; Zhao, J.W.; Wu, H.; Zhao, X.M.; Zhang, X.M.; Xu, J.Z.; Jiao, S.H.; Wang, X.G.; Zhou, C.L.; Jiang, Z.Y. Effects of oil-in-water based nanolubricant containing TiO2 nanoparticles in hot rolling of 304 stainless steel. *J. Mater. Process. Technol.* **2018**, *262*, 149–156. [CrossRef]
10. Chen, Y.; Renner, P.; Liang, H. Dispersion of Nanoparticles in Lubricating Oil: A Critical Review. *Lubricants* **2019**, *7*, 7. [CrossRef]
11. Gulzar, M.; Masjuki, H.H.; Kalam, M.A.; Varman, M.; Zulkifli, N.W.M.; Mufti, R.A.; Zahid, R. Tribological performance of nanoparticles as lubricating oil additives. *J. Nanopart. Res.* **2016**, *18*, 223. [CrossRef]
12. Huang, S.Q.; Lin, W.K.; Li, X.L.; Fan, Z.Q.; Wu, H.; Jiang, Z.Y.; Huang, H. Roughness-dependent tribological characteristics of water-based GO suspensions with ZrO$_2$ and TiO$_2$ nanoparticles as additives. *Tribol. Int.* **2021**, *161*, 107073. [CrossRef]
13. Wu, H.; Jia, F.H.; Zhao, J.W.; Huang, S.Q.; Wang, L.Z.; Jiao, S.H.; Huang, H.; Jiang, Z.Y. Effect of water-based nanolubricant containing nano-TiO$_2$ on friction and wear behaviour of chrome steel at ambient and elevated temperatures. *Wear* **2019**, *426*, 792–804. [CrossRef]
14. Wu, H.; Zhao, J.W.; Cheng, X.W.; Xia, W.Z.; He, A.S.; Yun, J.H.; Huang, S.Q.; Wang, L.Z.; Huang, H.; Jiao, S.H.; et al. Friction and wear characteristics of TiO$_2$ nano-additive water-based lubricant on ferritic stainless steel. *Tribol. Int.* **2018**, *117*, 24–38. [CrossRef]
15. Wu, H.; Zhao, J.W.; Xia, W.Z.; Cheng, X.W.; He, A.S.; Yun, J.H.; Wang, L.Z.; Huang, H.; Jiao, S.H.; Huang, L.; et al. A study of the tribological behaviour of TiO$_2$ nano-additive water-based lubricants. *Tribol. Int.* **2017**, *109*, 398–408. [CrossRef]
16. He, A.S.; Huang, S.Q.; Yun, J.H.; Wu, H.; Jiang, Z.Y.; Stokes, J.; Jiao, S.H.; Wang, L.Z.; Huang, H. Tribological Performance and Lubrication Mechanism of Alumina Nanoparticle Water-Based Suspensions in Ball-on-Three-Plate Testing. *Tribol. Lett.* **2017**, *65*, 40. [CrossRef]
17. He, A.S.; Huang, S.Q.; Yun, J.H.; Jiang, Z.Y.; Stokes, J.; Jiao, S.H.; Wang, L.Z.; Huang, H. The pH-dependent structural and tribological behaviour of aqueous graphene oxide suspensions. *Tribol. Int.* **2017**, *116*, 460–469. [CrossRef]
18. He, A.S.; Huang, S.Q.; Yun, J.H.; Jiang, Z.Y.; Stokes, J.R.; Jiao, S.H.; Wang, L.Z.; Huang, H. Tribological Characteristics of Aqueous Graphene Oxide, Graphitic Carbon Nitride, and Their Mixed Suspensions. *Tribol. Lett.* **2018**, *66*, 42. [CrossRef]
19. Huang, S.Q.; Li, X.; Yu, B.; Jiang, Z.; Huang, H. Machining characteristics and mechanism of GO/SiO$_2$ nanoslurries in fixed abrasive lapping. *J. Mater. Process. Technol.* **2020**, *277*, 116444. [CrossRef]
20. Huang, S.Q.; Li, X.L.; Zhao, Y.T.; Sun, Q.; Huang, H. A novel lapping process for single-crystal sapphire using hybrid nanoparticle suspensions. *Int. J. Mech. Sci.* **2021**, *191*, 106099. [CrossRef]
21. Huang, S.Q.; He, A.S.; Yun, J.H.; Xu, X.F.; Jiang, Z.Y.; Jiao, S.H.; Huang, H. Synergistic tribological performance of a water based lubricant using graphene oxide and alumina hybrid nanoparticles as additives. *Tribol. Int.* **2019**, *135*, 170–180. [CrossRef]
22. Lin, W.; Kampf, N.; Klein, J. Designer Nanoparticles as Robust Superlubrication Vectors. *ACS Nano* **2020**, *14*, 7008–7017. [CrossRef]
23. Lin, W.; Kampf, N.; Goldberg, R.; Driver, M.J.; Klein, J. Poly-phosphocholinated Liposomes Form Stable Superlubrication Vectors. *Langmuir* **2019**, *35*, 6048–6054. [CrossRef] [PubMed]
24. Wu, H.; Kamali, H.; Huo, M.; Lin, F.; Huang, S.; Huang, H.; Jiao, S.; Xing, Z.; Jiang, Z. Eco-Friendly Water-Based Nanolubricants for Industrial-Scale Hot Steel Rolling. *Lubricants* **2020**, *8*, 96. [CrossRef]
25. Wu, H.; Jia, F.; Li, Z.; Lin, F.; Huo, M.; Huang, S.; Sayyar, S.; Jiao, S.; Huang, H.; Jiang, Z. Novel water-based nanolubricant with superior tribological performance in hot steel rolling. *Int. J. Extrem. Manuf.* **2020**, *2*, 025002. [CrossRef]
26. Huo, M.; Wu, H.; Xie, H.; Zhao, J.; Su, G.; Jia, F.; Li, Z.; Lin, F.; Li, S.; Zhang, H.; et al. Understanding the role of water-based nanolubricants in micro flexible rolling of aluminium. *Tribol. Int.* **2020**, *151*, 106378. [CrossRef]

27. Wu, H.; Jiang, C.Y.; Zhang, J.Q.; Huang, S.Q.; Wang, L.Z.; Jiao, S.H.; Huang, H.; Jiang, Z.Y. Oxidation Behaviour of Steel During hot Rolling by Using TiO$_2$-Containing Water-Based Nanolubricant. *Oxid. Met.* **2019**, *92*, 315–335. [CrossRef]

28. Wu, H.; Zhao, J.W.; Luo, L.; Huang, S.Q.; Wang, L.Z.; Zhang, S.Q.; Jiao, S.H.; Huang, H.; Jiang, Z.Y. Performance Evaluation and Lubrication Mechanism of Water-Based Nanolubricants Containing Nano-TiO$_2$ in Hot Steel Rolling. *Lubricants* **2018**, *6*, 57. [CrossRef]

29. Wu, H.; Zhao, J.W.; Xia, W.Z.; Cheng, X.W.; He, A.S.; Yun, J.H.; Wang, L.Z.; Huang, H.; Jiao, S.H.; Huang, L.; et al. Analysis of TiO$_2$ nano-additive water-based lubricants in hot rolling of microalloyed steel. *J. Manuf. Process.* **2017**, *27*, 26–36. [CrossRef]

30. Yu, X.; Zhou, J.; Jiang, Z. Developments and Possibilities for Nanoparticles in Water-Based Lubrication During Metal Processing. *Rev. Nanosci. Nanotechnol.* **2016**, *5*, 136–163. [CrossRef]

31. Rahman, M.H.; Warneke, H.; Webbert, H.; Rodriguez, J.; Austin, E.; Tokunaga, K.; Rajak, D.K.; Menezes, P.L. Water-Based Lubricants: Development, Properties, and Performances. *Lubricants* **2021**, *9*, 73. [CrossRef]

32. Canter, N. Special Report: Trends in extreme pressure additives. *Tribol. Lubr. Technol.* **2007**, *63*, 10.

33. Choi, S.U.; Eastman, J.A. Enhanced Heat Transfer Using Nanofluids. U.S. Patent 6221275, 1 January 2001.

34. Akoh, H.; Tsukasaki, Y.; Yatsuya, S.; Tasaki, A. Magnetic properties of ferromagnetic ultrafine particles prepared by vacuum evaporation on running oil substrate. *J. Cryst. Growth* **1978**, *45*, 495–500. [CrossRef]

35. Wang, H.; Xu, J.-Z.; Zhu, J.-J.; Chen, H.-Y. Preparation of CuO nanoparticles by microwave irradiation. *J. Cryst. Growth* **2002**, *244*, 88–94. [CrossRef]

36. Sandhya, S.U.; Nityananda, S.A. A Facile One Step Solution Route to Synthesize Cuprous Oxide Nanofluid. *Nanomater. Nanotechnol.* **2013**, *3*, 5. [CrossRef]

37. Han, S.Y.; Shin, S.Y.; Lee, H.-J.; Lee, B.-J.; Lee, S.; Kim, N.J.; Kwak, J.-H. Effects of annealing temperature on microstructure and tensile properties in ferritic lightweight steels. *Metall. Mater. Trans. A Phys. Metall. Mater. Sci.* **2012**, *43*, 843–853. [CrossRef]

38. Sun, Y.; Mayers, B.; Herricks, T.; Xia, Y. Polyol Synthesis of Uniform Silver Nanowires: A Plausible Growth Mechanism and the Supporting Evidence. *Nano Lett.* **2003**, *3*, 955–960. [CrossRef]

39. Eastman, J.A.; Choi, S.U.S.; Li, S.; Yu, W.; Thompson, L.J. Anomalously increased effective thermal conductivities of ethylene glycol-based nanofluids containing copper nanoparticles. *Appl. Phys. Lett.* **2001**, *78*, 718–720. [CrossRef]

40. Hsin, Y.L.; Hwang, K.C.; Chen, F.-R.; Kai, J.-J. Production and in-situ Metal Filling of Carbon Nanotubes in Water. *Adv. Mater.* **2001**, *13*, 830–833. [CrossRef]

41. Lo, C.-H.; Tsung, T.-T.; Chen, L.-C. Shape-controlled synthesis of Cu-based nanofluid using submerged arc nanoparticle synthesis system (SANSS). *J. Cryst. Growth* **2005**, *277*, 636–642. [CrossRef]

42. Angayarkanni, S.A.; Philip, J. Review on thermal properties of nanofluids: Recent developments. *Adv. Colloid. Interface Sci.* **2015**, *225*, 146–176. [CrossRef] [PubMed]

43. Haddad, Z.; Abid, C.; Oztop, H.F.; Mataoui, A. A review on how the researchers prepare their nanofluids. *Int. J. Sci.* **2014**, *76*, 168–189. [CrossRef]

44. Shahnazar, S.; Bagheri, S.; Abd Hamid, S.B. Enhancing lubricant properties by nanoparticle additives. *Int. J. hydrogen Energy* **2016**, *41*, 3153–3170. [CrossRef]

45. Liu, G.; Li, X.; Qin, B.; Xing, D.; Guo, Y.; Fan, R. Investigation of the mending effect and mechanism of copper nano-particles on a tribologically stressed surface. *Tribol. Lett.* **2004**, *17*, 961–966. [CrossRef]

46. Zhao, J.; Yang, G.; Zhang, C.; Zhang, Y.; Zhang, S.; Zhang, P. Synthesis of water-soluble Cu nanoparticles and evaluation of their tribological properties and thermal conductivity as a water-based additive. *Friction* **2019**, *7*, 246–259. [CrossRef]

47. Zhang, C.; Zhang, S.; Song, S.; Yang, G.; Yu, L.; Wu, Z.; Li, X.; Zhang, P. Preparation and Tribological Properties of Surface-Capped Copper Nanoparticle as a Water-Based Lubricant Additive. *Tribol. Lett.* **2014**, *54*, 25–33. [CrossRef]

48. Radice, S.; Mischler, S. Effect of electrochemical and mechanical parameters on the lubrication behaviour of Al$_2$O$_3$ nanoparticles in aqueous suspensions. *Wear* **2006**, *261*, 1032–1041. [CrossRef]

49. Kong, L.; Sun, J.; Bao, Y.; Meng, Y. Effect of TiO$_2$ nanoparticles on wettability and tribological performance of aqueous suspension. *Wear* **2017**, *376–377*, 786–791. [CrossRef]

50. Sun, J.; Li, Y.; Xu, P.; Zhu, Z. Study on the lubricating performance of nano-TiO$_2$ in water-based cold rolling fluid. *Mater. Sci. Forum* **2015**, *3*, 3988–3992.

51. Zhu, Z.; Sun, J.; Wei, H.; Niu, T.; Zhu, Z. Research on Lubrication Behaviors of Nano-TiO$_2$ in Water-Based Hot Rolling Liquid. *Adv. Mater. Res.* **2013**, *643*, 139–143. [CrossRef]

52. Meng, Y.; Sun, J.; Wu, P.; Dong, C.; Yan, X. The Role of Nano-TiO$_2$ Lubricating Fluid on the Hot Rolled Surface and Metallographic Structure of SS41 Steel. *Nanomaterials* **2018**, *8*, 111. [CrossRef]

53. Zhao, C.; Chen, Y.K.; Ren, G. A Study of Tribological Properties of Water-Based Ceria Nanofluids. *Tribol. Trans.* **2013**, *56*, 275–283. [CrossRef]

54. Zhao, J.; Yang, G.; Zhang, Y.; Zhang, S.; Zhang, C.; Gao, C.; Zhang, P. Controllable synthesis of different morphologies of CuO nanostructures for tribological evaluation as water-based lubricant additives. *Friction* **2020**, *9*, 963–977. [CrossRef]

55. Pardue, T.; Acharya, B.; Curtis, C.; Krim, J. A Tribological Study of γ-Fe$_2$O$_3$ Nanoparticles in Aqueous Suspension. *Tribol. Lett.* **2018**, *66*, 130. [CrossRef]

56. Sun, J.; Meng, Y.; Zhang, B. Tribological Behaviors and Lubrication Mechanism of Water-based MoO$_3$ Nanofluid during Cold Rolling Process. *J. Manuf. Process.* **2021**, *61*, 518–526. [CrossRef]

57. Xiong, S.; Liang, D.; Kong, F. Effect of pH on the Tribological Behavior of Eu-Doped WO₃ Nanoparticle in Water-Based Fluid. *Tribol. Lett.* **2020**, *68*, 126. [CrossRef]

58. Ding, M.; Lin, B.; Sui, T.; Wang, A.; Yan, S.; Yang, Q. The excellent anti-wear and friction reduction properties of silica nanoparticles as ceramic water lubrication additives. *Ceram. Int.* **2018**, *44*, 14901–14906. [CrossRef]

59. Bao, Y.; Sun, J.; Kong, L. Tribological properties and lubricating mechanism of SiO₂ nanoparticles in water-based fluid. In *IOP Conference Series: Materials Science and Engineering*; IOP Publishing: Bristol, UK, 2017; Volume 182, p. 012025. [CrossRef]

60. Kogovšek, J.; Remškar, M.; Mrzel, A.; Kalin, M. Influence of surface roughness and running-in on the lubrication of steel surfaces with oil containing MoS2 nanotubes in all lubrication regimes. *Tribol. Int.* **2013**, *61*, 40–47. [CrossRef]

61. Kuznetsova, Y.; Rempel, S.V.; Popov, I.D.; Gerasimov, E.; Rempel, A. Stabilization of Ag₂S nanoparticles in aqueous solution by MPS. *Colloids Surf. Phys. Eng. Asp.* **2017**, *520*, 369–377. [CrossRef]

62. Zhao, J.; Yang, G.; Zhang, Y.; Zhang, S.; Zhang, P. A Simple Preparation of HDA-CuS Nanoparticles and Their Tribological Properties as a Water-Based Lubrication Additive. *Tribol. Lett.* **2019**, *67*, 88. [CrossRef]

63. Yanan, M.; Jianlin, S.; Jiaqi, H.; Xudong, Y.; Yu, P. Recycling prospect and sustainable lubrication mechanism of water-based MoS₂ nano-lubricant for steel cold rolling process. *J. Clean. Prod.* **2020**, *277*, 123991. [CrossRef]

64. Wang, Y.; Du, Y.; Deng, J.; Wang, Z. Friction reduction of water based lubricant with highly dispersed functional MoS₂ nanosheets. *Colloids Surf. A Phys. Eng. Asp.* **2019**, *562*, 321–328. [CrossRef]

65. Peña-Parás, L.; Maldonado-Cortés, D.; Kharissova, O.V.; Saldívar, K.I.; Contreras, L.; Arquieta, P.; Castaños, B. Novel carbon nanotori additives for lubricants with superior anti-wear and extreme pressure properties. *Tribol. Int.* **2019**, *131*, 488–495. [CrossRef]

66. Hu, Y.; Wang, Y.; Wang, C.; Ye, Y.; Zhao, H.; Li, J.; Lu, X.; Mao, C.; Chen, S.; Mao, J.; et al. One-pot pyrolysis preparation of carbon dots as eco-friendly nanoadditives of water-based lubricants. *Carbon* **2019**, *152*, 511–520. [CrossRef]

67. Liang, S.; Shen, Z.; Yi, M.; Liu, L.; Zhang, X.; Ma, S. In-situ exfoliated graphene for high-performance water-based lubricants. *Carbon* **2016**, *96*, 1181–1190. [CrossRef]

68. Jiao, Y.; Liu, S.; Sun, Y.; Yue, W.; Zhang, H. Bioinspired Surface Functionalization of Nanodiamonds for Enhanced Lubrication. *Langmuir* **2018**, *34*, 12436–12444. [CrossRef]

69. Si, Y.; Samulski, E.T. Synthesis of Water Soluble Graphene. *Nano Lett.* **2008**, *8*, 1679–1682. [CrossRef] [PubMed]

70. Song, H.-J.; Li, N. Frictional behavior of oxide graphene nanosheets as water-base lubricant additive. *Appl. Phys. A* **2011**, *105*, 827–832. [CrossRef]

71. Hummers, W.S.; Offeman, R.E. Preparation of Graphitic Oxide. *J. Am. Chem. Soc.* **1958**, *80*, 1339. [CrossRef]

72. Min, C.; He, Z.; Song, H.; Liang, H.; Liu, D.; Dong, C.; Jia, W. Fluorinated graphene oxide nanosheet: A highly efficient water-based lubricated additive. *Tribol. Int.* **2019**, *140*, 105867. [CrossRef]

73. Fan, K.; Liu, J.; Wang, X.; Liu, Y.; Lai, W.; Gao, S.; Qin, J.; Liu, X. Towards enhanced tribological performance as water-based lubricant additive: Selective fluorination of graphene oxide at mild temperature. *J. Colloid Interface Sci.* **2018**, *531*, 138–147. [CrossRef] [PubMed]

74. Liu, C.; Guo, Y.; Wang, D. PEI-RGO nanosheets as a nanoadditive for enhancing the tribological properties of water-based lubricants. *Tribol. Int.* **2019**, *140*, 105851. [CrossRef]

75. Hu, Y.; Wang, Y.; Zeng, Z.; Zhao, H.; Li, J.; Ge, X.; Wang, L.; Xue, Q.; Mao, C.; Chen, S. BLG-RGO: A novel nanoadditive for water-based lubricant. *Tribol. Int.* **2019**, *135*, 277–286. [CrossRef]

76. Meng, W.; Sun, J.; Wang, C.; Wu, P. pH-dependent lubrication mechanism of graphene oxide aqueous lubricants on the strip surface during cold rolling. *Surf. Interface Anal.* **2021**, *53*, 406–417. [CrossRef]

77. Xie, H.; Jiang, B.; Dai, J.; Peng, C.; Li, C.; Li, Q.; Pan, F. Tribological Behaviors of Graphene and Graphene Oxide as Water-Based Lubricant Additives for Magnesium Alloy/Steel Contacts. *Materials* **2018**, *11*, 206. [CrossRef] [PubMed]

78. Wu, P.; Chen, X.; Zhang, C.; Luo, J. Synergistic tribological behaviors of graphene oxide and nanodiamond as lubricating additives in water. *Tribol. Int.* **2019**, *132*, 177–184. [CrossRef]

79. Liu, Y.; Wang, X.; Pan, G.; Luo, J. A comparative study between graphene oxide and diamond nanoparticles as water-based lubricating additives. *Sci. China Technol. Sci.* **2013**, *56*, 152–157. [CrossRef]

80. Su, F.; Chen, G.; Huang, P. Lubricating performances of graphene oxide and onion-like carbon as water-based lubricant additives for smooth and sand-blasted steel discs. *Friction* **2020**, *8*, 47–57. [CrossRef]

81. Oh, S.-T.; Lee, J.-S.; Sekino, T.; Niihara, K. Fabrication of Cu dispersed Al₂O₃ nanocomposites using Al₂O₃/CuO and Al₂O₃/Cu-nitrate mixtures. *Scr. Mater.* **2001**, *44*, 2117–2120. [CrossRef]

82. Devendiran, D.K.; Amirtham, V.A. A review on preparation, characterization, properties and applications of nanofluids. *Renew. Sustain. Energy Rev.* **2016**, *60*, 21–40. [CrossRef]

83. Guo, P.; Chen, L.; Wang, J.; Geng, Z.; Lu, Z.; Zhang, G. Enhanced Tribological Performance of Aminated Nano-Silica Modified Graphene Oxide as Water-Based Lubricant Additive. *ACS Appl. Nano Mater.* **2018**, *1*, 6444–6453. [CrossRef]

84. Du, S.; Sun, J.; Wu, P. Preparation, characterization and lubrication performances of graphene oxide-TiO₂ nanofluid in rolling strips. *Carbon* **2018**, *140*, 338–351. [CrossRef]

85. Li, W.; Zou, C.; Li, X. Thermo-physical properties of cooling water-based nanofluids containing TiO₂ nanoparticles modified by Ag elementary substance for crystallizer cooling system. *Powder Technol.* **2018**, *329*, 434–444. [CrossRef]

86. Zheng, X.; Xu, Y.; Geng, J.; Peng, Y.; Olson, D.; Hu, X. Tribological behavior of Fe_3O_4/MoS_2 nanocomposites additives in aqueous and oil phase media. *Tribol. Int.* **2016**, *102*, 79–87. [CrossRef]

87. Lelonis, D.A.; Tereshko, J.W.; Andersen, C.M. Boron Nitride Powder—A High-Performance Alternative for Solid Lubrication. *GE Adv. Ceram.* **2003**, *4*, 81506.

88. Cho, D.-H.; Kim, J.-S.; Kwon, S.-H.; Lee, C.; Lee, Y.-Z. Evaluation of hexagonal boron nitride nano-sheets as a lubricant additive in water. *Wear* **2013**, *302*, 981–986. [CrossRef]

89. Bai, Y.; Wang, L.; Ge, C.; Liu, R.; Guan, H.; Zhang, X. Atomically Thin Hydroxylation Boron Nitride Nanosheets for Excellent Water-Based Lubricant Additives. *J. Am. Ceram. Soc.* **2020**, *103*, 6951–6960. [CrossRef]

90. Cheng, H.; Zhao, W. Regulating the Nb_2C nanosheets with different degrees of oxidation in water lubricated sliding toward an excellent tribological performance. *Friction* **2021**, 1–13. [CrossRef]

91. Nguyen, H.; Chung, K. Assessment of Tribological Properties of Ti_3C_2 as a Water-Based Lubricant Additive. *Materials* **2020**, *13*, 5545. [CrossRef]

92. Tang, W.; Jiang, Z.; Wang, B.; Li, Y. Black phosphorus quantum dots: A new-type of water-based high-efficiency lubricant additive. *Friction* **2021**, *9*, 1528–1542. [CrossRef]

93. Wang, H.; Liu, Y.; Chen, Z.; Wu, B.; Xu, S.; Luo, J. Layered Double Hydroxide Nanoplatelets with Excellent Tribological Properties under High Contact Pressure as Water-Based Lubricant Additives. *Sci. Rep.* **2016**, *6*, 22748. [CrossRef]

94. Wang, H.; Liu, Y.; Liu, W.; Liu, Y.; Wang, K.; Li, J.; Ma, T.; Eryilmaz, O.L.; Shi, Y.; Erdemir, A.; et al. Superlubricity of Polyalkylene Glycol Aqueous Solutions Enabled by Ultrathin Layered Double Hydroxide Nanosheets. *ACS Appl. Mater. Interfaces* **2019**, *11*, 20249–20256. [CrossRef] [PubMed]

95. Li, X.; Wang, Z.; Dong, G. Preparation of nanoscale liquid metal droplet wrapped with chitosan and its tribological properties as water-based lubricant additive. *Tribol. Int.* **2020**, *148*, 106349. [CrossRef]

96. Ye, X.; Wang, J.; Fan, M. Evaluating tribological properties of the stearic acid-based organic nanomaterials as additives for aqueous lubricants. *Tribol. Int.* **2019**, *140*, 105848. [CrossRef]

97. Odzak, N.; Kistler, D.; Behra, R.; Sigg, L. Dissolution of metal and metal oxide nanoparticles in aqueous media. *Environ. Pollut.* **2014**, *191*, 132–138. [CrossRef] [PubMed]

98. Kim, H.J.; Bang, I.C.; Onoe, J. Characteristic stability of bare Au-water nanofluids fabricated by pulsed laser ablation in liquids. *Opt. Lasers Eng.* **2009**, *47*, 532–538. [CrossRef]

99. Lv, T.; Xu, X.; Yu, A.; Niu, C.; Hu, X. Ambient air quantity and cutting performances of water-based Fe_3O_4 nanofluid in magnetic minimum quantity lubrication. *Int. J. Adv. Manuf. Technol.* **2021**, *115*, 1711–1722. [CrossRef]

100. Bao, Y.; Sun, J.; Kong, L. Effects of nano-SiO_2 as water-based lubricant additive on surface qualities of strips after hot rolling. *Tribol. Int.* **2017**, *114*, 257–263. [CrossRef]

101. Lv, T.; Xu, X.; Yu, A.; Hu, X. Oil mist concentration and machining characteristics of SiO_2 water-based nano-lubricants in electrostatic minimum quantity lubrication-EMQL milling. *J. Mater. Process. Technol.* **2021**, *290*, 116964. [CrossRef]

102. Gao, Y.; Chen, G.; Oli, Y.; Zhang, Z.; Xue, Q. Study on tribological properties of oleic acid-modified TiO_2 nanoparticle in water. *Wear* **2002**, *252*, 454–458. [CrossRef]

103. Gu, Y.; Zhao, X.; Liu, Y.; Lv, Y. Preparation and Tribological Properties of Dual-Coated TiO_2 Nanoparticles as Water-Based Lubricant Additives. *J. Nanomater.* **2014**, *2014*, 785680. [CrossRef]

104. Ohenoja, K.; Saari, J.; Illikainen, M.; Niinimäki, J. Effect of molecular weight of sodium polyacrylates on the particle size distribution and stability of a TiO_2 suspension in aqueous stirred media milling. *Powder Technol.* **2014**, *262*, 188–193. [CrossRef]

105. Najiha, M.S.; Rahman, M.M. Experimental investigation of flank wear in end milling of aluminum alloy with water-based TiO_2 nanofluid lubricant in minimum quantity lubrication technique. *Int. J. Adv. Manuf. Technol.* **2016**, *86*, 2527–2537. [CrossRef]

106. Kayhani, M.H.; Soltanzadeh, H.; Heyhat, M.M.; Nazari, M.; Kowsary, F. Experimental study of convective heat transfer and pressure drop of TiO_2/water nanofluid. *Int. Commun. Heat Mass Transf.* **2012**, *39*, 456–462. [CrossRef]

107. Ukamanal, M.; Chandra Mishra, P.; Kumar Sahoo, A. Temperature distribution during AISI 316 steel turning under TiO_2-water based nanofluid spray environments. *Mater. Today Proc.* **2018**, *5*, 20741–20749. [CrossRef]

108. Wang, L.; Tieu, A.K.; Zhu, H.; Deng, G.; Cui, S.; Zhu, Q. A study of water-based lubricant with a mixture of polyphosphate and nano-$TiO2$ as additives for hot rolling process. *Wear* **2021**, *477*, 203895. [CrossRef]

109. Cui, Y.; Ding, M.; Sui, T.; Zheng, W.; Qiao, G.; Yan, S.; Liu, X. Role of nanoparticle materials as water-based lubricant additives for ceramics. *Tribol. Int.* **2020**, *142*, 105978. [CrossRef]

110. Wu, C.; Hou, S.X.; Zhang, H.Q.; Jia, X.M. Study and Evaluation on Dispersion of Molybdenum Disulfide in Aqueous Solution. *Adv. Mater. Res.* **2013**, *750–752*, 2175–2178. [CrossRef]

111. Zhang, B.; Sun, J. Tribological performances of multilayer-MoS_2 nanoparticles in water-based lubricating fluid. In *IOP Conference Series: Materials Science and Engineering*; IOP Publishing: Bristol, UK, 2017; Volume 182, p. 012023. [CrossRef]

112. Xie, H.; Dang, S.; Jiang, B.; Xiang, L.; Zhou, S.; Sheng, H.; Yang, T.; Pan, F. Tribological performances of SiO_2/graphene combinations as water-based lubricant additives for magnesium alloy rolling. *Appl. Surf. Sci.* **2019**, *475*, 847–856. [CrossRef]

113. Xie, H.; Wei, Y.; Jiang, B.; Tang, C.; Nie, C. Tribological properties of carbon nanotube/SiO_2 combinations as water-based lubricant additives for magnesium alloy. *J. Mater. Res. Technol.* **2021**, *12*, 138–149. [CrossRef]

114. Zayan, M.; Rasheed, A.K.; John, A.; Khalid, M.; Ismail, A. Experimental Investigation on Rheological Properties of Water Based Novel Ternary Hybrid Nanofluids. *Nanoscience* **2021**. [CrossRef]

115. Wang, N.; Wang, H.; Ren, J.; Gao, G.; Chen, S.; Zhao, G.; Yang, Y.; Wang, J. Novel additive of PTFE@SiO$_2$ core-shell nanoparticles with superior water lubricating properties. *Mater. Des.* **2020**, *195*, 109069. [CrossRef]

116. Zhang, C.; Zhang, S.; Yu, L.; Zhang, Z.; Wu, Z.; Zhang, P. Preparation and tribological properties of water-soluble copper/silica nanocomposite as a water-based lubricant additive. *Appl. Surf. Sci.* **2012**, *259*, 824–830. [CrossRef]

117. Liu, T.; Zhou, C.; Gao, C.; Zhang, Y.; Yang, G.; Zhang, P.; Zhang, S. Preparation of Cu@SiO$_2$ composite nanoparticle and its tribological properties as water-based lubricant additive. *Lubr. Sci.* **2020**, *32*, 69–79. [CrossRef]

118. He, J.; Sun, J.; Meng, Y.; Pei, Y. Superior lubrication performance of MoS$_2$-Al$_2$O$_3$ composite nanofluid in strips hot rolling. *J. Manuf. Process.* **2020**, *57*, 312–323. [CrossRef]

119. Kumar, A.S.; Deb, S.; Paul, S. Tribological characteristics and micromilling performance of nanoparticle enhanced water based cutting fluids in minimum quantity lubrication. *J. Manuf. Process.* **2020**, *56*, 766–776. [CrossRef]

120. Giwa, S.O.; Sharifpur, M.; Ahmadi, M.H.; Sohel Murshed, S.M.; Meyer, J.P. Experimental Investigation on Stability, Viscosity, and Electrical Conductivity of Water-Based Hybrid Nanofluid of MWCNT-Fe(2)O(3). *Nanomaterials* **2021**, *11*, 136. [CrossRef] [PubMed]

121. Song, H.; Huang, J.; Jia, X.; Sheng, W. Facile synthesis of core–shell Ag@C nanospheres with improved tribological properties for water-based additives. *New J. Chem.* **2018**, *42*, 8773–8782. [CrossRef]

122. Gara, L.; Zou, Q. Friction and Wear Characteristics of Water-Based ZnO and Al$_2$O$_3$ Nanofluids. *Tribol. Trans.* **2012**, *55*, 345–350. [CrossRef]

123. Liang, D.; Ling, X.; Xiong, S. Preparation, characterisation and lubrication performances of Eu doped WO$_3$ nanoparticle reinforce Mn$_3$B$_7$O$_{13}$ Cl as water-based lubricant additive for laminated Cu-Fe composite sheet during hot rolling. *Lubr. Sci.* **2021**, *33*, 142–152. [CrossRef]

124. Wang, Y.; Cui, L.; Cheng, G.; Yuan, N.; Ding, J.; Pesika, N.S. Water-Based Lubrication of Hard Carbon Microspheres as Lubricating Additives. *Tribol. Lett.* **2018**, *66*, 148. [CrossRef]

125. Peng, Y.; Hu, Y.; Wang, H. Tribological behaviors of surfactant-functionalized carbon nanotubes as lubricant additive in water. *Tribol. Lett.* **2007**, *25*, 247–253. [CrossRef]

126. Sun, X.; Han, B.; Kang, H.; Fan, Z.; Liu, Y.; Umar, A.; Guo, Z. Frictional Reduction with Partially Exfoliated Multi-Walled Carbon Nanotubes as Water-Based Lubricant Additives. *J. Nanosci. Nanotechnol.* **2018**, *18*, 3427–3432. [CrossRef] [PubMed]

127. Min, C.; He, Z.; Liu, D.; Zhang, K.; Dong, C. Urea Modified Fluorinated Carbon Nanotubes: Unique Self-Dispersed Characteristic in Water and High Tribological Performance as Water-Based Lubricant Additives. *New J. Chem.* **2019**, *43*, 14684–14693. [CrossRef]

128. Kristiansen, K.; Zeng, H.; Wang, P.; Israelachvili, J. Microtribology of Aqueous Carbon Nanotube Dispersions. *Adv. Funct. Mater.* **2011**, *21*, 4555–4564. [CrossRef]

129. Ye, X.; E, S.; Fan, M. The influences of functionalized carbon nanotubes as lubricating additives: Length and diameter. *Diam. Relat. Mater.* **2019**, *100*, 107548. [CrossRef]

130. Tang, W.; Wang, B.; Li, J.; Li, Y.; Zhang, Y.; Quan, H.; Huang, Z. Facile pyrolysis synthesis of ionic liquid capped carbon dots and subsequent application as the water-based lubricant additives. *J. Mater. Sci.* **2019**, *54*, 1171–1183. [CrossRef]

131. Xiao, H.; Liu, S.; Xu, Q.; Zhang, H. Carbon quantum dots: An innovative additive for water lubrication. *Sci. China Technol. Sci.* **2019**, *62*, 587–596. [CrossRef]

132. Fan, K.; Liu, X.; Liu, Y.; Li, Y.; Chen, Y.; Meng, Y.; Liu, X.; Feng, W.; Luo, L. Covalent functionalization of fluorinated graphene through activation of dormant radicals for water-based lubricants. *Carbon* **2020**, *167*, 826–834. [CrossRef]

133. Ma, L.; Li, Z.; Jia, W.; Hou, K.; Wang, J.; Yang, S. Microwave-assisted synthesis of hydroxyl modified fluorinated graphene with high fluorine content and its high load-bearing capacity as water lubricant additive for ceramic/steel contact. *Colloids Surf. A* **2021**, *610*, 125931. [CrossRef]

134. Ye, X.; Ma, L.; Yang, Z.; Wang, J.; Wang, H.; Yang, S. Covalent Functionalization of Fluorinated Graphene and Subsequent Application as Water-based Lubricant Additive. *ACS Appl. Mater. Interfaces* **2016**, *8*, 7483–7488. [CrossRef] [PubMed]

135. Qiang, R.; Hu, L.; Hou, K.; Wang, J.; Yang, S. Water-Soluble Graphene Quantum Dots as High-Performance Water-Based Lubricant Additive for Steel/Steel Contact. *Tribol. Lett.* **2019**, *67*, 64. [CrossRef]

136. Piatkowska, A.; Romaniec, M.; Grzybek, D.; Mozdzonek, M.; Rojek, A.; Diduszko, R. A study on antiwear properties of graphene water-based lubricant and its contact with metallic materials. *Tribologia* **2018**, *281*, 71–81. [CrossRef]

137. Mirzaamiri, R.; Akbarzadeh, S.; Ziaei-Rad, S.; Shin, D.-G.; Kim, D.-E. Molecular dynamics simulation and experimental investigation of tribological behavior of nanodiamonds in aqueous suspensions. *Tribol. Int.* **2021**, *156*, 106838. [CrossRef]

138. Kinoshita, H.; Nishina, Y.; Alias, A.A.; Fujii, M. Tribological properties of monolayer graphene oxide sheets as water-based lubricant additives. *Carbon* **2014**, *66*, 720–723. [CrossRef]

139. Elomaa, O.; Singh, V.K.; Iyer, A.; Hakala, T.J.; Koskinen, J. Graphene oxide in water lubrication on diamond-like carbon vs. stainless steel high-load contacts. *Diam. Relat. Mater.* **2015**, *52*, 43–48. [CrossRef]

140. Singh, S.; Chen, X.; Zhang, C.; Tyagi, R.; Luo, J. Investigation on the lubrication potential of graphene oxide aqueous dispersion for self-mated stainless steel tribo-pair. *Vacuum* **2019**, *166*, 307–315. [CrossRef]

141. Bai, M.; Liu, J.; He, J.; Li, W.; Wei, J.; Chen, L.; Miao, J.; Li, C. Heat transfer and mechanical friction reduction properties of graphene oxide nanofluids. *Diam. Relat. Mater.* **2020**, *108*, 107982. [CrossRef]

142. Gan, C.; Liang, T.; Li, X.; Li, W.; Li, H.; Fan, X.; Zhu, M. Ultra-dispersive monolayer graphene oxide as water-based lubricant additive: Preparation, characterization and lubricating mechanisms. *Tribol. Int.* **2021**, *155*, 106768. [CrossRef]

143. Kim, H.-J.; Kim, D.-E. Water Lubrication of Stainless Steel using Reduced Graphene Oxide Coating. *Sci. Rep.* **2015**, *5*, 17034. [CrossRef]

144. Kinoshita, H.; Suzuki, K.; Suzuki, T.; Nishina, Y. Tribological properties of oxidized wood-derived nanocarbons with same surface chemical composition as graphene oxide for additives in water-based lubricants. *Diam. Relat. Mater.* **2018**, *90*, 101–108. [CrossRef]

145. Wei, Q.; Fu, T.; Yue, Q.; Liu, H.; Ma, S.; Cai, M.; Zhou, F. Graphene oxide/brush-like polysaccharide copolymer nanohybrids as eco-friendly additives for water-based lubrication. *Tribol. Int.* **2021**, *157*, 106895. [CrossRef]

146. Li, X.; Lu, H.; Guo, J.; Tong, Z.; Dong, G. Synergistic water lubrication effect of self-assembled nanofilm and graphene oxide additive. *Appl. Surf. Sci.* **2018**, *455*, 1070–1077. [CrossRef]

147. Hu, Y.; Wang, Y.; Zeng, Z.; Zhao, H.; Ge, X.; Wang, K.; Wang, L.; Xue, Q. PEGlated graphene as nanoadditive for enhancing the tribological properties of water-based lubricants. *Carbon* **2018**, *137*, 41–48. [CrossRef]

148. Shariatzadeh, M.; Grecov, D. Cellulose Nanocrystals Suspensions as Water-Based Lubricants for Slurry Pump Gland Seals. *Int. J. Aerosp. Mech. Eng.* **2018**, *12*, 603–607. [CrossRef]

149. Shariatzadeh, M.; Grecov, D. Aqueous suspensions of cellulose nanocrystals as water-based lubricants. *Cellulose* **2019**, *26*, 4665–4677. [CrossRef]

150. Lei, H.; Guan, W.; Luo, J. Tribological behavior of fullerene–styrene sulfonic acid copolymer as water-based lubricant additive. *Wear* **2002**, *252*, 345–350. [CrossRef]

151. Jiang, G.; Guan, W.; Zheng, Q. A study on fullerene–acrylamide copolymer nanoball—A new type of water-based lubrication additive. *Wear* **2005**, *258*, 1625–1629. [CrossRef]

152. Wang, Y.; Yang, W.; Yu, Q.; Zhang, J.; Ma, Z.; Zhang, M.; Zhang, L.; Bai, Y.; Cai, M.; Zhou, F.; et al. Significantly Reducing Friction and Wear of Water-Based Fluids with Shear Thinning Bicomponent Supramolecular Hydrogels. *Adv. Mater. Interfaces* **2020**, *7*, 2001084. [CrossRef]

153. Yang, D.; Du, X.; Li, W.; Han, Y.; Ma, L.; Fan, M.; Zhou, F.; Liu, W. Facile Preparation and Tribological Properties of Water-Based Naphthalene Dicarboxylate Ionic Liquid Lubricating Additives. *Tribol. Lett.* **2020**, *68*, 84. [CrossRef]

154. Zhang, J.; Zhang, Y.; Zhang, S.; Yu, L.; Zhang, P.; Zhang, Z. Preparation of Water-Soluble Lanthanum Fluoride Nanoparticles and Evaluation of their Tribological Properties. *Tribol. Lett.* **2013**, *52*, 305–314. [CrossRef]

155. Zheng, D.; Wang, X.; Liu, Z.; Ju, C.; Xu, Z.; Xu, J.; Yang, C. Synergy between two protic ionic liquids for improving the antiwear property of glycerol aqueous solution. *Tribol. Int.* **2020**, *141*, 105731. [CrossRef]

156. Dong, R.; Yu, Q.; Bai, Y.; Wu, Y.; Ma, Z.; Zhang, J.; Zhang, C.; Yu, B.; Zhou, F.; Liu, W.; et al. Towards superior lubricity and anticorrosion performances of proton-type ionic liquids additives for water-based lubricating fluids. *Chem. Eng. J.* **2020**, *383*, 123201. [CrossRef]

157. Khanmohammadi, H.; Wijanarko, W.; Espallargas, N. Ionic Liquids as Additives in Water-Based Lubricants: From Surface Adsorption to Tribofilm Formation. *Tribol. Lett.* **2020**, *68*, 130. [CrossRef]

158. Kreivaitis, R.; Gumbytė, M.; Kupčinskas, A.; Kazancev, K.; Ta, T.N.; Horng, J.H. Investigation of tribological properties of two protic ionic liquids as additives in water for steel–steel and alumina–steel contacts. *Wear* **2020**, *456–457*, 203390. [CrossRef]

159. He, J.; Sun, J.; Meng, Y.; Yan, X. Preliminary investigations on the tribological performance of hexagonal boron nitride nanofluids as lubricant for steel/steel friction pairs. *Surf. Topogr. Metrol. Prop.* **2019**, *7*, 015022. [CrossRef]

160. Abdollah, M.F.B.; Amiruddin, H.; Azmi, M.A.; Tahir, N.A.M. Lubrication mechanisms of hexagonal boron nitride nano-additives water-based lubricant for steel–steel contact. *J. Eng. Tribol.* **2020**, *235*, 1038–1046. [CrossRef]

161. Lin, B.; Ding, M.; Sui, T.; Cui, Y.; Yan, S.; Liu, X. Excellent Water Lubrication Additives for Silicon Nitride to Achieve Superlubricity under Extreme Conditions. *Langmuir* **2019**, *35*, 14861–14869. [CrossRef] [PubMed]

162. Wang, W.; Xie, G.; Luo, J. Black phosphorus as a new lubricant. *Friction* **2018**, *6*, 116–142. [CrossRef]

163. Wang, Q.; Hou, T.; Wang, W.; Zhang, G.; Gao, Y.; Wang, K. Tribological behavior of black phosphorus nanosheets as water-based lubrication additives. *Friction* **2021**, 1–14. [CrossRef]

164. Ali, N.; Amaral Teixeira, J.; Addali, A. A Review on Nanofluids: Fabrication, Stability, and Thermophysical Properties. *J. Nanomater.* **2018**, *2018*, 6978130. [CrossRef]

165. Dey, D.; Kumar, P.; Samantaray, S. A review of nanofluid preparation, stability, and thermo-physical properties. *Heat Transf. Asian Res.* **2017**, *46*, 1413–1442. [CrossRef]

166. Ghadimi, A.; Saidur, R.; Metselaar, H.S.C. A review of nanofluid stability properties and characterization in stationary conditions. *Int. J. Heat Mass Transf.* **2011**, *54*, 4051–4068. [CrossRef]

167. Wu, D.; Zhu, H.; Wang, L.; Liu, L. Critical Issues in Nanofluids Preparation, Characterization and Thermal Conductivity. *Curr. Nanosci.* **2009**, *5*, 103–112. [CrossRef]

168. Zhu, H.; Li, C.; Wu, D.; Zhang, C.; Yin, Y. Preparation, characterization, viscosity and thermal conductivity of $CaCO_3$ aqueous nanofluids. *Sci. China Technol. Sci.* **2010**, *53*, 360–368. [CrossRef]

169. Urmi, W.T.; Rahman, M.M.; Kadirgama, K.; Ramasamy, D.; Maleque, M.A. An overview on synthesis, stability, opportunities and challenges of nanofluids. *Mater. Today Proc.* **2021**, *41*, 30–37. [CrossRef]

170. Fang, Y.; Ma, L.; Luo, J. Modelling for water-based liquid lubrication with ultra-low friction coefficient in rough surface point contact. *Tribol. Int.* **2020**, *141*, 105901. [CrossRef]

171. Azman, N.F.; Samion, S. Dispersion Stability and Lubrication Mechanism of Nanolubricants: A Review. *Int. J. Precis. Eng. Manuf.-Green Technol.* **2019**, *6*, 393–414. [CrossRef]

172. Cacua, K.; Murshed, S.M.S.; Pabón, E.; Buitrago, R. Dispersion and thermal conductivity of TiO_2/water nanofluid: Effects of ultrasonication, agitation and temperature. *J. Therm. Anal. Calorim.* **2019**, *140*, 109–114. [CrossRef]

173. Lee, K.; Hwang, Y.; Cheong, S.; Kwon, L.; Kim, S.; Lee, J. Performance evaluation of nano-lubricants of fullerene nanoparticles in refrigeration mineral oil. *Curr. Appl. Phys.* **2009**, *9*, e128–e131. [CrossRef]

174. Ghadimi, A.; Metselaar, H.; LotfizadehDehkordi, B. Nanofluid stability optimization based on UV-Vis spectrophotometer measurement. *J. Eng. Sci. Technol.* **2015**, *10*, 32–40.

175. Jiang, L.; Gao, L.; Sun, J. Production of aqueous colloidal dispersions of carbon nanotubes. *J. Colloid Interface Sci.* **2003**, *260*, 89–94. [CrossRef]

176. Yu, W.; Xie, H. A Review on Nanofluids: Preparation, Stability Mechanisms, and Applications. *J. Nanomater.* **2012**, *2012*, 128. [CrossRef]

177. Sajid, M.U.; Ali, H.M. Thermal conductivity of hybrid nanofluids: A critical review. *Int. J. Heat Mass Transf.* **2018**, *126*, 211–234. [CrossRef]

178. Alawi, O.A.; Mallah, A.R.; Kazi, S.N.; Sidik, N.A.C.; Najafi, G. Thermophysical properties and stability of carbon nanostructures and metallic oxides nanofluids. *J. Therm. Anal. Calorim.* **2019**, *135*, 1545–1562. [CrossRef]

179. Kumar, M.S.; Vasu, V.; Gopal, A.V. Thermal conductivity and rheological studies for Cu–Zn hybrid nanofluids with various basefluids. *J. Taiwan Inst. Chem. Eng.* **2016**, *66*, 321–327. [CrossRef]

180. Yu, F.; Chen, Y.; Liang, X.; Xu, J.; Lee, C.; Liang, Q.; Tao, P.; Deng, T. Dispersion stability of thermal nanofluids. *Prog. Nat. Sci. Mater. Int.* **2017**, *27*, 531–542. [CrossRef]

181. Cremaschi, L.; Bigi, A.; Wong, T.; Deokar, P. Thermodynamic properties of Al_2O_3 nanolubricants: Part 1—Effects on the two-phase pressure drop. *Sci. Technol. Built Environ.* **2015**, *21*, 607–620. [CrossRef]

182. Huminic, G.; Huminic, A.; Fleacă, C.; Dumitrache, F.; Morjan, I. Experimental study on viscosity of water based Fe–Si hybrid nanofluids. *J. Mol. Liq.* **2021**, *321*, 114938. [CrossRef]

183. Haghighi, E.; Nikkam, N.; Saleemi, M.; Behi, R.; Mirmohammadi, S.A.; Poth, H.; Khodabandeh, R.; Toprak, M.; Muhammed, M.; Palm, B. Shelf stability of nanofluids and its effect on thermal conductivity and viscosity Shelf stability of nanofluids and its effect on thermal conductivity and viscosity. *Meas. Sci. Technol.* **2013**, *24*, 105301–105311. [CrossRef]

184. Baghbanzadeh, M.; Rashidi, A.; Soleimanisalim, A.H.; Rashtchian, D. Investigating the rheological properties of nanofluids of water/hybrid nanostructure of spherical silica/MWCNT. *Thermochim. Acta* **2014**, *578*, 53–58. [CrossRef]

185. Zhu, H.; Zhang, C.; Tang, Y.; Wang, J.; Ren, B.; Yin, Y. Preparation and thermal conductivity of suspensions of graphite nanoparticles. *Carbon* **2007**, *45*, 226–228. [CrossRef]

186. Li, Y.; Zhou, J.; Tung, S.; Schneider, E.; Xi, S. A review on development of nanofluid preparation and characterization. *Powder Technol.* **2009**, *196*, 89–101. [CrossRef]

187. Mukherjee, S.; Paria, S. Preparation and Stability of Nanofluids-A Review. *IOSR J. Mech. Civ. Eng.* **2013**, *9*, 63–69. [CrossRef]

188. Qamar, A.; Anwar, Z.; Ali, H.; Shaukat, R.; Imran, S.; Arshad, A.; Ali, H.M.; Korakianitis, T. Preparation and dispersion stability of aqueous metal oxide nanofluids for potential heat transfer applications: A review of experimental studies. *J. Therm. Anal. Calorim.* **2020**, 1–24. [CrossRef]

189. Oh, D.-W.; Jain, A.; Eaton, J.K.; Goodson, K.E.; Lee, J.S. Thermal conductivity measurement and sedimentation detection of aluminum oxide nanofluids by using the 3ω method. *Int. J. Heat Fluid Flow* **2008**, *29*, 1456–1461. [CrossRef]

190. Peng, X.F.; Yu, X.; Xia, L.F.; Zhong, X. Influence factors on suspension stability of nanofluids. *J. Zhejiang Univ.* **2007**, *41*, 577–580.

191. Azizian, R.; Doroodchi, E.; Moghtaderi, B. Influence of Controlled Aggregation on Thermal Conductivity of Nanofluids. *J. Heat Transf.* **2016**, *138*, 021301. [CrossRef]

192. Jama, M.; Singh, T.; Mahmoud, S.; Koç, M.; Samara, A.; Isaifan, R.; Atieh, M. Critical Review on Nanofluids: Preparation, Characterization, and Applications. *J. Nanomater.* **2016**, *2016*, 6717624. [CrossRef]

193. Kumar Dubey, M.; Bijwe, J.; Ramakumar, S.S.V. PTFE based nano-lubricants. *Wear* **2013**, *306*, 80–88. [CrossRef]

194. Lee, G.-J.; Rhee, C.K. Enhanced thermal conductivity of nanofluids containing graphene nanoplatelets prepared by ultrasound irradiation. *J. Mater. Sci.* **2014**, *49*, 1506–1511. [CrossRef]

195. Mahbubul, I.M.; Elcioglu, E.B.; Saidur, R.; Amalina, M.A. Optimization of ultrasonication period for better dispersion and stability of TiO2–water nanofluid. *Ultrason. Sonochem.* **2017**, *37*, 360–367. [CrossRef]

196. Tang, E.; Cheng, G.; Ma, X.; Pang, X.; Zhao, Q. Surface modification of zinc oxide nanoparticle by PMAA and its dispersion in aqueous system. *Appl. Surf. Sci.* **2006**, *252*, 5227–5232. [CrossRef]

197. Neouze, M.-A.; Schubert, U. Surface Modification and Functionalization of Metal and Metal Oxide Nanoparticles by Organic Ligands. *Mon. Chem.-Chem. Mon.* **2008**, *139*, 183–195. [CrossRef]

198. Yang, X.-F.; Liu, Z.-H. Pool boiling heat transfer of functionalized nanofluid under sub-atmospheric pressures. *Int. J. Therm. Sci.* **2011**, *50*, 2402–2412. [CrossRef]

199. Sezer, N.; Atieh, M.A.; Koç, M. A comprehensive review on synthesis, stability, thermophysical properties, and characterization of nanofluids. *Powder Technol.* **2019**, *344*, 404–431. [CrossRef]

200. Narendar, G.; Gupta, A.V.S.S.K.S.; Krishnaiah, A.; Satyanarayana, M.G.V. Experimental investigation on the preparation and applications of Nano fluids. *Mater. Today Proc.* **2017**, *4*, 3926–3931. [CrossRef]

201. Xia, G.; Jiang, H.; Liu, R.; Zhai, Y. Effects of surfactant on the stability and thermal conductivity of Al_2O_3/de-ionized water nanofluids. *Int. J. Therm. Sci.* **2014**, *84*, 118–124. [CrossRef]

202. Kakati, H.; Mandal, A.; Laik, S. Promoting effect of Al$_2$O$_3$/ZnO-based nanofluids stabilized by SDS surfactant on CH$_4$+C$_2$H$_6$+C$_3$H$_8$ hydrate formation. *J. Ind. Eng. Chem.* **2016**, *35*, 357–368. [CrossRef]

203. Tomala, A.; Karpinska, A.; Werner, W.S.M.; Olver, A.; Störi, H. Tribological properties of additives for water-based lubricants. *Wear* **2010**, *269*, 804–810. [CrossRef]

204. Wen, P.; Lei, Y.; Li, W.; Fan, M. Synergy between Covalent Organic Frameworks and Surfactants to Promote Water-Based Lubrication and Corrosion-Resistance. *ACS Appl. Nano Mater.* **2020**, *3*, 1400–1411. [CrossRef]

205. Popa, I.; Gillies, G.; Papastavrou, G.; Borkovec, M. Attractive and Repulsive Electrostatic Forces between Positively Charged Latex Particles in the Presence of Anionic Linear Polyelectrolytes. *J. Phys. Chem. B* **2010**, *114*, 3170–3177. [CrossRef] [PubMed]

206. Tadros, T. Chapter 2—Colloid and interface aspects of pharmaceutical science. In *Colloid and Interface Science in Pharmaceutical Research and Development*; Ohshima, H., Makino, K., Eds.; Elsevier: Amsterdam, The Netherlands, 2014; pp. 29–54.

207. Du, Y.; Yuan, X. Coupled hybrid nanoparticles for improved dispersion stability of nanosuspensions: A review. *J. Nanopart. Res.* **2020**, *22*, 261. [CrossRef]

208. Byrd, T.; Walz, J. Interaction Force Profiles between Cryptosporidium parvum Oocysts and Silica Surfaces. *Environ. Sci. Technol.* **2006**, *39*, 9574–9582. [CrossRef] [PubMed]

209. Napper, D.H. Steric stabilization. *J. Colloid Interface Sci.* **1977**, *58*, 390–407. [CrossRef]

210. Zhulina, E.B.; Borisov, O.V.; Priamitsyn, V.A. Theory of steric stabilization of colloid dispersions by grafted polymers. *J. Colloid Interface Sci.* **1990**, *137*, 495–511. [CrossRef]

211. Gerber, P.; Moore, M.A. Comments on the Theory of Steric Stabilization. *Macromolecules* **1977**, *10*, 476–481. [CrossRef]

212. Dutta, N.; Green, D. Impact of Solvent Quality on Nanoparticle Dispersion in Semidilute and Concentrated Polymer Solutions. *Langmuir* **2010**, *26*, 16737–16744. [CrossRef]

213. Munkhbayar, B.; Tanshen, M.R.; Jeoun, J.; Chung, H.; Jeong, H. Surfactant-free dispersion of silver nanoparticles into MWCNT-aqueous nanofluids prepared by one-step technique and their thermal characteristics. *Ceram. Int.* **2013**, *39*, 6415–6425. [CrossRef]

214. Hatami, M.; Ali, F.; Alsabery, A.; Hu, S.; Jing, D.; Hameed, K. mixed convection heat transfer of SiO$_2$-water and alumina-pao nano-lubricants used in a mechanical ball bearing. *J. Therm. Eng.* **2021**, *7*, 134–161. [CrossRef]

215. Chen, L.; Cheng, M.; Yang, D.; Yang, L. Enhanced Thermal Conductivity of Nanofluid by Synergistic Effect of Multi-Walled Carbon Nanotubes and Fe$_2$O$_3$ Nanoparticles. *Appl. Mech. Mater.* **2014**, *548–549*, 118–123. [CrossRef]

216. Botha, S.S.; Ndungu, P.; Bladergroen, B.J. Physicochemical Properties of Oil-Based Nanofluids Containing Hybrid Structures of Silver Nanoparticles Supported on Silica. *Ind. Eng. Chem. Res.* **2011**, *50*, 3071–3077. [CrossRef]

217. Nine, M.J.; Munkhbayar, B.; Rahman, M.S.; Chung, H.; Jeong, H. Highly productive synthesis process of well dispersed Cu$_2$O and Cu/Cu$_2$O nanoparticles and its thermal characterization. *Mater. Chem. Phys.* **2013**, *141*, 636–642. [CrossRef]

218. Valdes, M.; Gonzalo, J.; Marín, A.; Rodriguez, M.; Betancur, J. Tribometry: How is friction research quantified? A review. *Int. J. Eng. Res. Technol.* **2020**, *13*, 2596–2610. [CrossRef]

219. Paul, G.; Hirani, H.; Kuila, T.; Murmu, N. Nanolubricants Dispersed with Graphene and its Derivatives: An Assessment and Review of the Tribological Performance. *Nanoscale* **2019**, *11*, 3458–3483. [CrossRef] [PubMed]

220. Sagraloff, N.; Dobler, A.; Tobie, T.; Stahl, K.; Ostrowski, J. Development of an Oil Free Water-Based Lubricant for Gear Applications. *Lubricants* **2019**, *7*, 33. [CrossRef]

221. Zhang, T.; Jiang, F.; Yan, L.; Jiang, Z.; Xu, X. A novel ultrahigh-speed ball-on-disc tribometer. *Tribol. Int.* **2021**, *157*, 106901. [CrossRef]

222. Chen, W.; Amann, T.; Kailer, A.; Rühe, J. Macroscopic Friction Studies of Alkylglucopyranosides as Additives for Water-Based Lubricants. *Lubricants* **2020**, *8*, 11. [CrossRef]

223. Cheng, X.; Jiang, Z.; Wei, D.; Wu, H.; Jiang, L. Adhesion, friction and wear analysis of a chromium oxide scale on a ferritic stainless steel. *Wear* **2019**, *426–427*, 1212–1221. [CrossRef]

224. Pawlak, Z.; Urbaniak, W.; Oloyede, A. The relationship between friction and wettability in aqueous environment. *Wear* **2011**, *271*, 1745–1749. [CrossRef]

225. Liu, Y.; Chen, X.; Li, J.; Luo, J. Enhancement of friction performance enabled by a synergetic effect between graphene oxide and molybdenum disulfide. *Carbon* **2019**, *154*, 266–276. [CrossRef]

226. Wu, H.; Li, Y.; Lu, Y.; Li, Z.; Cheng, X.; Hasan, M.; Zhang, H.; Jiang, Z. Influences of Load and Microstructure on Tribocorrosion Behaviour of High Strength Hull Steel in Saline Solution. *Tribol. Lett.* **2019**, *67*, 124. [CrossRef]

227. Tang, W.; Zhu, X.; Li, Y. Tribological performance of various metal-doped carbon dots as water-based lubricant additives and their potential application as additives of poly(ethylene glycol). *Friction* **2021**, *1*, 1–18. [CrossRef]

228. Kim, H.J.; Shin, D.G.; Kim, D.-E. Frictional behavior between silicon and steel coated with graphene oxide in dry sliding and water lubrication conditions. *Int. J. Precis. Eng. Manuf.-Green Technol.* **2016**, *3*, 91–97. [CrossRef]

229. Rosa, W.O.; Vereda, F.; de Vicente, J. Tribological Behavior of Glycerol/Water-Based Magnetorheological Fluids in PMMA Point Contacts. *Front. Mater.* **2019**, *6*, 32. [CrossRef]

230. Kotia, A.; Borkakoti, S.; Deval, P.; Ghosh, S.K. Review of interfacial layer's effect on thermal conductivity in nanofluid. *Heat Mass Transf.* **2017**, *53*, 2199–2209. [CrossRef]

231. Kotia, A.; Rajkhowa, P.; Rao, G.S.; Ghosh, S.K. Thermophysical and tribological properties of nanolubricants: A review. *Heat Mass Transf.* **2018**, *54*, 3493–3508. [CrossRef]

232. Tang, Z.; Li, S. A review of recent developments of friction modifiers for liquid lubricants (2007–present). *Curr. Opin. Solid State Mater. Sci.* **2014**, *18*, 119–139. [CrossRef]

233. Kong, L.; Sun, J.; Bao, Y. Preparation, characterization and tribological mechanism of nanofluids. *RSC Adv.* **2017**, *7*, 12599–12609. [CrossRef]

234. Liu, L.; Zhou, M.; Jin, L.; Li, L.; Mo, Y.; Su, G.; Li, X.; Zhu, H.; Tian, Y. Recent advances in friction and lubrication of graphene and other 2D materials: Mechanisms and applications. *Friction* **2019**, *7*, 199–216. [CrossRef]

235. Zhao, J.; Huang, Y.; He, Y.; Shi, Y. Nanolubricant additives: A review. *Friction* **2021**, *9*, 891–917. [CrossRef]

236. Sarno, M.; Scarpa, D.; Senatore, A.; Mustafa, W. rGO/GO Nanosheets in Tribology: From the State of the Art to the Future Prospective. *Lubricants* **2020**, *8*, 31. [CrossRef]

237. Laad, M.; Jatti, V.K.S. Titanium oxide nanoparticles as additives in engine oil. *J. King Saud Univ. Eng. Sci.* **2018**, *30*, 116–122. [CrossRef]

238. Khadem, M.; Penkov, O.; Pukha, V.; Maleyev, M.; Kim, D.-E. Ultra-thin carbon-based nanocomposite coatings for superior wear resistance under lubrication with nano-diamond additives. *RSC Adv.* **2016**, *6*, 56918–56929. [CrossRef]

239. Chiñas-Castillo, F.; Spikes, H. Mechanism of Action of Colloidal Solid Dispersions. *J. Tribol.* **2003**, *125*, 552–557. [CrossRef]

240. Rapoport, L.; Leshchynsky, V.; Lvovsky, M.; Nepomnyashchy, O.; Volovik, Y.; Tenne, R. Mechanism of friction of fullerene. *Ind. Lubr. Tribol.* **2002**, *54*, 171–176. [CrossRef]

241. Wu, Y.Y.; Tsui, W.C.; Liu, T.C. Experimental analysis of tribological properties of lubricating oils with nanoparticle additives. *Wear* **2007**, *262*, 819–825. [CrossRef]

242. Aldana, P.U.; Dassenoy, F.; Vacher, B.; Le Mogne, T.; Thiebaut, B. WS_2 nanoparticles anti-wear and friction reducing properties on rough surfaces in the presence of ZDDP additive. *Tribol. Int.* **2016**, *102*, 213–221. [CrossRef]

243. Ku, B.-C.; Han, Y.-C.; Lee, J.-E.; Lee, J.-K.; Park, S.-H.; Hwang, Y.-J. Tribological effects of fullerene (C60) nanoparticles added in mineral lubricants according to its viscosity. *Int. J. Precis. Eng. Manuf.* **2010**, *11*, 607–611. [CrossRef]

244. Peng, D.; Kang, Y.; Hwang, R.; Shyr, S.; Chang, Y. Tribological properties of diamond and SiO_2 nanoparticles added in paraffin. *Tribol. Int.* **2009**, *42*, 911–917. [CrossRef]

245. Srivyas, P.; Charoo, M.S. A Review on Tribological Characterization of Lubricants with Nano Additives for Automotive Applications. *Tribol. Ind.* **2018**, *40*, 594–623. [CrossRef]

246. Xiao, H.; Liu, S. 2D nanomaterials as lubricant additive: A review. *Mater. Des.* **2017**, *135*, 319–332. [CrossRef]

247. Flores-Castañeda, M.; Camps, E.; Camacho-López, M.; Muhl, S.; García, E.; Figueroa, M. Bismuth nanoparticles synthesized by laser ablation in lubricant oils for tribological tests. *J. Alloy Compd.* **2015**, *643*, S67–S70. [CrossRef]

248. Kato, H.; Komai, K. Tribofilm formation and mild wear by tribo-sintering of nanometer-sized oxide particles on rubbing steel surfaces. *Wear* **2007**, *262*, 36–41. [CrossRef]

249. Song, X.; Zheng, S.; Zhang, J.; Li, W.; Chen, Q.; Cao, B. Synthesis of monodispersed $ZnAl_2O_4$ nanoparticles and their tribology properties as lubricant additives. *Mater. Res. Bull.* **2012**, *47*, 4305–4310. [CrossRef]

250. Uflyand, I.E.; Zhinzhilo, V.A.; Burlakova, V.E. Metal-containing nanomaterials as lubricant additives: State-of-the-art and future development. *Friction* **2019**, *7*, 93–116. [CrossRef]

251. Lee, C.-G.; Hwang, Y.-J.; Choi, Y.-M.; Lee, J.-K.; Choi, C.; Oh, J.-M. A study on the tribological characteristics of graphite nano lubricants. *Int. J. Precis. Eng. Manuf.* **2009**, *10*, 85–90. [CrossRef]

252. Lee, K.; Hwang, Y.; Cheong, S.; Choi, Y.; Kwon, L.; Lee, J.; Kim, S.H. Understanding the Role of Nanoparticles in Nano-oil Lubrication. *Tribol. Lett.* **2009**, *35*, 127–131. [CrossRef]

253. Tevet, O.; Von-Huth, P.; Popovitz-Biro, R.; Rosentsveig, R.; Wagner, H.D.; Tenne, R. Friction mechanism of individual multilayered nanoparticles. *Proc. Natl. Acad. Sci. USA* **2011**, *108*, 19901–19906. [CrossRef]

254. Cizaire, L.; Vacher, B.; Le Mogne, T.; Martin, J.M.; Rapoport, L.; Margolin, A.; Tenne, R. Mechanisms of ultra-low friction by hollow inorganic fullerene-like MoS_2 nanoparticles. *Surf. Coat. Technol.* **2002**, *160*, 282–287. [CrossRef]

255. Joly-Pottuz, L.; Martin, J.; Dassenoy, F.; Belin, M.; Montagnac, G.; Reynard, B.; Fleischer, N. Pressure-induced exfoliation of inorganic fullerene-like WS2 particles in a Hertzian contact. *J. Appl. Phys.* **2006**, *99*, 023524. [CrossRef]

256. Rapoport, L.; Feldman, Y.; Homyonfer, M.; Cohen, H.; Sloan, J.; Hutchison, J.L.; Tenne, R. Inorganic fullerene-like material as additives to lubricants: Structure–function relationship. *Wear* **1999**, *225–229*, 975–982. [CrossRef]

257. Spikes, H. Friction Modifier Additives. *Tribol. Lett.* **2015**, *60*, 5. [CrossRef]

258. Lin, W.; Klein, J. Control of surface forces through hydrated boundary layers. *Curr. Opin. Colloid Interface Sci.* **2019**, *44*, 94–106. [CrossRef]

259. Klein, J. Hydration lubrication. *Friction* **2013**, *1*, 1–23. [CrossRef]

260. Suresh, S.; Venkitaraj, K.P.; Selvakumar, P.; Chandrasekar, M. Synthesis of Al_2O_3–Cu/water hybrid nanofluids using two step method and its thermo physical properties. *Colloids Surf. A* **2011**, *388*, 41–48. [CrossRef]

261. Kedzierski, M.A.; Brignoli, R.; Quine, K.T.; Brown, J.S. Viscosity, density, and thermal conductivity of aluminum oxide and zinc oxide nanolubricants. *Int. J. Refrig.* **2017**, *74*, 3–11. [CrossRef]

262. Mehrali, M.; Sadeghinezhad, E.; Latibari, S.T.; Kazi, S.N.; Mehrali, M.; Zubir, M.N.B.M.; Metselaar, H.S.C. Investigation of thermal conductivity and rheological properties of nanofluids containing graphene nanoplatelets. *Nanoscale Res. Lett.* **2014**, *9*, 15. [CrossRef]

263. Kulkarni, D.P.; Das, D.K.; Chukwu, G.A. Temperature dependent rheological property of copper oxide nanoparticles suspension (nanofluid). *J. Nanosci. Nanotechnol.* **2006**, *6*, 1150–1154. [CrossRef]

264. Pawelski, O.; Rasp, W.; Draese, S. Influence of Hydrodynamic Lubricant Entrainment on Friction Effects in Cold-Rolling. *Steel Res.* **1994**, *65*, 488–493. [CrossRef]

265. Qu, J.; Truhan, J.J.; Dai, S.; Luo, H.; Blau, P.J. Ionic liquids with ammonium cations as lubricants or additives. *Tribol. Lett.* **2006**, *22*, 207–214. [CrossRef]

266. Hild, W.; Opitz, A.; Schaefer, J.A.; Scherge, M. The effect of wetting on the microhydrodynamics of surfaces lubricated with water and oil. *Wear* **2003**, *254*, 871–875. [CrossRef]

267. Xia, W.Z.; Zhao, J.W.; Wu, H.; Zhao, X.M.; Zhang, X.M.; Xu, J.Z.; Hee, A.C.; Jiang, Z.Y. Effects of Nano-TiO_2 Additive in Oil-in-Water Lubricant on Contact Angle and Antiscratch Behavior. *Tribol. Trans.* **2017**, *60*, 362–372. [CrossRef]

268. Jiang, Z.Y.; Tang, J.; Sun, W.; Tieu, A.K.; Wei, D. Analysis of tribological feature of the oxide scale in hot strip rolling. *Tribol. Int.* **2010**, *43*, 1339–1345. [CrossRef]

269. Hao, L.; Wu, H.; Wei, D.B.; Cheng, X.W.; Zhao, J.W.; Luo, S.Z.; Jiang, L.Z.; Jiang, Z.Y. Wear and friction behaviour of high-speed steel and indefinite chill material for rolling ferritic stainless steels. *Wear* **2017**, *376*, 1580–1585. [CrossRef]

270. Colás, R.; Ramírez, J.; Sandoval, I.; Morales, J.C.; Leduc, L.A. Damage in hot rolling work rolls. *Wear* **1999**, *230*, 56–60. [CrossRef]

271. Najiha, M.S.; Rahman, M.M.; Kadirgama, K. Performance of water-based TiO_2 nanofluid during the minimum quantity lubrication machining of aluminium alloy, AA6061-T6. *J. Clean. Prod.* **2016**, *135*, 1623–1636. [CrossRef]

272. Williams, K. Tribology in Metal Working±New Developments. In Proceedings of the Echanical Engineering Conference, London, UK, 7–9 May 1980; pp. 4–6.

273. Zhu, Z.; Sun, J.; Niu, T.; Liu, N. Experimental research on tribological performance of water-based rolling liquid containing nano-TiO_2. *J. Nanomater. Nanoeng. Nanosyst.* **2015**, *229*, 104–109. [CrossRef]

274. Jia, T.; Liu, Z.Y.; Hu, H.F.; Wang, G.D. The Optimal Design for the Production of Hot Rolled Strip with "Tight Oxide Scale" by Using Multi-objective Optimization. *ISIJ Int.* **2011**, *51*, 1468–1473. [CrossRef]

275. Jiang, Z.Y.; Tieu, A.K.; Sun, W.H.; Tang, J.N.; Wei, D.B. Characterisation of thin oxide scale and its surface roughness in hot metal rolling. *Mater. Sci. Eng. A* **2006**, *435–436*, 434–438. [CrossRef]

276. Xiong, S.; Liang, D.; Wu, H.; Lin, W.; Chen, J.; Zhang, B. Preparation, characterization, tribological and lubrication performances of Eu doped $CaWO_4$ nanoparticle as anti-wear additive in water-soluble fluid for steel strip during hot rolling. *Appl. Surf. Sci.* **2021**, *539*, 148090. [CrossRef]

277. Cheng, X.; Jiang, Z.; Wei, D.; Hao, L.; Zhao, J.; Jiang, L. Oxide scale characterization of ferritic stainless steel and its deformation and friction in hot rolling. *Tribol. Int.* **2015**, *84*, 61–70. [CrossRef]

278. Yu, X.; Jiang, Z.; Zhao, J.; Wei, D.; Zhou, C.; Huang, Q. Microstructure and microtexture evolutions of deformed oxide layers on a hot-rolled microalloyed steel. *Corros. Sci.* **2015**, *90*, 140–152. [CrossRef]

279. Yu, X.; Jiang, Z.; Zhao, J.; Wei, D.; Zhou, C.; Huang, Q. Effects of grain boundaries in oxide scale on tribological properties of nanoparticles lubrication. *Wear* **2015**, *332–333*, 1286–1292. [CrossRef]

280. Dohda, K.; Boher, C.; Rezai-Aria, F.; Mahayotsanun, N. Tribology in metal forming at elevated temperatures. *Friction* **2015**, *3*, 1–27. [CrossRef]

281. Tominaga, J.; Wakimoto, K.; Mori, T.; Murakami, M.; Yoshimura, T. Manufacture of wire rods with good descaling property. *Trans. ISIJ* **1982**, *22*, 646–656. [CrossRef]

282. Sun, W.; Tieu, A.K.; Jiang, Z.; Zhu, H.; Lu, C. Oxide scales growth of low-carbon steel at high temperatures. *J. Mater. Process. Technol.* **2004**, *155–156*, 1300–1306. [CrossRef]

283. Zhao, J.; Jiang, Z. Thermomechanical processing of advanced high strength steels. *Prog. Mater. Sci.* **2018**, *94*, 174–242. [CrossRef]

284. Verlinden, B.; Driver, J.; Samajdar, I.; Doherty, R.D. *Thermo-Mechanical Processing of Metallic Materials*; Elsevier: Amsterdam, The Netherlands, 2007.

285. Hou, H.; Chen, Q.; Liu, Q.; Dong, H. Grain refinement of a Nb–Ti microalloyed steel through heavy deformation controlled cooling. *J. Mater. Process. Technol.* **2003**, *137*, 173–176. [CrossRef]

286. Cannio, M.; Ponzoni, C.; Gualtieri, M.L.; Lugli, E.; Leonelli, C.; Romagnoli, M. Stabilization and thermal conductivity of aqueous magnetite nanofluid from continuous flows hydrothermal microwave synthesis. *Mater. Lett.* **2016**, *173*, 195–198. [CrossRef]

287. Özerinç, S.; Kakaç, S.; Yazıcıoğlu, A.G. Enhanced thermal conductivity of nanofluids: A state-of-the-art review. *Microfluid. Nanofluid.* **2010**, *8*, 145–170. [CrossRef]

288. Tang, S.; Liu, Z.Y.; Wang, G.D.; Misra, R.D.K. Microstructural evolution and mechanical properties of high strength microalloyed steels: Ultra Fast Cooling (UFC) versus Accelerated Cooling (ACC). *Mater. Sci. Eng. A* **2013**, *580*, 257–265. [CrossRef]

289. Ginzburg, V.B. Steel-rolling technology. *Theory Pract.* **1989**, *328*, 791.

290. Eghbali, B.; Abdollah-zadeh, A. Influence of deformation temperature on the ferrite grain refinement in a low carbon Nb–Ti microalloyed steel. *J. Mater. Process. Technol.* **2006**, *180*, 44–48. [CrossRef]

291. Raulf, M.; Persson, K. Rolling of Steel. In *Encyclopedia of Lubricants and Lubrication*; Mang, T., Ed.; Springer: Berlin/Heidelberg, Germany, 2014; pp. 1663–1680. [CrossRef]

292. Zhang, S.; Ma, T.; Erdemir, A.; Li, Q. Tribology of two-dimensional materials: From mechanisms to modulating strategies. *Mater. Today* **2018**, *26*, 67–86. [CrossRef]

293. Song, J.; She, J.; Chen, D.; Pan, F. Latest research advances on magnesium and magnesium alloys worldwide. *J. Magnes. Alloy* **2020**, *8*, 1–41. [CrossRef]

294. Xie, H.; Jiang, B.; He, J.; Xia, X.; Pan, F. Lubrication performance of MoS_2 and SiO_2 nanoparticles as lubricant additives in magnesium alloy-steel contacts. *Tribol. Int.* **2016**, *93*, 63–70. [CrossRef]

295. Huang, W.; Du, C.; Li, Z.; Liu, M.; Liu, W. Tribological characteristics of magnesium alloy using N-containing compounds as lubricating additives during sliding. *Wear* **2006**, *260*, 140–148. [CrossRef]

296. Huang, W.; Fu, Y.; Wang, J.; Li, Z.; Liu, M. Effect of chemical structure of borates on the tribological characteristics of magnesium alloy during sliding. *Tribol. Int.* **2005**, *38*, 775–780. [CrossRef]

297. Xia, Y.; Jia, Z.; Jia, J. Tribological Behavior of AZ91D Magnesium Alloy against SAE52100 Steel under Ionic Liquid Lubricated Conditions. In *Advanced Tribology*; Springer: Berlin, Germany, 2009; pp. 896–898.